

STRIVE

Report Series No.79

Nanotechnology: Environmental and Human Health Impacts

STRIVE

Environmental Protection
Agency Programme

2007-2013

Environmental Protection Agency

The Environmental Protection Agency (EPA) is a statutory body responsible for protecting the environment in Ireland. We regulate and police activities that might otherwise cause pollution. We ensure there is solid information on environmental trends so that necessary actions are taken. Our priorities are protecting the Irish environment and ensuring that development is sustainable.

The EPA is an independent public body established in July 1993 under the Environmental Protection Agency Act, 1992. Its sponsor in Government is the Department of the Environment, Community and Local Government.

OUR RESPONSIBILITIES

LICENSING

We license the following to ensure that their emissions do not endanger human health or harm the environment:

- waste facilities (e.g., landfills, incinerators, waste transfer stations);
- large scale industrial activities (e.g., pharmaceutical manufacturing, cement manufacturing, power plants);
- intensive agriculture;
- the contained use and controlled release of Genetically Modified Organisms (GMOs);
- large petrol storage facilities;
- waste water discharges.

NATIONAL ENVIRONMENTAL ENFORCEMENT

- Conducting over 2,000 audits and inspections of EPA licensed facilities every year.
- Overseeing local authorities' environmental protection responsibilities in the areas of - air, noise, waste, waste-water and water quality.
- Working with local authorities and the Gardaí to stamp out illegal waste activity by co-ordinating a national enforcement network, targeting offenders, conducting investigations and overseeing remediation.
- Prosecuting those who flout environmental law and damage the environment as a result of their actions.

MONITORING, ANALYSING AND REPORTING ON THE ENVIRONMENT

- Monitoring air quality and the quality of rivers, lakes, tidal waters and ground waters; measuring water levels and river flows.
- Independent reporting to inform decision making by national and local government.

REGULATING IRELAND'S GREENHOUSE GAS EMISSIONS

- Quantifying Ireland's emissions of greenhouse gases in the context of our Kyoto commitments.
- Implementing the Emissions Trading Directive, involving over 100 companies who are major generators of carbon dioxide in Ireland.

ENVIRONMENTAL RESEARCH AND DEVELOPMENT

- Co-ordinating research on environmental issues (including air and water quality, climate change, biodiversity, environmental technologies).

STRATEGIC ENVIRONMENTAL ASSESSMENT

- Assessing the impact of plans and programmes on the Irish environment (such as waste management and development plans).

ENVIRONMENTAL PLANNING, EDUCATION AND GUIDANCE

- Providing guidance to the public and to industry on various environmental topics (including licence applications, waste prevention and environmental regulations).
- Generating greater environmental awareness (through environmental television programmes and primary and secondary schools' resource packs).

PROACTIVE WASTE MANAGEMENT

- Promoting waste prevention and minimisation projects through the co-ordination of the National Waste Prevention Programme, including input into the implementation of Producer Responsibility Initiatives.
- Enforcing Regulations such as Waste Electrical and Electronic Equipment (WEEE) and Restriction of Hazardous Substances (RoHS) and substances that deplete the ozone layer.
- Developing a National Hazardous Waste Management Plan to prevent and manage hazardous waste.

MANAGEMENT AND STRUCTURE OF THE EPA

The organisation is managed by a full time Board, consisting of a Director General and four Directors.

The work of the EPA is carried out across four offices:

- Office of Climate, Licensing and Resource Use
- Office of Environmental Enforcement
- Office of Environmental Assessment
- Office of Communications and Corporate Services

The EPA is assisted by an Advisory Committee of twelve members who meet several times a year to discuss issues of concern and offer advice to the Board.

EPA STRIVE Programme 2007–2013

Nanotechnology: Environmental and Human Health Impacts

**A Human Blood–brain Barrier Model for Screening
Nanoparticle Uptake and Access**

(2007-FS-EH-7-M5-2)

STRIVE Report

Prepared for the Environmental Protection Agency

by

University College Dublin

Authors:

**Michelle Nic Raghnaill, Meredith Brown, Dong Ye, Mattia Bramini,
Kenneth Dawson and Iseult Lynch**

ENVIRONMENTAL PROTECTION AGENCY

An Ghníomhaireacht um Chaomhnú Comhshaoil
PO Box 3000, Johnstown Castle, Co. Wexford, Ireland

Telephone: +353 53 916 0600 Fax: +353 53 916 0699

Email: info@epa.ie Website: www.epa.ie

ACKNOWLEDGEMENTS

This report is published as part of the Science, Technology, Research and Innovation for the Environment (STRIVE) Programme 2007–2013. The programme is financed by the Irish Government under the National Development Plan 2007–2013. It is administered on behalf of the Department of the Environment, Community and Local Government by the Environmental Protection Agency which has the statutory function of co-ordinating and promoting environmental research.

Parts of the work were conducted under the framework of the INSPIRE programme, funded by the Irish Government's Programme for Research in Third Level Institutions, Cycle 4, National Development Plan 2007–2013. Funding from the European Commission FP7 project NeuroNano (NMP4-SL-2008-214547) is also acknowledged.

DISCLAIMER

Although every effort has been made to ensure the accuracy of the material contained in this publication, complete accuracy cannot be guaranteed. Neither the Environmental Protection Agency nor the author(s) accept any responsibility whatsoever for loss or damage occasioned or claimed to have been occasioned, in part or in full, as a consequence of any person acting, or refraining from acting, as a result of a matter contained in this publication. All or part of this publication may be reproduced without further permission, provided the source is acknowledged.

The EPA STRIVE Programme addresses the need for research in Ireland to inform policy makers and other stakeholders on a range of questions in relation to environmental protection. These reports are intended as contributions to the necessary debate on the protection of the environment.

EPA STRIVE PROGRAMME 2007–2013

Published by the Environmental Protection Agency, Ireland

ISBN: 978-1-84095-409-8

Online version

Price: Free

Details of Project Partners

Michelle Nic Raghnaill

Centre for BioNano Interactions
School of Chemistry & Chemical Biology
and
UCD Conway Institute
University College Dublin
Belfield
Dublin 4
Ireland
Tel.: +353 1 716 6928
Email: michelle.nicraghnaill@cbni.ucd.ie

Meredith Brown

School of Agriculture, Food Science &
Veterinary Medicine
Veterinary Science Centre
University College Dublin
Belfield
Dublin 4
Ireland
Tel.: +353 1 716 6928
Email: brownmer@gmail.com

Dong Ye

Centre for BioNano Interactions
School of Chemistry & Chemical Biology
and
UCD Conway Institute
University College Dublin
Belfield
Dublin 4
Ireland
Tel.: +353 1 716 6928
Email: dong.ye@cbni.ucd.ie

Mattia Bramini

Centre for BioNano Interactions
School of Chemistry & Chemical Biology
and
UCD Conway Institute
University College Dublin
Belfield
Dublin 4
Ireland
Tel.: +353 1 716 6928
Email: mattia.bramini@cbni.ucd.ie

Kenneth Dawson

Centre for BioNano Interactions
School of Chemistry & Chemical Biology
and
UCD Conway Institute
University College Dublin
Belfield
Dublin 4
Ireland
Tel.: +353 1 716 6928
Email: kenneth.a.dawson@cbni.ucd.ie

Iseult Lynch

Centre for BioNano Interactions
School of Chemistry & Chemical Biology
and
UCD Conway Institute
University College Dublin
Belfield
Dublin 4
Ireland
Tel.: +353 1 716 6928
Email: iseult.lynch@cbni.ucd.ie

Table of Contents

Acknowledgements	ii
Disclaimer	ii
Details of Project Partners	iii
Executive Summary	vii
1 Introduction	1
2 Objectives	4
3 Background to the Project	5
4 Establishment of the <i>in vitro</i> Human Blood–brain Barrier Model	7
4.1 Optimisation of the Barrier Growth Conditions	9
5 Validation of the Model in Terms of Structure and Function	11
5.1 Validation of Tight Junction Formation in the Blood–brain Barrier Model	12
5.2 hCMEC/D3 Barrier Integrity Validation on Various Porous Transwells	14
5.3 Internal Validation of the Apparent Permeability of the <i>In Vitro</i> Blood-brain Barrier Model – Paracellular Transport	16
5.4 Internal Validation of the Apparent Permeability of the <i>In Vitro</i> Blood-brain Barrier Model – Transcellular Transport	18
6 Initial Screening of a Range of Nanoparticles for Passage through the Model Blood–brain Barrier	19
6.1 Nanoparticle Equilibration in Different Types of Transwells	19
6.2 Nanoparticle Adherence to Transwell Membranes	20
7 Selection of the Nanoparticles to be used for Deeper Studies	24
7.1 Characterisation of the Selected Nanoparticles in the Assay Medium	24
7.2 Pre-incubation of the Nanoparticles in the Assay Medium – Effect of the Protein Corona on Particle Stability	26
8 Determination of Mechanisms for Nanoparticle Passage through the Blood–brain Barrier Model	30
8.1 Transport of 50 nm SiO ₂ Nanoparticles Through the <i>In Vitro</i> Blood–brain Barrier Model	30
8.2 Effect of SiO ₂ Nanoparticles Size on Efficiency of Crossing the Blood–brain Barrier Model	31
8.3 Temperature-dependent Nanoparticle Transport Across the Blood–brain Barrier Model	33
8.4 Bi-directional Transport Assays through the hCMEC/D3 Blood–brain Barrier Monolayers	35
8.5 Endocytosis and Internalisation of SiO ₂ Nanoparticles by hCMEC/D3 Cells	37

8.6	Co-localisation of SiO ₂ Nanoparticles in Lysosomes of hCMEC/D3 Cells	38
8.7	Visualisation of Cellular Endocytosis of 50 nm SiO ₂ Nanoparticles by hCMEC/D3 Cells using Electron Microscopy	39
8.8	Transcytosis of 50 nm SiO ₂ Nanoparticles across the hCMEC/D3 Blood–brain Barrier Model	40
9	Correlation of Protein Coronas on Particles with Passage through the Blood–brain Barrier	43
10	Development of a Risk-assessment Protocol for Nanoparticle Uptake into the Brain	45
10.1	Exposure Assessment	45
10.2	Hazard Assessment	46
10.3	Risk Assessment	48
11	Validation of the Human Blood–brain Barrier Model Against <i>In Vivo</i> Biodistribution Data	49
11.1	Intra-cerebro-ventricular Injection of Animals with Nanoparticles	49
12	Conclusions and Recommendations	52
13	Key Messages for Policy Makers	54
	References	55
	Acronyms and Annotations	60
	Appendix I: Experimental Details	62

Executive Summary

Neurodegenerative diseases currently affect over 1.6% of the European population, with dramatically rising incidence that is likely (in part) due to the increase in the average age of the population. There are persistent claims, based on the epidemiology, that pollution may be a cofactor in Alzheimer's disease, although the evidence is controversial. The risk that engineered nanoparticles could introduce unforeseen hazards to human health is now a matter of deep and growing concern in regulatory bodies, governments and industry. However, at present there is only circumstantial evidence that nanoparticles could impact on such diseases.

The 'blood-brain barrier' (BBB) is a protective mechanism that separates the bloodstream from brain tissue while allowing passage of essential nutrients to the brain. Due to their small size and large surface area that is rapidly coated with proteins, which thereby confer on them a biological identity, nanoparticles have unique access to the cellular machinery and can potentially cross biological barriers such as the BBB, offering extraordinary hope for treatment of diseases such as HIV and Alzheimer's disease, but also raising significant concerns regarding their safety.

This report presents the work of an EPA STRIVE Fellowship of almost 2¼ years that aimed to establish and validate an *in vitro* model for assessment of the human BBB, and to use this to screen nanoparticle transport through the BBB and correlate nanoparticle

access to the brain with the nanoparticle physico-chemical characteristics and their protein corona. Specifically, the project intended to develop a rational framework within which to understand which properties of nanoparticles lead to them reaching the brain, and the mechanism(s) by which nanoparticles cross the BBB.

Based on the large quantity of uptake and localisation data generated within the project, a preliminary risk assessment of the potential for silicon dioxide (SiO₂) nanoparticles to induce neurotoxicity was performed. The low potential of the SiO₂ nanoparticles to reach the brain via the BBB (less than 5% of the applied dose of 50 nm SiO₂ nanoparticles was transcytosed in 4 hours), coupled with the low hazard of these nanoparticles (no cytotoxicity observed at 100 µg/mL after 48 hours of exposure), implies a very limited potential for these nanoparticles to induce neurotoxicity. However, these are only very short-term acute exposure tests, and additional longer-term, chronic and repeat-dose experiments are required urgently.

The recommendations of the report for policy makers include the need to consider nanomaterials as biological entities as distinct from chemicals, and as such to develop a strategy to monitor the likely environmental exposure to nanomaterials, and to fund additional research into the environmental and human health impacts of nanomaterials.

1 Introduction

The 'blood–brain barrier' (BBB) is a protective mechanism that separates the bloodstream from brain tissue while allowing passage of essential nutrients to the brain. The BBB is composed of high-density cells that restrict the passage of substances from the bloodstream much more than is done by endothelial cells in capillaries elsewhere in the body. This 'barrier' functionality results from the selectivity of the tight junctions that form between endothelial cells in the blood vessels of the central nervous system (CNS), which restricts the passage of solutes. At the interface between blood and the brain, endothelial cells are stitched together by these tight junctions, which are composed of smaller subunits, such as transmembrane proteins. The BBB has evolved to prevent harmful chemicals and foreign entities from reaching the extremely sensitive cells and tissues of the brain. The primary components of the BBB are the tight junctions formed between the endothelial cells, supporting cells (astrocytes, pericytes and microglia), enzymes, receptors, transporters and efflux pumps that control and limit the access of molecules to the brain, as shown in [Fig. 1.1](#).

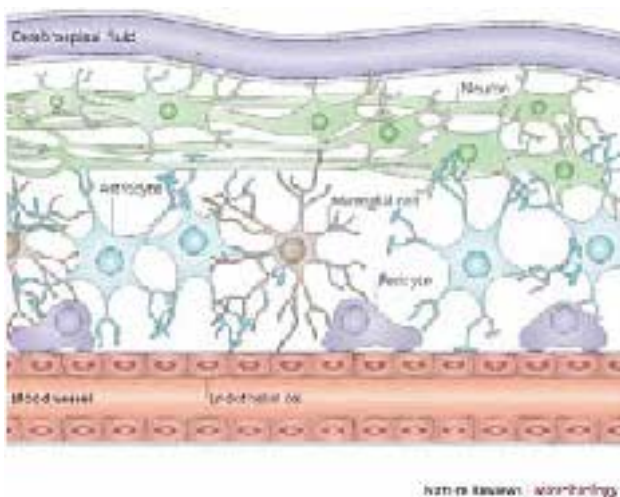


Figure 1.1. The primary component of the blood–brain barrier is the tight junctions between endothelial cells. The blood–brain barrier regulates the flow of material from the systemic circulation to the central nervous system. (Source: Abbott et al., 2006.)

Several methods of transport across the BBB have been identified, including paracellular or transcellular pathways, transport proteins, receptor-mediated transcytosis, and adsorptive transcytosis (see [Fig. 1.2](#)). Indeed, many biological molecules manage to cross the BBB as part of the natural functioning of the body – these are termed endogenous BBB transporters, and can be classified into three categories: carrier-mediated transport (CMT), active efflux transport (AET) and receptor-mediated transport (RMT). Whereas the CMT and AET systems are responsible for the transport of small molecules between blood and brain, the RMT systems are responsible for the transport across the BBB of certain endogenous large molecules. For example, insulin in blood undergoes RMT across the BBB via the endogenous BBB insulin receptor.

Although the neuroprotective function is vital, the BBB also impedes the passage of pharmacologically beneficial substances in instances of CNS diseases, such as Alzheimer's disease, Parkinson's disease, neuro-AIDS, stroke and dementia. Thus, despite the existence of these transport pathways, pharmaceutical companies have invested significant sums in the design of drugs that can cross the BBB, with very limited success. The limited penetration of drugs into the brain is the rule, not the exception, and in fact more than 98% of all small molecules do not cross the BBB (Pardridge, 2007). Essentially, 100% of large-molecule pharmaceuticals, including peptides, recombinant proteins, monoclonal antibodies, RNA interference based drugs and gene therapies, do not cross the BBB (Pardridge, 2001). There are more than 7000 drugs in the Comprehensive Medicinal Chemistry database, and only 5% of these drugs treat the CNS; the drugs that do treat the CNS are limited to the treatment of depression, schizophrenia and insomnia (Ghose et al., 1999).

Considerable effort has been deployed by the pharmaceutical industry to understand how the BBB functions, and to understand which physico-chemical properties of drugs will promote their passage across the BBB (Pardridge, 2007).

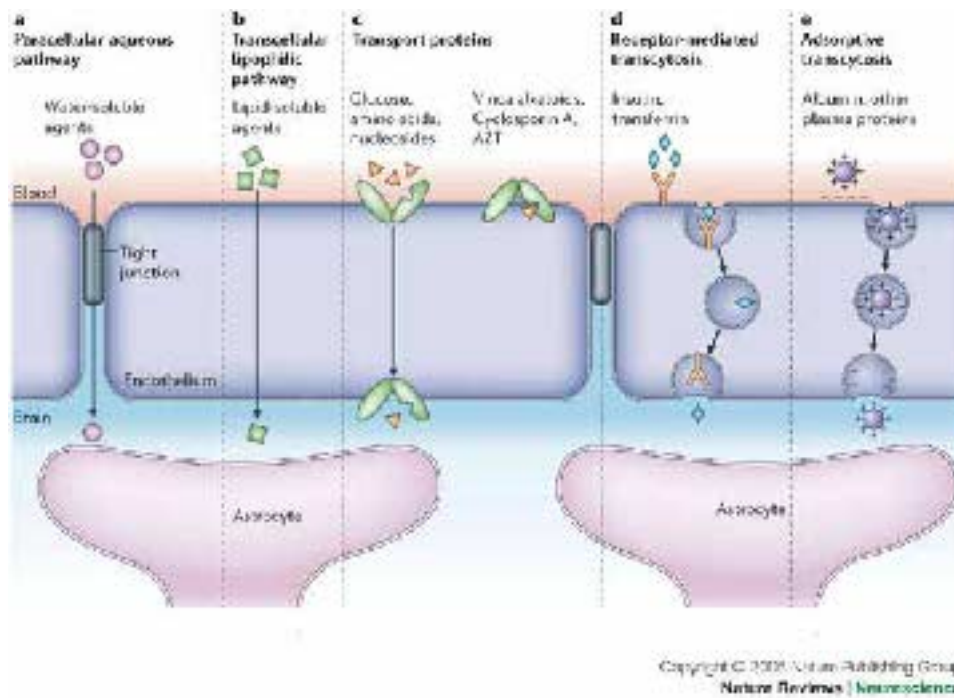


Figure 1.2. Pathways across the blood–brain barrier. Size, surface charge and molecular signalling influence the ability of substances to cross the blood–brain barrier through these various pathways. (Source: Abbott et al., 2006.)

As a general rule, the BBB permeability of a drug decreases by one log order of magnitude for each pair of hydrogen bonds (H-bonds) added to the molecule in the form of polar functional groups (Pardridge and Mietus, 1979). Based on H-bonding rules (Stein, 1967; Diamond and Wright, 1969), the number of H-bonds that a given drug forms with water can be calculated by inspection of the chemical structure. Once the number of H-bonds is greater than eight, it is unlikely that the drug crosses the BBB via lipid-mediated free diffusion in pharmacologically significant amounts (see Fig. 1.3).

The other important parameter determining free diffusion of small molecules across the BBB is the molecular weight (MW) of the drug. Once the MW is over 400 Da, the BBB permeability of the drug does not increase in proportion to lipid solubility (Fischer et al., 1998). The biophysical basis for the MW threshold appears to be the transitory formation of pores within the phospholipid bilayer that are created as the free fatty acyl side-chains kink in the process of normal molecular motion within the phospholipid bilayer (Trauble, 1971; Marrink et al., 1996). The pores are of finite size and restrict the movement of small molecules that have a

spherical volume in excess of the pore volume. BBB permeation decreases 100-fold as the surface area of the drug is increased from 52 Å (e.g. a drug with an MW of 200 Da), to 105 Å (e.g. a drug with an MW of 450 Da) (Fischer et al., 1998).

Based on the MW and H-bonding for a given drug, a reasonable prediction can be made as to whether the drug crosses the BBB in pharmacologically significant amounts via lipid-mediated free diffusion (see Fig. 1.3). Interestingly, the presence of more than one carboxyl group (-COOH) or a quaternary ammonium group (permanently positively charged, irrespective of pH) on a drug was also found to inhibit passage through the BBB (Pardridge, 2007).

However, it has recently emerged that nanoparticles do not seem to be subject to the restrictions of small molecules, and increasing numbers of reports of nanoparticles being able to pass through the BBB are emerging in the literature (Michaelis et al., 2006; Sarin et al., 2008; Chattopadhyay et al., 2008; Brigger et al., 2002; Silva, 2008). While this unprecedented access of nanoparticles to the brain via the BBB offers

BOX 1

Two-step method for prediction of whether a small-molecule drug crosses the BBB via lipid-mediated free diffusion

Step 1: determine molecular weight (MW) of drug
 Step 2: determine H-bonding based on drug chemical structure

H-bonding rules:
 4 H-bonds for each terminal amide group
 3 H-bonds for each internal amide, primary amino group or carboxyl group
 2 H-bonds for each hydroxyl group
 1 H-bond for each ether or carbonyl group
 Add total H-bonds formed between drug and solvent water

Parameter	Unrestricted BBB transport	Restricted BBB transport
MW	<400 Da	>400 Da
Total H-bonding	<8	>8

If the MW of the drug is >400 Da and/or the drug forms eight or more H-bonds, then the drug is probably a poor CNS-penetrating molecule.

Certain functional groups abort BBB transport, for example:
 Quaternary ammonium group
 More than one carboxyl group

Figure 1.3. Summary of the two-step method for prediction of small-molecule penetration of the blood–brain barrier, based on the drug molecular weight and the number of hydrogen bonds that the molecule is capable of forming. (Source: Pardridge, 2007.)

enormous potential for therapeutics, it also raises the possibility of unintended nanoparticle access to the brain (Olivier et al., 1999). There is also significant *in vivo* evidence (Semmler et al., 2004; Kreyling et al., 2002), now incontrovertible (Kreyling et al., 2007), that some engineered nanoparticles (e.g. 6 nm and 18 nm gold nanoparticles) entering intravenously or via the lungs can reach the brains of small animals. Indeed, the uptaken nanoparticles lodge in almost all parts of the brain, and there are no efficient clearance mechanisms to remove them once there. Furthermore, there are suggestions that nanoscale particles arising from urban pollution reach the brains of animals (Calderón-Garcidueñas et al., 2002, 2003; Elder et al., 2007). The relevant particle fractions arise from pollution, but their structure and size are similar to engineered carbon nanostructures. Thus, there are sufficient concerns to warrant urgent research on the mechanism(s) by which nanoparticles reach the brain, and to correlate nanoparticle access to the brain via the BBB with the nanoparticle physico-

chemical characteristics and the nature of the adsorbed proteins that mediate the surface of the nanoparticles and engage with the cellular receptors of the BBB. This information would potentially enable production of those nanoparticles that pose a risk of access to the brain and allow for controlled design to ensure only those particles intended for therapy reach the brain.

To date there are no well validated *in vitro* models of the human BBB that could be used as the basis of a nanoparticle screening and risk-assessment programme for the more than 30,000 different nanoparticles that will emerge from research labs and industry around the world over the coming years. The aim of this project was to establish and validate such an *in vitro* BBB model and to screen a range of relevant nanoparticles for their ability to pass through the barrier. Comparison with literature animal studies of ultrafine and nanoparticle uptake and translocation will help to establish the risk parameters.

2 Objectives

The aim of the project was to develop a rational framework within which to understand which properties of nanoparticles lead to them reaching the brain (e.g. surface area, surface composition, shape, etc.), and the mechanism(s) by which nanoparticles cross the BBB. Specifically, the project intended to establish and validate an *in vitro* (cell culture) model of the human BBB, and to use this to screen nanoparticle transport through the BBB and correlate nanoparticle access to the brain with the nanoparticle physico-chemical characteristics and their protein corona compositions.

It was intended to focus on nanoparticles that were of immediate environmental importance, such as cerium oxide nanoparticles (which are already in use as fuel additives in Turkey) and carbon nanotubes (which are in kilogram scale production in several sites worldwide), as well as model polymeric particles whose surface characteristics can be controlled and modified extensively, thereby offering exceptional versatility and a unique opportunity to conduct a systematic study and produce much-needed scientific data to address this issue. However, a key factor in determining the uptake of the nanoparticles into the cells, and quantifying the amount of nanoparticles traversing the barrier (reaching the basolateral chamber of the experimental set-up), is the need for a method of detection of the nanoparticles, such as a fluorescent signal. Thus, the project focused primarily on the mechanism of transport of commercially available, fluorescently labelled SiO₂ and polystyrene nanoparticles through the BBB. These particles are also on the Organisation for Economic Cooperation and Development (OECD) list of priority nanoparticles for testing within their sponsorship programme, due to their current or predicted future production volumes and their industrial applications, (OECD, 2008) and as such are considered of high importance for risk assessment.

To achieve this, the overall objective was further divided into a series of sub-objectives aimed at understanding and quantifying the potential for nanoparticles to reach the brain, as follows:

- **Understand what constitutes a lead nanoparticle candidate for passing the BBB.** It is recognised that not all particles that could be toxic will in fact pass the BBB. Part of the strategy is to carry out early screening of the particles using the BBB model and to complement this with limited animal studies within the European Commission Seventh Framework Programme (EU FP7) NeuroNano project.
- **Quantify transport efficiency to the brain.** The project seeks to quantify the amount of nanoparticles that pass through the model BBB compared to the amount delivered via different routes. It will also attempt to show how this amount depends on the material, both in the conventional sense (size, zeta potential, etc.) and according to the concept of surface expression, or the evolving protein corona.
- **Understand the detailed pathways that nanoparticles take to reach the brain.** Microscopy and imaging will be used to learn (for the first time) as much as possible about how the particles reached their destination, and the detailed nature of what is expressed on their surface as they pass through the barrier cells on the way to the brain will be determined using proteomic approaches.

The overall output will thus be a paradigm to classify the risk factors of nanoparticles in terms of their biomolecule corona and their potential to cross the BBB, resulting in a preliminary framework for risk assessment of nanoparticles.

3 Background to the Project

Neurodegenerative diseases currently affect over 1.6% of the European population (Alzheimer Europe, 2006), with dramatically rising incidence that is likely (in part) due to the increase of the average age of the population. This is a major concern for all industrialised societies, including Ireland. Data from the Alzheimer's Society of Ireland indicates that dementia affects almost 44,000 people and touches the lives of 50,000 carers and hundreds of thousands of family members in Ireland, with Alzheimer's disease accounting for 66% of all cases of dementia. Estimates suggest that within 20 years the numbers of people affected will double, and by 2036 some 104,000 people will be affected. By 2036, the number of people with dementia in Ireland is expected to increase by 300%, while the total population is likely to increase by less than 40%.

There are persistent claims, based on the epidemiology, that pollution may be a cofactor in Alzheimer's disease, although the evidence is controversial. Furthermore, there are suggestions that nanoscale particles arising from urban pollution reach the brains of animals (Calderón-Garcidueñas et al., 2002, 2003; Elder et al., 2007), and nanoscale particles have been found in target brain areas (olfactory bulb, frontal cortex) in children resident in Mexico City (Calderón-Garcidueñas et al., 2004). The relevant particle fractions arise from pollution but their structure and size are similar to engineered carbon nanostructures. Due to their similar size to the ultrafine fraction of pollution, the risk that engineered nanoparticles could introduce unforeseen hazards to human health is now also a matter of deep and growing concern for many regulatory bodies, governments and industry. Some comments about the topic have also appeared in the more general literature (Ball, 2006; Phibbs-Rizzuto, 2007).

As nanoparticles have appeared and will increasingly appear in everyday consumer products, there has been considerable interest in ensuring that these materials are safe and are introduced safely into the market. Applications range from nano-sized titanium dioxide and zinc oxide in sun creams, clay nanoparticles in beer bottles, silver nanoparticles in food storage containers, and nano-hydroxyapatite in toothpaste, as well as

a range of inorganic nanoparticles and nanotubes being developed for use in the information technology industry. Careful and thorough attention to detail from both governmental institutions and researchers in this arena has now begun to prevail, and broadly speaking early fears of great hazard (associated solely with the nanoscale) have declined, being replaced by cautious disciplined efforts to ensure safety of the various applications. Besides the very evident everyday advantages for consumer products, some of the greatest hopes for bionano science involve biomedical applications including new therapies and diagnostic tools for some of the most deadly and intractable human diseases.

One approach to ensuring safe application of nanomaterials in biology is to obtain a deep mechanistic understanding of the interactions between nanomaterials and living systems (bionano interactions). To this end, this project reports on the establishment and quality management by internal benchmarking of a human cell model of the BBB for use as a tool for screening nanoparticle interactions, and assessing the critical nanoscale parameters that determine transcytosis (crossing of the BBB). Nanoparticles have recently been shown to be able to enter the CNS by crossing the BBB. Thus, nanoparticles may need to be considered as a separate class of chemicals under the Registration, Evaluation, and Authorization of Chemicals (REACH) guidelines that are currently being developed, due to their different behaviour *in vivo* as compared to standard chemicals and drugs. Note that less than 2% of all drugs developed can reach the BBB (see Section 1). It will be important in the longer term to study a range of different nanoparticle types in terms of the classical divisions, such as organic, inorganic and metallic, but even more important is to choose nanoparticles that are industrially relevant and/or high-risk particles, with some urgency.

As described briefly in Section 1, transport of drugs across the BBB is considered the holy grail of targeted delivery, due to the extreme effectiveness of this barrier at preventing passage of non-essential molecules through to the brain. This has caused severe limitations for therapeutics for many brain-associated diseases,

such as HIV and neurodegenerative diseases. Nanomaterials, as a result of their small size (in the order of many protein–lipid clusters routinely transported by cells) and large surface area (which acts as a scaffold for proteins, thereby rendering nanoparticles as biological entities), offer great promise for neuro-therapeutics. However, in parallel with developing neuro-therapeutic applications based on nanotechnology, it is essential to ensure their safety and long-term consequences on reaching the brain.

Among the various non-invasive approaches to neurotherapy, nanoparticulate carriers and particularly polymeric nanoparticles seem to present one of the most interesting strategies. These nanoparticles are vectors with a size of 10–100 nm, and drugs can be loaded into them, adsorbed or chemically linked to their surface (Chang et al., 2009). These carriers possess a higher stability in biological fluids and against the enzymatic metabolism than other colloidal carriers, such as liposomes or lipidic vesicles (Huwlyer et al., 1996). Many attempts to use nanoparticles as CNS drug delivery systems were performed with some success (Blasi et al., 2007; Tosi et al., 2007), thus demonstrating the feasibility of drug delivery to the CNS by using these carriers. Poly(butyl cyanoacrylate) nanoparticles coated with polysorbate 80 are able to cross the BBB when administered intravenously (Ambruosi et al., 2006). Similar results were obtained in the presence of Polyethylene oxide coated (PEGylated) polycyanoacrylate nanoparticles (Calvo et al., 2001). Poly(butyl cyanoacrylate) nanoparticles coated with polysorbate 80 were used to encapsulate dalargin, loperamide, (*N*-methyl *D*-aspartate)-receptor antagonists and doxorubicin (Ambruosi et al., 2006). The mechanism of drug delivery across the BBB using surfactant-coated nanoparticles appears to result from adsorption of apolipoprotein E or apolipoprotein A-1 after injection into the bloodstream, followed by

receptor-mediated endocytosis of the particles by the brain capillary endothelial cells (BCECs) (Kreuter et al., 2002; Kim et al., 2007). This hypothesis is supported by the finding that covalent coupling of apolipoprotein E or A-1 to human serum albumin nanoparticles leads to similar effects (Michaelis et al., 2006; Petri et al., 2007; Kreuter et al., 2007).

Specific receptors have been identified in the brain capillary endothelium that are utilised for uptake of essential nutrients such as the low-density lipoprotein (LDL) receptor that is used for uptake of cholesterol (Dehouck et al., 1997), the insulin receptor (Frank et al., 1986), the folic acid receptor (Wu and Pardridge, 1999) and the transferrin receptor (Descamps et al., 1996). These receptors can be targeted with suitable ligands, including with nanoparticles functionalised with ligands to these receptors. Receptor-mediated transcytosis has been illustrated for insulin, transferrin and LDL, among others (Duffy and Pardridge, 1987; Descamps et al., 1996; Dehouck et al., 1997).

The basis of nanoparticles as the new hope in therapeutics involves several key factors. First, the endogenous biological transport processes are mainly on the scale of some tens of nanometres, and by exploiting these, nanoparticles may facilitate unique access to hitherto inaccessible disease sites. Second, the primary immune system is less active for objects measuring somewhat less than several hundred nanometres, allowing for longer circulation or processing times before clearance. There are clear hopes that a fundamental understanding and control of how the nanoparticle surface is affected and read by living organisms will enable major developments in medicine. It should also not be forgotten that pharmaceutical products involving the more basic applications of nanotechnology have already been approved for clinical uses, and there are more than 300 nano-enabled products at various stages of preclinical development (Dobrovolskaia, 2007).

4 Establishment of the *in vitro* Human Blood–brain Barrier Model

The development of a reliable *in vitro* BBB model has been a goal in the field of neuro-therapeutics for a long time. In the past, efforts to establish appropriate models were made by co-culturing various primary BCECs with astrocytes to mimic the *in vivo* situation. In this combination, BCECs are surrounded by astrocytes and pericytes, which are crucial for cell maturation and development of tight junctions *in vivo*. These models exhibited high electrical resistances, low permeability to small molecular weight compounds, and functional expression of the most important drug transporters (Mahley, 1988). However, as the isolation of primary or low-passage brain capillary endothelial cells (BCECs) is very laborious and time-consuming, this method was replaced by the use of different immortalised rat or mouse brain endothelial cell lines, such as RBE4 (Roux et al., 1994), GPNT (Regina et al., 1999) and b.End3 (Omidi et al., 2003).

Species differences in these *in vitro* animal models, in terms of the mechanisms of BBB function, led researchers to develop immortalised human *in vitro* BBB models. So far, only three human immortalised cell lines have been developed: BB19 (Prudhomme et al., 1996; Kusch-Poddar et al., 2005), NKIM-6 (Kusch-Poddar et al., 2005) and immortalised human capillary microvascular endothelial cells (hCMEC/D3) (Weksler et al., 2005). Immortalised human brain endothelial cell model BB19 has been used to study cytoadherence of *Plasmodium falciparum*-infected erythrocytes *in vitro* (Kusch-Poddar et al., 2005). BB19 cells have been reported to display much higher sucrose permeability than primary porcine BCECs, and non-discrimination between its paracellular and transcytotic permeability, suggesting a further improvement of cell monolayer tightness is needed in this model (Kusch-Poddar et al., 2005). Another immortalised human brain endothelial cell model, NKIM-6, initially reported by Ketabi-Kiyanvash et al. (2007), has not been validated with any permeability

studies so far, although this model reportedly retains most endothelial characteristics. Comparatively, the hCMEC/D3 cell line has been well characterised, and data on active transport of insulin, sucrose, lucifer yellow, morphine, propranolol and midazolam have been reported (Poller et al., 2008), hence this was selected for this study.

The hCMEC/D3 cell line was developed in 2005 by immortalisation of primary human BCECs through expression of hTERT and the SV40 large T antigen via a lentiviral vector system. Similarly to primary BCECs, the hCMEC/D3 cell line constitutively expresses typical endothelial markers, including junction proteins PECAM-1, VE-cadherin, ZO-1, JAM-A and claudin-5 (Weksler et al., 2005). Moreover, a series of adhesion molecules and chemokine receptors were detected as well, such as ICAM-1, ICAM-2, and CD-4, which were known to facilitate leukocyte migration into the CNS under *in vivo* inflammatory conditions (Weksler et al., 2005). These conclusions show that hCMEC/D3 cells have many key characteristics of the *in vivo* BBB, and provide a promising tool to study compound delivery across the BBB. Like other immortalised *in vitro* models, however, a consistently low transendothelial electrical resistance (TEER) has been observed in the hCMEC/D3 cell model compared to the primary endothelial model or the astrocyte co-culturing model. In addition, the paracellular and transcytotic permeability of the hCMEC/D3 cell model has been evaluated, and the permeabilities of compounds with various molecular weights and hydrophobicities – such as insulin, sucrose, lucifer yellow, propranolol, morphine, midazolam – have been reported (Poller et al., 2008).

In the hCMEC/D3 cell model, a collagen-coated porous membrane is used to support cellular differentiation and to allow fluid diffusion between both sides of the membrane, as shown schematically in [Fig. 4.1](#).

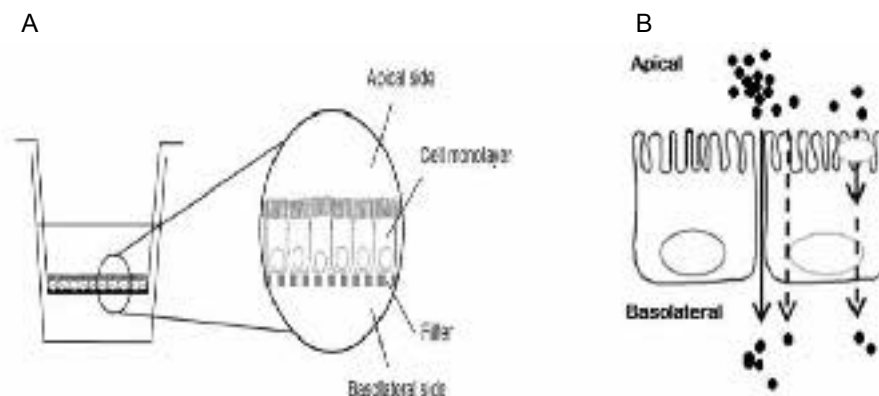


Figure 4.1. The model diagram of the hCMEC/D3 monolayer on a permeable membrane. (A) A so-called ‘transwell’, consisting of an upper insert membrane (apical chamber) and lower acceptor well (basolateral chamber). (B) The upper (apical) chamber mimics the microvascular bloodstream, and the lower (basolateral) chamber, in contrast, can be seen as ‘brain side’ or ‘central nervous system side’.

Recently, the hCMEC/D3 *in vitro* model has been improved to mimic *in vivo* BBB functions. hCMEC/D3 cells were reported to grow in endothelial basal media (EBM-2) supplemented with vascular endothelial growth factor (VEGF), insulin-like growth factor 1 (IGF-1), epidermal growth factor (EGF), basic fibroblast growth factor (bFGF), foetal calf serum (FCS) and hydrocortisone. The method consists of ‘seeding’ cells onto a porous membrane (see [Fig. 4.1A](#)) for one week to form a differentiated, contact-inhibited monolayer, which can then be used to study BBB transport mechanisms. In this system, the different chambers mimic different *in vivo* microenvironments, with the apical chamber mimicking the blood and the basolateral chamber mimicking the brain, as shown in [Fig. 4.1B](#). Thus, molecules loaded into the apical chamber are presented to the cellular barrier formed on the filter, which can then be taken up by the cells by a receptor-mediated (transcytosis) process ([Fig. 4.1B](#)), and in some rare cases the nanoparticles are released to the basolateral chamber.

While it is clearly desirable to apply these established models to study nanoparticle passage across the BBB, it transpires that there are very significant challenges in achieving this for nanomaterials, specifically in terms of gaining reproducible data on nanoparticle flux across the barrier. The difficulties far exceed those in molecular applications of these models, and it is useful to discuss them at some length based on extensive experience in this area. For example, interactions of the nanoparticles with the filter material, including potential for blocking

of the pores, are complicated issues that impact on the amount of nanoparticles that reach the basolateral chamber.

It should also be recognised that extraction of the cell-barrier transport property requires the subtraction of the flux from the filter support alone from the flux of the combined *in vitro* BBB model. This requires the flux through the filter to be significantly higher than that of the cell-barrier (and the combination); otherwise, a small flux must be determined from the difference between two large (noisy) fluxes. These issues therefore lay quite a lot of attention on the nature of the filter, and its interactions with particles under flow. It should also be noted that many of the challenges laid out here are by no means fully resolved, and all aspects of the problem continue to be explored in an effort to produce a truly quantitative and ultimately validatable model. The present report should be considered a ‘status report’ on the efforts so far, suggesting the need for considerable advancement.

In [Fig. 4.1B](#), apical to basolateral (ab) transport illustrates fluid migration via either a paracellular or a transcellular pathway. The reverse transport, basolateral to apical (ba), is another possible way of assessing compound transport. Both transports are usually studied together in order to evaluate the compound uptake ratio $P_{app'ba}/P_{app'ab}$ (where P_{app} is apparent permeability) or the efflux ratio $P_{app'ab}/P_{app'ba}$, and to determine whether the transport is via a passive or an active transport pathway (Hubatsch et al., 2007).

4.1 Optimisation of the Barrier Growth Conditions

In order for the hCMEC/D3 cells to function as a barrier, it is essential that they form a confluent monolayer and tight junctions with their neighbouring endothelial cells, which prevents paracellular (between cells) transport. Extensive transmission electron microscopy (TEM) imaging has been used to characterise the phenotype of the cells and their organisation on the transwell filters in advance of the transport assays.

In order to confirm the differentiated cell morphology, and to confirm that the cell growth protocol results in the formation of a homogeneous monolayer of human endothelial cells on the transwell filter, the cells grown under different culture conditions were evaluated with TEM, as shown in [Fig. 4.2](#) for hCMEC/D3 cells grown on a 0.4 μm transwell filter.

The hCMEC/D3 cells were cultivated in the two sets of media – the growth medium and the assay medium. The major difference between the media was the species of growth factors contained in each medium, which are capable of simulating cellular growth, proliferation and differentiation. The assay medium contained only bFGF. In contrast, the growth medium contained bFGF and three other growth factors: VEGF, IGF-1 and EGF. As shown in [Fig. 4.2A](#), hCMEC/D3 cells appeared aggregated and overgrown when grown in the growth-factor rich medium on a 0.4 μm porous membrane. In the assay medium ([Fig. 4.2B](#)), however, a monolayer was found on the membrane with a morphology of cell

to cell contact inhibition after 7 days of growth, which maintained sufficient cellular differentiation without cell aggregation. Furthermore, in [Fig. 4.2C](#), tight junctions were observed between adjacent cells after cultivation in the assay medium. Using electron microscopy, the tight junctions appeared as high electron-dense areas that discriminated themselves from the other cellular structures.

The comparison above indicates that the growth-factor rich medium (i.e. the growth medium) prompted rapid cell propagation rather than cell differentiation, and caused a loss of cellular capacity to form a homogeneous monolayer. Additionally, it has been demonstrated that when hCMEC/D3 cells are cultivated in a growth-factor-depleted medium, the cells are able to maintain physiological barrier properties similar to the *in vivo* human BBB even without co-culture with astrocytes (Weksler et al., 2005; Forster et al., 2008; Cucullo et al., 2007). For example, the *in vitro* hCMEC/D3 cell model retained the expression of several endothelial cell markers (Weksler et al., 2005) in the aerobic metabolic pathway, and showed features of barrier disorganisation and extravasation of leucocytes in response to an inflammatory response (Cucullo et al., 2007). Thus, the growth medium for cell propagation or proliferation was used to modulate hCMEC/D3 cell responses *in vitro*, and the assay medium was used to obtain a differentiated monolayer barrier for the transport studies and for assessment of the access of nanoparticles through the model *in vitro* BBB.

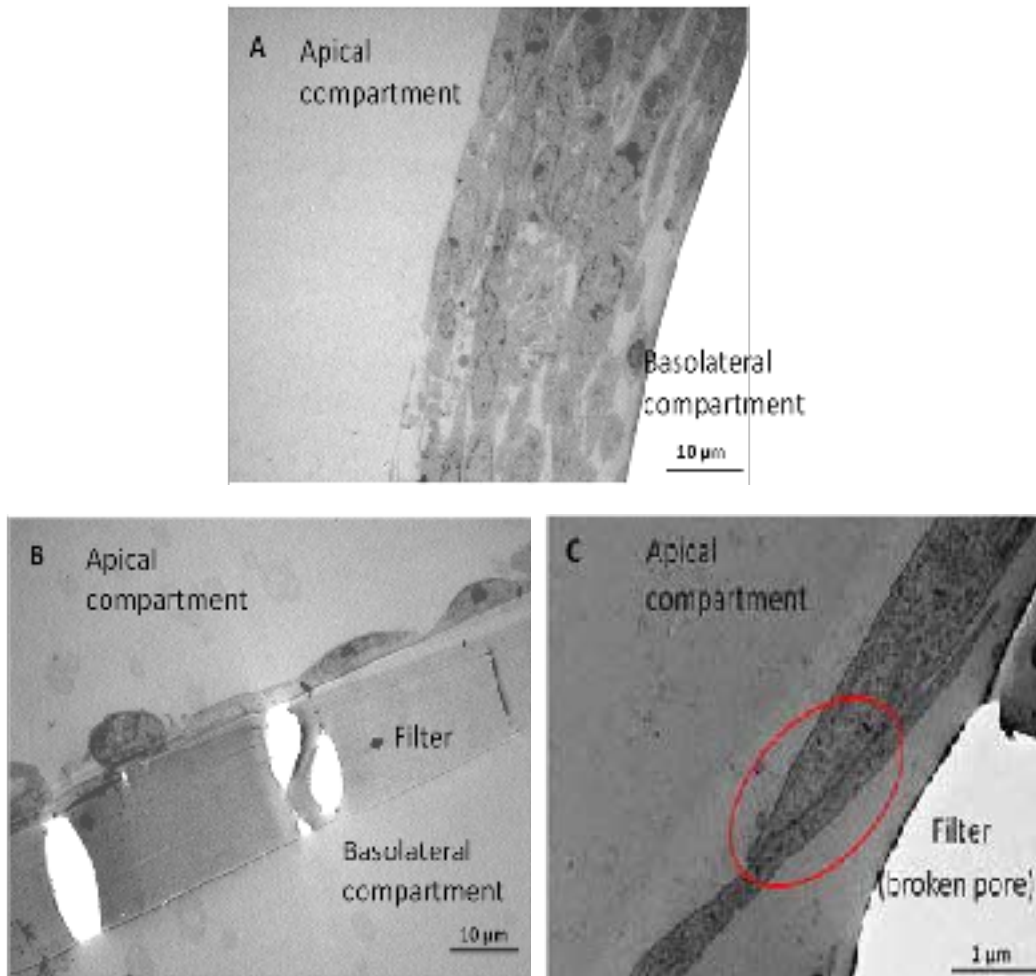


Figure 4.2. Transmission electron microscopy analysis of an *in vitro* blood–brain barrier model cultivated in different media. (A) hCMEC/D3 cells formed a multilayer after 7 days in the growth medium. Here, the transwell membrane detached from the barrier while the sample was being processed for electron microscopy. Scale bar indicates 10 µm. (B) The cells were differentiated to a monolayer after 7 days of growth in the assay medium. Scale bar indicates 10 µm. (C) An electron-dense area (red border) shows the tight junction formed between adjacent cells. Scale bar indicates 1 µm. In all three images, the cells were grown on a 0.4 µm collagen-fibronectin coated polyester transwell (Corning Costar 3460).

5 Validation of the Model in Terms of Structure and Function

Significant effort was put into devising and implementing a robust protocol for the establishment of the *in vitro* BBB model, and validating it via an internal benchmarking process to ensure that the protocol was robust and suitable for application to the study and screening of nanomaterials, as this has not been done previously. Using hCMEC/D3 cells (a gift from Florence Miller, B.B. Weksler, INSERM, France), this section details the optimisation and internal benchmarking validation of the *in vitro* human BBB model for screening of nanoparticle interactions and mechanism(s) of passage across the BBB.

The key steps in validating the BBB model are as follows:

- Confirmation of the formation of tight junctions, typically by measurement of the TEER, followed by TEM imaging to confirm that monolayers and tight junctions were formed, and later by staining of the key proteins present in the tight junctions (e.g. via staining of occludin).
- Assessment of the permeability properties and active transport via the BBB. Paracellular or transcellular permeabilities of fluorescein isothiocyanate labelled 4 kDa dextran (FD4) and apolipoprotein E (ApoE) were measured as controls.

In order to conduct the internal benchmarking validation, two teams, each consisting of one postdoctoral researcher and one postgraduate student researcher, were tasked with following an identical protocol for growth of the hCMEC/D3 cell line for 7 days according to the detailed protocol described in Appendix I. On day 7, the barrier integrity was determined by each team, by calculating the apparent permeability using FD4. Results were compared to the literature values for this cell line. Once it was clear that both teams could obtain the same barrier strength, significant additional work was performed, using TEM to confirm that monolayers and tight junctions were formed, and assessment of the passage of fluorescently labelled ApoE, as a positive control for receptor-mediated uptake was conducted.

Generally speaking, compound transport from the apical to the basolateral side of the model BBB can be considered to mimic intravenous injection and subsequent transport to the brain. Conversely, transport from the basolateral to the apical side could be used to evaluate the efflux mechanism from brain to bloodstream. It has been reported that drug-resistance proteins or adenosine-5'-triphosphate (ATP)-binding cassette transporters, such as P-glycoprotein, which are expressed on both the apical membrane and the luminal surface of BCECs, are able to limit the entry of drugs or toxic compounds from the blood to the brain and thus to pump out small hydrophobic molecules from the brain to the blood (Schinkel, 1999).

Fluorescein isothiocyanate-labelled-dextran (FITC-dextran, FD4) has been used as a paracellular transport marker to test tight junction quality in the hCMEC/D3 cell model, with reported published values acting as a valuable quality control reference for the model presented here. Consecutive fluxes of compounds through the BBB model can be detected as fluorescent or radioactive signals from fluorescently- or radio-labelled compounds. Apparent permeability measures the compound transport rate over the assay duration.

Another parameter introduced in the transport study is the apparent permeability index (P_{app}). This index was introduced as part of a screening process to study drug absorption in *in vitro* or *in vivo* experiments, and is widely used in *in vitro* Caco-2 model studies (Palumbo et al., 2008). The index is defined as the initial flux of compound through a membrane (normalised by membrane surface area and donor concentration) and is computed by adapting a straight line to the initial portion of recorded amounts in the transwell basolateral chamber. To calculate the BBB apparent permeability to FD4, an equation developed by Hubatsch et al. (2007) was used:

$$(Eq. 5.1) \quad P_{app} = \frac{dQ}{dt} \times \frac{1}{A \times C_0},$$

where dQ/dt is the steady state of FD4 flux curve (the

slope of the line as specified in the 'standard curve'), A is the surface area of the transwell (in cm^2), and C_0 is the initial concentration of FD4 (200 $\mu\text{g}/\text{ml}$).

5.1 Validation of Tight Junction Formation in the Blood–brain Barrier Model

Transendothelial electrical resistance (TEER) measurement, which is a standard technique to assess *in vitro* endothelial barriers, was used to examine the electrical resistance generated by the cell monolayer as a measurement of tight junction quality. During barrier growth, TEER values were recorded in a transwell by connecting the top and bottom chambers with two electrodes, and then the resistance was read from a

voltmeter. As seen in [Fig. 5.1A](#), the resistance in the *in vitro* BBB model was about 50 $\Omega \text{ cm}^2$ after 2 days, then it reached a plateau between 40 and 50 $\Omega \text{ cm}^2$. In addition, in [Fig. 5.1B](#), the BBB model showed similar TEER values to other hCMEC/D3 barrier models reported in the literature (Weksler et al., 2005; Forster et al., 2008).

Another measure of the 'tightness' of the BBB model can be determined as the apparent permeability based on the flux of a molecule of known MW across the barrier (from the apical to the basolateral chambers, as measured by the change in fluorescence). For simple molecules, the fluid flux is linearly proportional to the dose applied, with more substance transport being observed at higher apical doses. However, due to physical and/or chemical factors, nanoparticle interactions with living

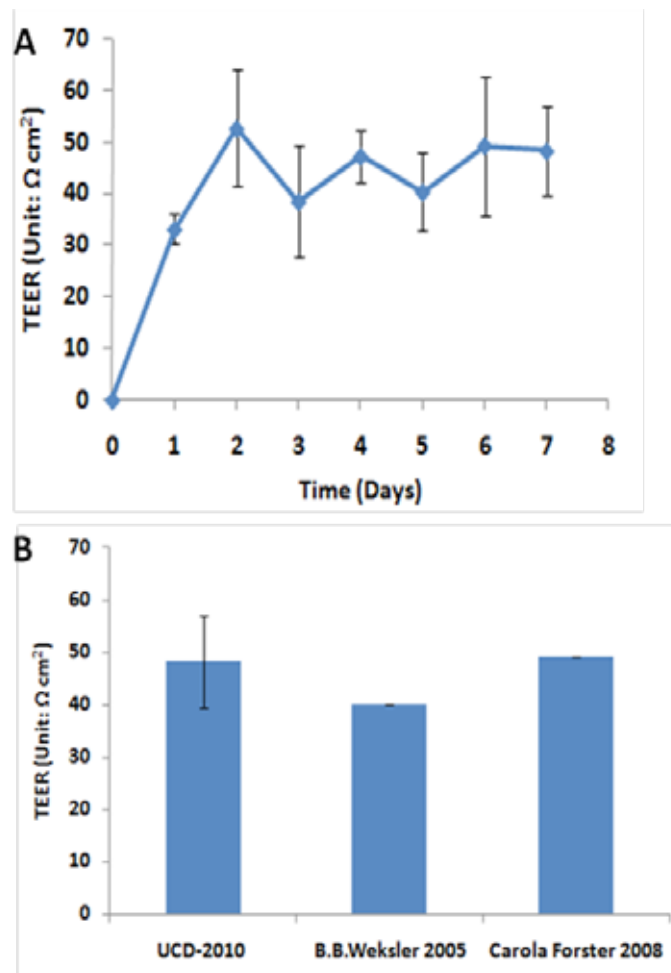


Figure 5.1. Transendothelial electrical resistance (TEER) of the blood–brain barrier (BBB) grown on 0.4 μm collagen-fibronectin coated polyester transwells in the assay medium over 7 days. (A) Consecutive resistance values of the BBB model were plotted over 7 days. (B) The barrier resistance on the 7th day of growth (UCD-2010) was compared with the reference values, reported by Weksler et al. (2005) and Forster et al. (2008). (Data represents mean of $n = 12 \pm$ standard deviation).

systems do not often follow this general rule, as in many cases nanoparticle agglomeration increases at higher particle concentrations, and large particle-aggregates are unable to transport across the BBB. Note, however, that *in vivo*, larger particles or particle-aggregates may be carried across the BBB in macrophages, and indeed this is the transport method utilised by many viruses.

To further validate the hCMEC/D3 BBB model, a paracellular permeability marker, FD4 was applied to the apical chamber, and the amount that transported to the basolateral chamber was determined in order to assess

the tight junction integrity of the hCMEC/D3 monolayer. As shown in Fig. 5.2A, approximately 6.2 µg FD4 was transported across the hCMEC/D3 monolayer to the basolateral chamber after 2 hours. That accounted for 6% of initial concentration of FD4 (0.5 ml 200 µg/ml FD4 at $T = 0$ minutes) applied to the apical chamber. Comparatively, in the blank transwell (with no cell monolayer present), 13% of the initial amount of FD4 accumulated in the basolateral chamber, which was significantly higher than the amount in the monolayer case, showing a significant barrier effect from the presence of the hCMEC/D3 cell monolayer.

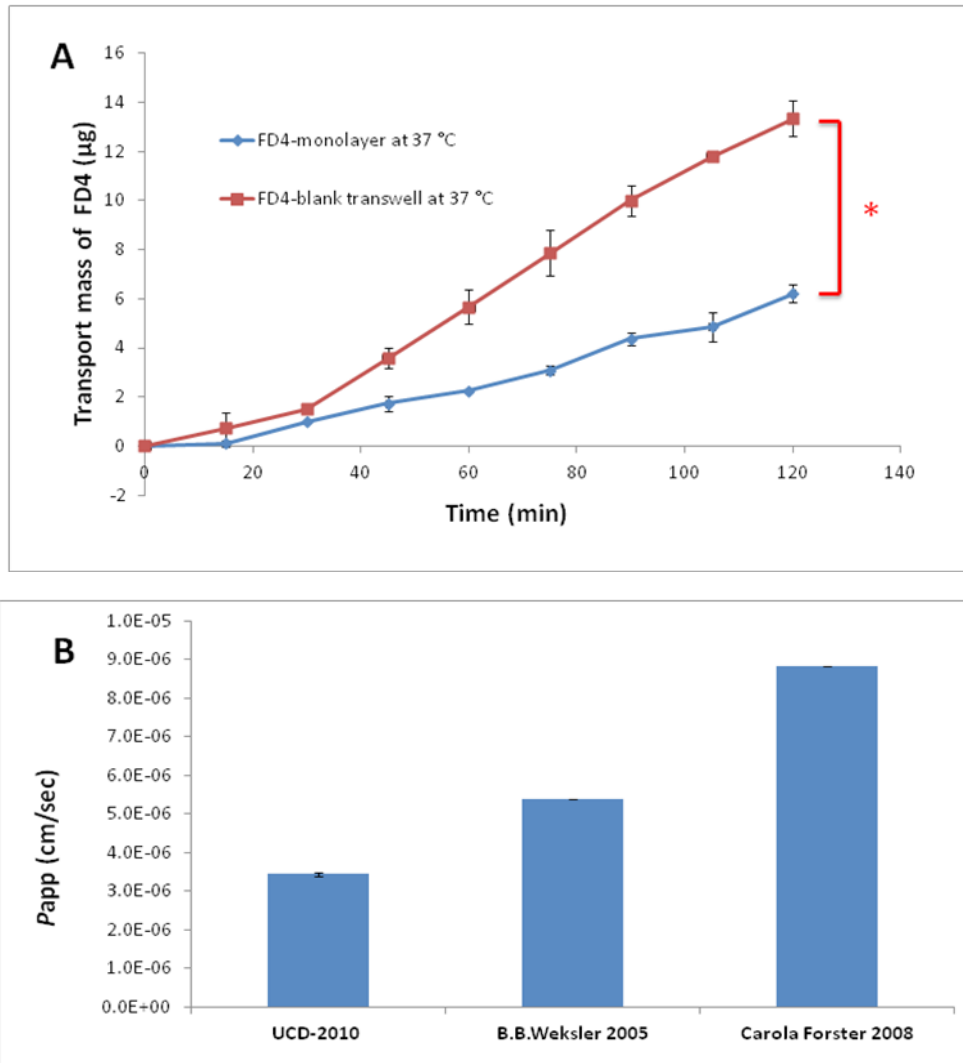


Figure 5.2. Transport of 4 kDa fluorescein isothiocyanate labelled dextrin (FD4) through hCMEC/D3 BBB monolayer on 0.4 µm collagen-fibronectin coated polyester transwells. (A) FD4 flux curves over 2 hours of transport across blank transwells and hCMEC/D3 monolayers. 'FD4-monolayer at 37°C' represents FD4 transport across the transwell with the blood-brain barrier (BBB) monolayer at 37°C; 'FD4-blank transwell at 37°C' represents FD4 transport through the blank transwells without the cell monolayer at 37°C. (B) Paracellular permeability (P_{app}) of the BBB to FD4 (UCD-2010) was compared with the reported values from Weksler et al. (2005) and Forster et al. (2008). (Data are mean values \pm standard deviation, $n = 12$. Student t -test, * indicates $p < 0.05$.)

To calculate the apparent permeability coefficient P_{app} of the hCMEC/D3 BBB model to FD4, Eq. 5.1 was used. Figure 5.2B shows that the permeability of the hCMEC/D3 monolayer BBB model was 3.45×10^{-6} cm/s, which was relatively lower than the reference values 5.40×10^{-6} cm/s of Weksler et al. (2005) and 8.60×10^{-6} cm/s of Forster et al. (2008). The comparison suggests that the barrier integrity obtained in this BBB model is tighter than those obtained previously.

Together, the FD4 transport study and the TEER measurements clarified that the hCMEC/D3 BBB model exerted high-quality tight junctions in culture conditions.

5.2 hCMEC/D3 Barrier Integrity Validation on Various Porous Transwells

In Section 5.1, the tightness of the BBB monolayer was studied with the FD4 assay on 0.4 μ m collagen-fibronectin coated PET transwells. In order to explore the barriers' growth compatibilities on the different transwell filter membranes and their coated growth substrates, cells were grown to form monolayers on two different transwell materials – polyester (PET) and polytetrafluoroethylene (PTFE) – then the FD4 transport assay was applied to test their individual permeability. This approach aimed to optimise the human endothelial cell model for nanoparticle application.

The hCMEC/D3 cell monolayers were formed on 0.4 μ m and 3 μ m porous transwells, and their individual barrier permeability was investigated with FD4. Before cell seeding, the PET transwells were coated with rat tail collagen I and fibronectin. PTFE transwells were pre-coated by the manufacturer with type I and type III collagen (Corning Costar). After 7 days, FD4 was applied to the transwells with or without the cell barrier. The transwell details and permeability values of the resultant BBB are given in Table 5.1.

Comparing transwells with same pore size, the results showed that the barrier permeability was three times lower on the 0.4 μ m PET transwell than on the 0.4 μ m PTFE transwell, as shown in Fig 5.3. Consistently, the barrier permeability using the 3.0 μ m PET membrane was a factor of two lower than the 3.0 μ m PTFE transwell, as shown in Fig. 5.4. The comparison indicated that PET membranes significantly improved the barrier tightness compared to PTFE membranes, probably due to either the different coating substrate or a preferable cell growth membrane. Additionally, for the same type of membrane, the 3.0 μ m PET transwell permeability to FD4 was double that of the FD4 permeability of the 0.4 μ m PET transwell in the presence of a monolayer. Moreover, no difference in barrier permeability was observed between the 0.4 μ m and 3.0 μ m PTFE transwells. In addition, all blank

Table 5.1. Details of various coated transwells and their barrier permeability to FD4.

Pore size (μ m)	Material of membrane	Type I collagen pre-coated	Extra growth substrate added before cell seeding	With or without cell layer on transwell	Apparent permeability to FD4 ($\times 10^{-6}$ cm/s)
0.4	PET	No	Rat tail collagen I and fibronectin	Cell layer	3.45 ± 0.04
0.4	PET	No	Rat tail collagen I and fibronectin	No cells	11.96 ± 0.74
3.0	PET	No	Rat tail collagen I and fibronectin	Cell layer	6.49 ± 1.41
3.0	PET	No	Rat tail collagen I and fibronectin	No cells	24.00 ± 2.36
0.4	PTFE	Yes	Pre-coated collagen	Cell layer	11.6 ± 2.58
0.4	PTFE	Yes	Pre-coated collagen	No cells	21.76 ± 7.23
3.0	PTFE	Yes	Pre-coated collagen	Cell layer	12.9 ± 1.31
3.0	PTFE	Yes	Pre-coated collagen	No cells	18.73 ± 6.22

transwells were relatively more permeable to FD4 than the transwells with the cell barrier. Permeability values for 0.4 μm and 3.0 μm blank PET transwells were always three times higher than the values for 0.4 μm and 3.0 μm PET transwells with the cell barrier. Similarly, permeability values on 0.4 μm and 3.0 μm blank PTFE transwells were almost double those found with the monolayer grown on the 0.4 μm and 3.0 μm transwells. The characterisation of the different barriers grown on the various membranes also included light microscopy imaging, as shown in [Figs 5.3](#) and [5.4](#).

For barrier morphology evaluation, light microscopy analysis was applied following the FD4 assay. As the images show, the monolayer was formed on 0.4 μm and 3.0 μm PET ([Fig. 5.3](#)) and PTFE transwells ([Fig. 5.4](#)). However, cell invasion was observed on the 3 μm PET

transwell, where a double layer of cells occurred on both sides of the transwell, suggesting an effect of the substrate coating procedure during barrier formation on the 3 μm porous membrane ([Fig. 5.3](#)).

These experiments showed that hCMEC/D3 cells tended to form tighter barriers on the 0.4 μm PET transwell coated with collagen and fibronectin. The 3 μm PET transwell were not able to support an hCMEC/D3 monolayer due to cell invasion through the pores, which meant that the barrier was not a polarised monolayer, explaining its higher permeability to FD4 relative to the 0.3 μm PET transwell. Additionally, both of the PTFE transwells had a relatively high permeability, although the hCMEC/D3 cells grew into an intact monolayer on these transwells.

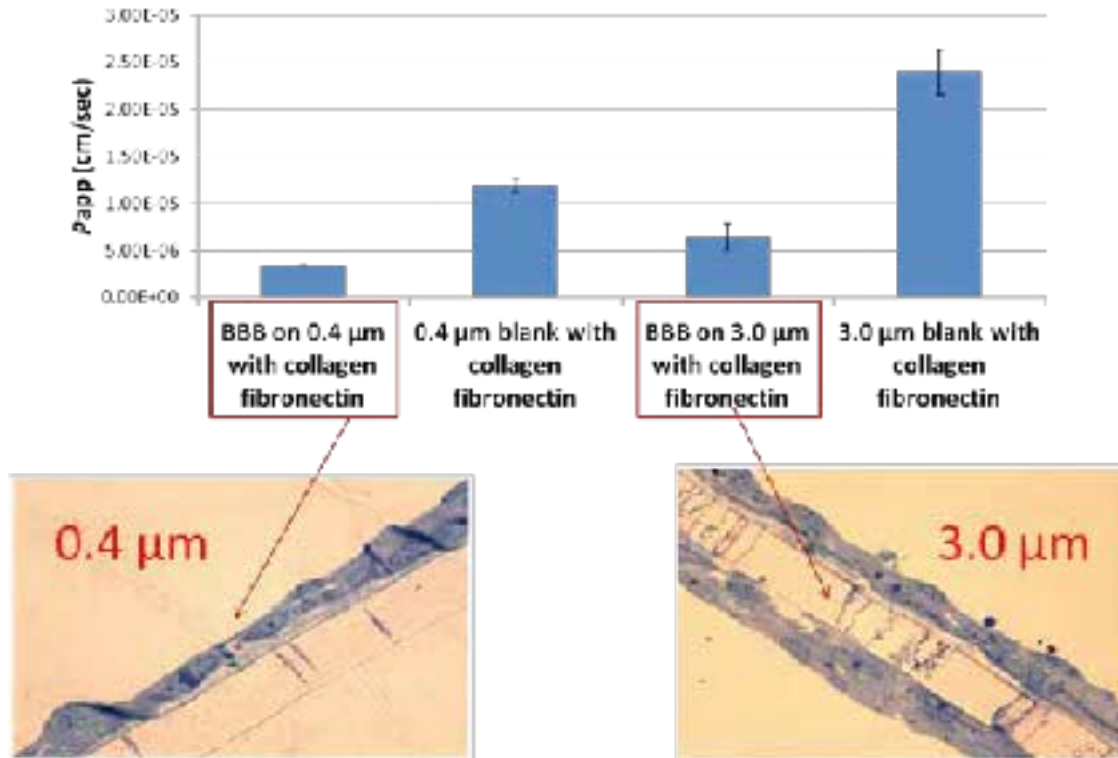


Figure 5.3. Paracellular permeability of the blood–brain barrier (BBB) monolayer to 4 kDa fluorescein isothiocyanate labelled dextrin (FD4) and the barrier morphologies on polyester (PET) transwells of different pore sizes. The BBB cells were grown on 0.4 μm and 3 μm type I rat tail collagen-fibronectin coated PET transwells (Corning Costar 3460 and 3462, respectively). BBB permeability values for FD4 were twice as high in the 3.0 μm PET transwells compared to the BBB permeability of the 0.4 μm PET transwells, which suggests some interaction with the pores of the filter.

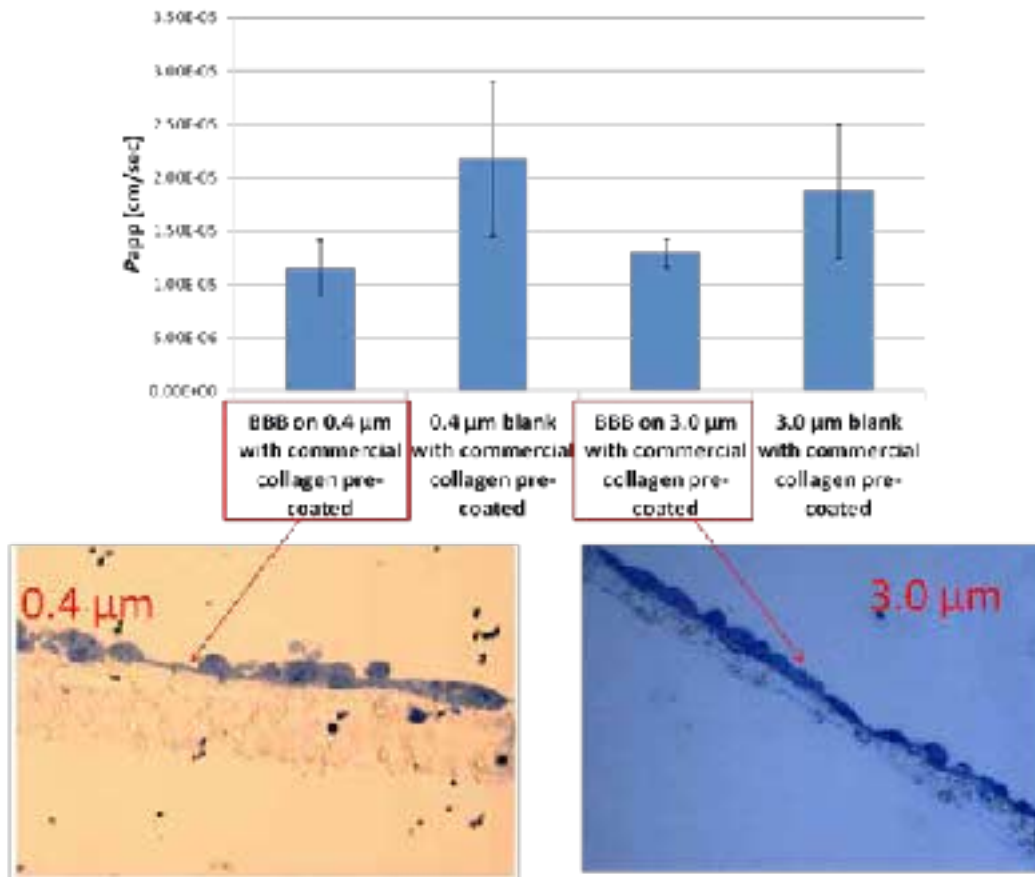


Figure 5.4. Paracellular permeability of the blood–brain barrier (BBB) monolayer to 4 kDa fluorescein isothiocyanate labelled dextrin (FD4 and the barrier morphologies on polytetrafluoroethylene (PTFE) transwells of different pore sizes. The BBB cell monolayer formed on 0.4 μm and 3 μm collagen I and III pre-coated PTFE transwells (Corning Costar 3493 and 3494, respectively). Similar BBB permeability values were found in both transwells. Blank transwells were used as negative controls to FD4 permeability of the BBB monolayer.

5.3 Internal Validation of the Apparent Permeability of the *In Vitro* Blood–brain Barrier Model – Paracellular Transport

The apparent permeability (P_{app}) of the model, grown on the collagen-fibronectin filters into a BBB, was determined as part of the internal benchmarking process, and the values obtained by the two teams were compared to those in the literature for FD4. FD4 is used as a marker for paracellular permeability of the endothelial monolayer and has been found

to be consistently low in this *in vitro* BBB model, due to the close contact of the hCMEC/D3 cells and their successful functioning as a barrier. The values are shown in Fig. 5.5, and the UCD values sit within the range of literature values. The data also show the robust nature of the barriers, as the spread of the values for the two internal UCD teams is small (indicated by the error bars) despite the barriers being prepared at different times and by the different teams.

An example of the time-resolved passage of FD4 through the blank filter and the hCMEC/D3 barrier is

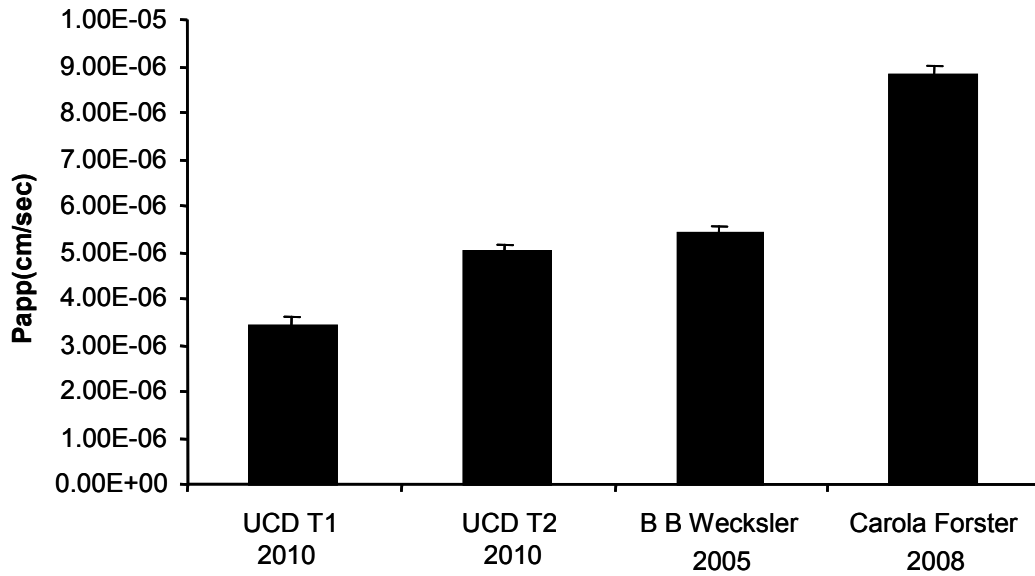


Figure 5.5. Comparison of the apparent permeability (P_{app}) values of the two teams in the mini-Round Robin (RR) with the literature values for fluorescein isothiocyanate labelled dextrin (FD4). Each of the UCD values is the mean of 12 replicates, and the standard deviation is shown, indicating the degree of reproducibility of the barriers (Nic Raghnaill et al., 2011). Excellent reproducibility between the two teams is observed, indicating the robustness of the protocol.

shown in Fig. 5.6. The 'blank' refers to the transport of FD4 through the filter alone, with no cellular barrier grown on top. It is clear that the small pore size of the filter (0.4 μm) exerts a significant barrier effect in the hCMEC/D3 monolayer itself, even for the small FD4 molecules, as initially 100 μg of FD4 was applied to the apical side of the transwell, and an average of 14 μg of FD4 passed through the filter after 2 hours. It is also clear that paracellular transport is significantly reduced in the presence of the hCMEC/D3 monolayer, as approximately 2.5 μg of FD4 was found to bypass the hCMEC/D3 cells after 2 hours of exposure.

Quantification of the TEER by this *in vitro* BBB model was carried out as an additional method to evaluate monolayer integrity. As shown in Fig. 5.7, both teams found TEER values of approximately 40 Ω by the seventh day of monolayer formation, which is very similar to the published values.

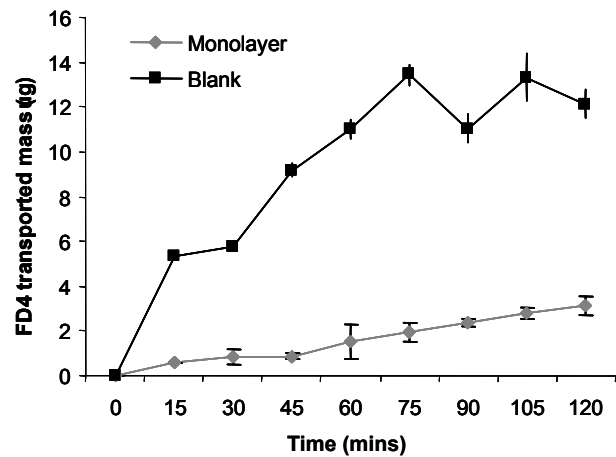


Figure 5.6. Transport of FD4 through the *in vitro* BBB model (blank filter and filter with cell monolayer) as a function of time. An increased flux of fluorescein isothiocyanate labelled dextrin (FD4) was found through the blank filter membrane compared to the monolayer over 2 hours.

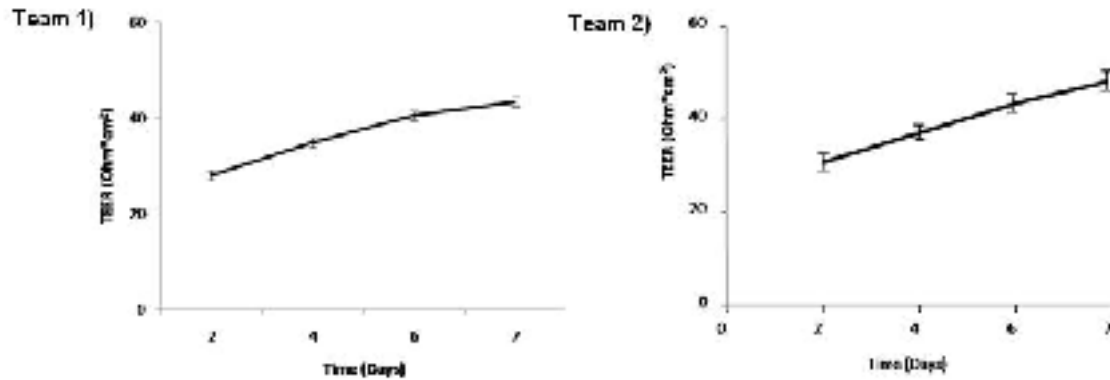


Figure 5.7. Transendothelial electrical resistance (TEER) values of the *in vitro* blood–brain barrier (BBB) during the 7 days of monolayer growth as reported during the internal benchmarking process. Teams 1 and 2 (see parts A and B, respectively) reported similar TEER values over the BBB culture period, increasing to approximately 40 Ω . Two-way ANOVA showed no significant difference between the two teams' TEER measurements over time.

5.4 Internal Validation of the Apparent Permeability of the *In Vitro* Blood–brain Barrier Model – Transcellular Transport

Despite being designed to keep foreign entities out, there are many transport pathways that are specifically designed to transport essential nutrients (including proteins and lipids) across the BBB, as was shown schematically in Fig. 1.2. Apolipoprotein E (ApoE) was chosen as a positive control for transcellular transport (pathway d in Fig. 1.2) across the BBB *in vitro* model,

as it is known to access the brain through a receptor-mediated mechanism, and has been shown to enhance the uptake of drugs and nanoparticles into the brain *in vivo* (Michaelis et al., 2006). The transported mass of ApoE across the BBB model was assessed, and the values are shown in Fig. 5.8. These studies confirm that the hCMEC/D3 BBB *in vitro* barrier model that was established is capable of the transcytosis of ApoE in a quantitatively reproducible manner, as similar amounts of ApoE transport were found by both teams.

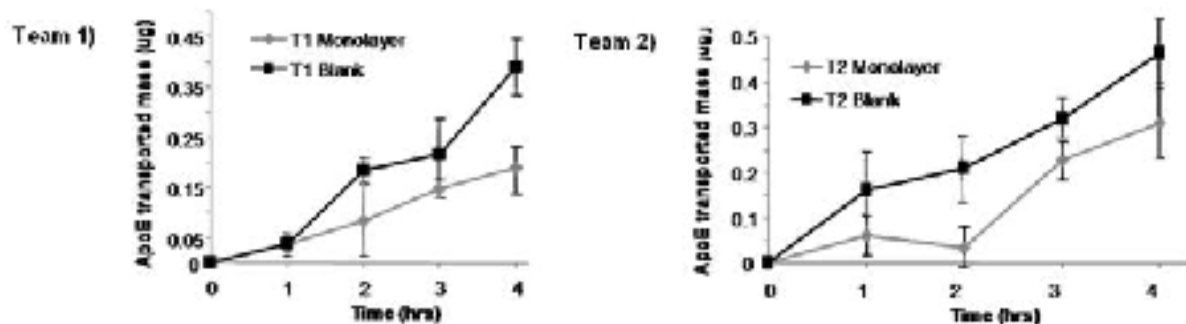


Figure 5.8. Comparison of apolipoprotein E (ApoE) transport through the *in vitro* blood–brain barrier during the internal benchmarking study. The transport of ApoE was found to be reproducible through both the monolayer and the blank filter membrane. (Data are mean \pm standard deviation, $3 \leq n \leq 6$. Two-way ANOVA showed no significant differences of ApoE transport in the two teams for either monolayer or blank values over time.)

6 Initial Screening of a Range of Nanoparticles for Passage through the Model Blood–brain Barrier

An important element to control in terms of assessing the capacity of nanomaterials to cross the *in vitro* BBB barrier is to assess the interaction of the transwell membranes with the various candidate nanomaterials in the absence of a cellular layer, as due to their large surface area nanoparticles are considered ‘sticky’ and may potentially interact with the membranes, which would confound the assessment of their apparent permeability through the *in vitro* BBB model. Part of this assessment included assessing the effect of the nanoparticle protein corona on the equilibration of the particles between the apical and basolateral chambers.

6.1 Nanoparticle Equilibration in Different Types of Transwells

In order to screen the appropriate transwells for nanoparticle application and to test the equilibration capability of different sizes of nanoparticles, several commercially available transwells were tested with three sizes of carboxylate modified polystyrene (PS-COOH) nanoparticles and three sizes of non-modified SiO₂ nanoparticles in a 24-hour equilibration study.

Forty nm, 100 nm, 200 nm PS-COOH and 50 nm, 100 nm, 200 nm SiO₂ nanoparticles were individually dispersed within the assay medium. Nanoparticles were subsequently applied to the top (apical) chamber of the transwell and were equilibrated at 37°C at 100 revolutions per minute (rpm) over 24 hours. Nanoparticle distribution throughout a transwell could be determined using the fluorescence dyes that are covalently bound to the nanoparticles, and determining the fluorescence

distribution between the two chambers and within the filter itself. Ideally, nanoparticles were expected to reach equilibrium with the same concentration in each of the two transwell compartments, with no nanoparticles remaining in the filters. Thus, by measuring the fluorescence intensity from both chambers of the transwell, it was possible to assess if the equilibrium could be achieved, and if the transwell permeability properties were suitable for the nanoparticle study. This was also used to determine the candidate nanoparticles for detailed mechanistic studies of the passage of nanoparticles through the *in vitro* BBB model.

[Figures 6.1](#) and [6.2](#) show representative data from the assessment of the equilibration of the polystyrene and silica nanoparticles of various sizes through transwell filters of two different pore sizes (0.4 µm or 3 µm) with different compositions of the membrane filter. The characteristics of the five types of transwells that were screened are presented in [Table 6.1](#).

Results showed that all sizes of PS-COOH nanoparticles (40 nm, 100 nm, 200 nm) did not equilibrate in any of the porous transwells at 37°C over 24 hours, meaning that the presence of the membrane itself interfered with the passage of the polystyrene nanoparticles through to the basolateral chamber, possibly as a consequence of electrostatic repulsion resulting from the negative charge on these particles from the carboxylic acid surface functionality. [Figures 6.1](#) and [6.2](#) indicate that most of the PS-COOH nanoparticles stayed in the apical compartment and could not go through the pores, even in the case of the 3 µm pore size, which was much

Table 6.1. Characteristics of transwell membranes.

	Polyester (PET)	Polycarbonate	Polytetrafluoroethylene (PTFE)
Pore sizes	0.4 µm, 3.0 µm (Corning Costar & Becton Dickinson)	3.0 µm	0.4 µm
Optical properties	Clear	Not clear	Clear when wet
Cell visibility	Good	Poor	Cell outlines
Membrane thickness	10 µm (parameter unavailable for Becton Dickinson 3 µm)	10 µm	30 µm
Collagen coated	No	No	Yes

bigger than the PS-COOH particles' nominal diameters. A possible explanation was that polystyrene particles were trapped in the pores of the filter membrane and gradually accumulated and blocked the pores over 24 hours, preventing nanoparticle passage.

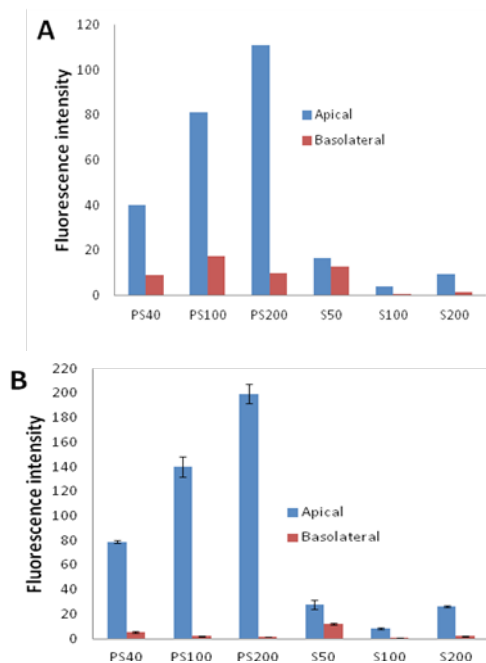


Figure 6.1. The 24-hour equilibration of nanoparticles through 0.4 μm blank transwells. (A) Equilibration study of yellow-green fluorophore labelled carboxylate modified polystyrene (PS-COOH) nanoparticles and yellow-green fluorophore labelled non-modified SiO_2 nanoparticles in 0.4 μm collagen pre-coated polytetrafluoroethylene (PTFE) transwells (Corning Costar 3493). (B) PS-COOH and SiO_2 non-modified nanoparticles equilibration study in 0.4 μm polyester (PET) transwells (Corning Costar 3460). PS40, PS100 and PS200 were 40 nm, 100 nm and 200 nm PS-COOH nanoparticles, respectively. S50, S100 and S200 were 50 nm, 100 nm and 200 nm SiO_2 nanoparticles, respectively. Blue (apical) represents the fluorescence intensity of the nanoparticles remaining in the apical chamber of the transwell after 24 hours; red (basolateral) represents the fluorescence intensity of the nanoparticles accumulated in the basolateral chamber of the transwell after 24 hours.

In the case of the SiO_2 nanoparticles (also shown in [Figs 6.1](#) and [6.2](#)), generally all of the 3 μm membranes were more permeable than the 0.4 μm membranes to these nanoparticles. In the three types of 3 μm transwells, 50 nm, 100 nm and 200 nm SiO_2 nanoparticles reached a balance of fluorescence intensity between the apical and basolateral chambers that indicated an equal concentration of nanoparticles in both compartments ([Fig. 6.2](#)). In addition, compared to 100 nm and 200 nm SiO_2 nanoparticles in 0.4 μm PTFE and PET transwells ([Fig. 6.1](#)) only 50 nm SiO_2 nanoparticles achieved equilibrium. In contrast, 100 nm and 200 nm SiO_2 nanoparticles showed very little capability to equilibrate across the two types of transwells tested.

Thus, it was concluded that PS-COOH nanoparticles were not suitable to be applied to the 0.4 μm or 3.0 μm transwells due to their low equilibration, possibly due to interaction with the membranes. However, SiO_2 nanoparticles were capable of diffusing through both the 0.4 μm and 3 μm transwells, therefore they were better candidates to be used in the BBB model. These particles were chosen for the detailed assessment of the mechanism by which nanoparticles interact with and pass through the *in vitro* BBB model (see Section 8).

6.2 Nanoparticle Adherence to Transwell Membranes

To clearly understand why the polystyrene nanoparticles did not diffuse well from one chamber to the other, and to prove the previous assumption that nanoparticles were trapped within the transwell membranes, transmission electron microscopy was used to study the location of nanoparticles within the transwell membranes, and to assess the potential adherence of the PS-COOH nanoparticles to the transwell membrane pores.

In [Fig. 6.3A](#), a 0.4 μm PET membrane was visualised using electron microscopy, and the two membrane pores shown were magnified to show additional details as shown in [Figs 6.3B](#) and [6.3C](#), illustrating that very few 50 nm SiO_2 nanoparticles were observed in the pores of PET membranes.

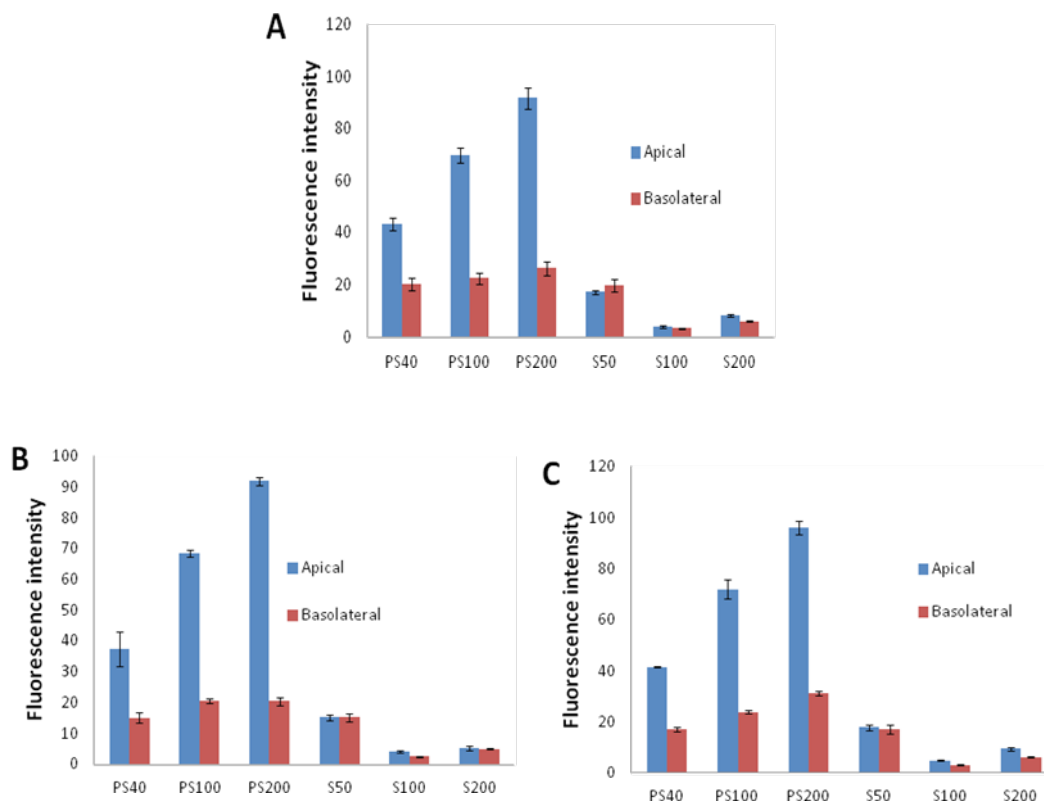


Figure 6.2. 24-hour nanoparticle equilibration study through 3 µm blank transwells. (A) Carboxylate modified polystyrene (PS-COOH) and non-modified SiO₂ nanoparticles equilibration study in 3 µm polyester (PET) transwells (Corning Costar 3462). (B) PS-COOH and non-modified SiO₂ nanoparticles equilibration across 3 µm polyester transwells (Becton Dickinson 353181). (C) PS-COOH and non-modified SiO₂ nanoparticles equilibration across 3 µm polycarbonate transwells (Corning Costar 3402). PS40, PS100 and PS200 represent 40 nm, 100 nm and 200 nm PS-COOH nanoparticles, respectively; S50, S100 and S200 represent 50 nm, 100 nm and 200 nm SiO₂ nanoparticles, respectively. Blue (apical) represents the fluorescence of the nanoparticles remaining in the apical chamber of the transwell after 24 hours; red (basolateral) represents the fluorescence accumulating in the basolateral chamber of the transwell after 24 hours.

In [Fig. 6.4A](#), a 0.4 µm PTFE membrane was sectioned after epoxy resin embedding and the membrane section was observed using electron microscopy. The PTFE membrane showed a different texture that was much more porous and permeable than the PET membrane. The pores were expanded so severely that some pore sizes visually far exceeded the transwell's nominal pore size (0.4 µm). In [Fig. 6.4B](#), at higher magnification, aggregated SiO₂ nanoparticles were

found surrounding pores, showing a large amount of adherence between pores and SiO₂ nanoparticles. The trapped nanoparticles were mostly adhering to the pores in the upper area of the membrane. The lower area of the PTFE membrane was very clean, without many nanoparticles accumulating, suggesting an inability of the nanoparticles to penetrate through the membrane.

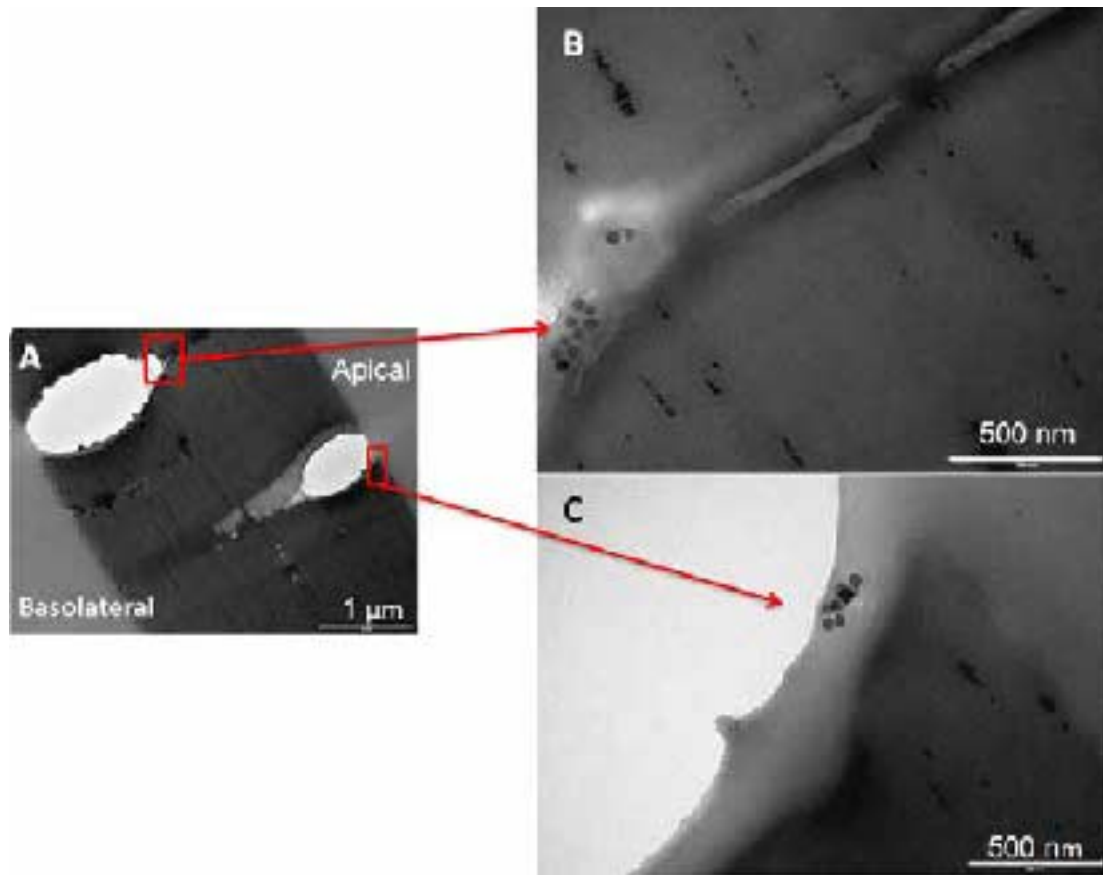


Figure 6.3. 50 nm SiO₂ adherence to a 0.4 µm polyester (PET) transwell (Corning Costar 3460). (A) Overview of a PET membrane using electron microscopy; scale bar represents 5 µm. (B, C) Magnified images of two separate pores showing nanoparticles within the membrane pores from image A; both scale bars represent 500 nm.

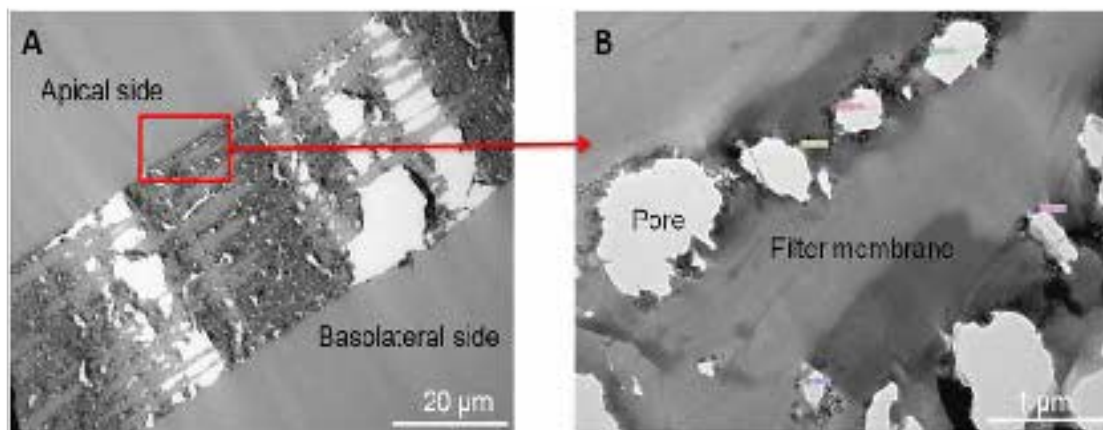


Figure 6.4. 50 nm SiO₂ nanoparticles adherence to a 0.4 µm collagen pre-coated polytetrafluoroethylene (PTFE) transwell (Corning Costar 3493). (A) Overview of PTFE membranes under electron microscopy; scale bar represents 20 µm. (B) At high magnification, the 50 nm SiO₂ nanoparticles were seen adhering to the membrane pores in the upper area of the membrane; scale bar represents 1 µm.

In addition, the 3 μm PTFE membrane, whose pore size (Fig. 6.5A), which was significantly bigger than the 50 nm SiO_2 nanoparticles, showed nanoparticle adherence as well. As shown in Fig. 6.5B, a large amount of nanoparticles accumulated in the pore vicinity. In Fig. 6.5A, the pores of PTFE membranes expanded due to electron beam exposure and damage. It is unknown why SiO_2 nanoparticles adhered to pores in 0.4 μm or 3 μm PTFE transwells; possible explanations could be either physical absorption between the PTFE material and SiO_2 nanoparticles, or the tortuous paths of the PTFE membrane pores that led to nanoparticle accumulation.

According to the manufacturer, the pore density of the 0.4 μm PET membrane is 4×10^6 pores/ cm^2 , but the PTFE membrane does not have a defined pore density due to its tortuous path, thus their permeability properties cannot be compared directly. It was observed using electron microscopy that the PET membrane was less porous than the PTFE membrane, suggesting higher permeability properties for the PTFE membrane; however, the severe nanoparticle deposit found in the 0.4 μm and 3.0 μm PTFE membranes limits application of these types of membrane for the study of nanoparticles in the BBB model. Thus, the 0.4 μm PET membrane is the more acceptable option for this study.

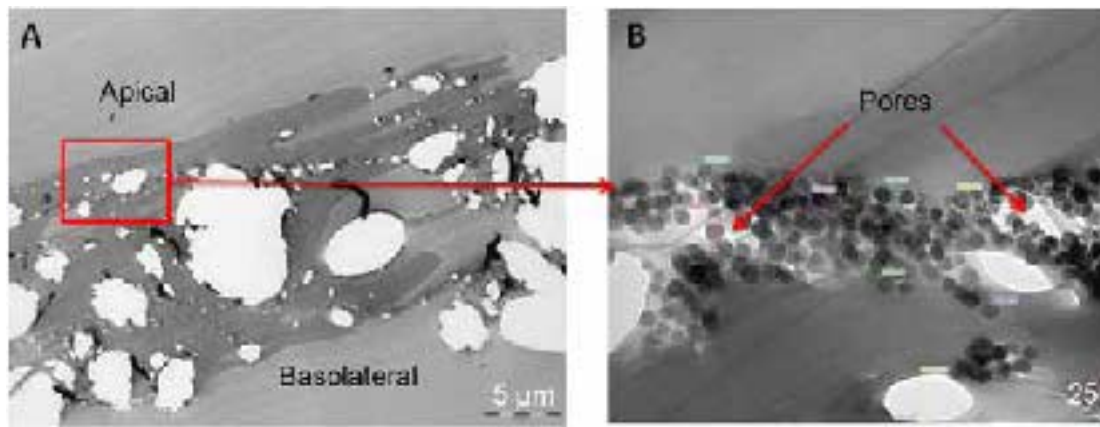


Figure 6.5. Adherence of 50 nm SiO_2 nanoparticles to a 3 μm collagen pre-coated polytetrafluoroethylene (PTFE) transwell (Corning Costar 3494). (A) Overview of the PTFE membrane by electron microscopy; scale bar represents 5 μm . (B) Nanoparticles covering the membrane pores, leading to pore blockage and restricted passage of nanoparticles; scale bar represents 250 nm.

7 Selection of the Nanoparticles to be used for Deeper Studies

Prior to all studies of nanoparticle interaction with cells, it is essential to characterise the nanoparticle dispersion under the conditions in which they will be presented to the cells – i.e. in the assay medium, and for the duration of the exposure. This is necessary in order to understand the dose of nanoparticles that is being presented to cells, as significant agglomeration of the nanoparticles in the assay media would reduce the available nanoparticle dose, and if the samples are not prepared in an identical manner for each experiment, the resultant dose could be completely different from experiment to experiment.

7.1 Characterisation of the Selected Nanoparticles in the Assay Medium

Nanoparticles display different dispersion properties in different dispersing agents. Because using an assay medium to sustain barrier viability during the transport studies, is inevitable when nanoparticles are applied in a transport study, it was necessary to evaluate the SiO₂ nanoparticles' dispersion properties in the assay medium. Dynamic light scattering (DLS) was used to measure the hydrodynamic sizes of all SiO₂ nanoparticles in water and in the assay medium (which contains 3% foetal calf serum, and thus will result in the formation of a protein corona around the nanoparticles that changes their surface presentation to cells) (Lynch et al., 2009; Walczyk et al., 2010). The diameter measured in DLS is a value that refers to how a particle diffuses within a fluid, so it is referred to as a 'hydrodynamic diameter'. According to the manufacturer of the SiO₂ nanoparticles used in this study (Kisker-Biotech), the particle sizes were nominally 50 nm, 100 nm and 200 nm.

As dispersed in de-ionised water at 37°C (Table 7.1), the SiO₂ hydrodynamic diameters were close to the values provided by the manufacturer, and the particles were monodisperse but there was some deviation of the average size from that indicated by the manufacturer. Polydispersity index (PDI) values are also indicated in Table 7.1. The PDI is a measure of the distribution of molecular mass in a polymer sample and usually has a value equal to or greater than 1. In DLS, a lower PDI value close to zero usually indicates that the compound is monodispersed. As seen in the Table 7.1, all three sizes of SiO₂ nanoparticles showed a PDI value lower than 0.1 in de-ionised water.

Once the 50 nm, 100 nm and 200 nm SiO₂ nanoparticles were dispersed in the assay medium (Table 7.2), they showed a rapid size increase after one hour of incubation at 37°C and at 4°C. As shown in Table 7.2, the size of 50 nm SiO₂ in the assay medium remained stable at ~220 nm over 4 hours of incubation at 37°C, nearly four times the size in water (Table 7.1). At 4°C the hydrodynamic size of 50 nm SiO₂ was mostly steady over 4 hours between 250 nm and 300 nm, close to the sizes at 37°C. In addition, 100 nm and 200 nm SiO₂ nanoparticles at 37°C remained in the ranges ~280 nm and ~400 nm, respectively, over 4 hours in the assay medium, and the apparent sizes were much bigger than their individual sizes in water (95 nm and 167 nm; Table 7.1). Also, at 4°C, the sizes of 100 nm and 200 nm SiO₂ nanoparticles increased to >400 nm and >550 nm, respectively, and at 37°C over 4 hours they far exceeded the limit of the pore size of 0.4 µm PET transwells, indicating that little transport would be expected.

Table 7.1. Average sizes (Z-ave) of SiO₂ nanoparticles in de-ionised water.

SiO ₂ nanoparticles	Temperature (°C)	Z-ave (diameter, nm)	Standard deviation	PDI
50 nm	37	61	± 1.2	0.03
100 nm	37	95	± 2.1	0.074
200 nm	37	167	± 1.0	0.007

Table 7.2. Average sizes (Z-ave) of SiO₂ nanoparticles at the indicated temperatures and incubation times in the assay medium (S.D. indicates standard deviation).

SiO ₂ nanoparticles	Incubation (°C)	1 hour			2 hours			3 hours			4 hours		
		Z-ave (nm)	S.D.	PDI	Z-ave (nm)	S.D.	PDI	Z-ave (nm)	S.D.	PDI	Z-ave (nm)	S.D.	PDI
50 nm	37	227	± 11	0.49	238	± 15	0.50	247	± 11	0.50	258	± 15	0.51
100 nm	37	275	± 16	0.50	282	± 11	0.48	293	± 16	0.45	290	± 9	0.49
200 nm	37	462	± 9	0.34	423	± 11	0.32	414	± 10	0.31	393	± 13	0.32
50 nm	4	256	± 3	0.267	442	± 11	0.49	305	± 12	0.37	295	± 5	0.28
100 nm	4	422	± 37	0.492	437	± 20	0.53	416	± 41	0.53	433	± 35	0.46
200 nm	4	583	± 27	0.433	600	± 61	0.44	670	± 40	0.44	550	± 43	0.34

In order to further illustrate the evolution of the particle size under the exposure conditions and over the time course of the transport assay, [Fig. 7.1](#) shows the size distribution of the 50 nm SiO₂ nanoparticles in the transport assay medium over the time course of the transport experiments (4 hours), determined using DLS. The data in [Table 7.3](#) also highlight a key limitation of the DLS technique: it gives a mean value, which is

actually physically quite meaningless in the presence of multiple peaks such as are observed here. However, for the purpose of the transport assays here, the data show that after the initial decrease of the mean particle peak, the size distribution remains relatively constant over the 4 hours of the experiment, suggesting that the available nanoparticle dose remains relatively constant throughout the assay.

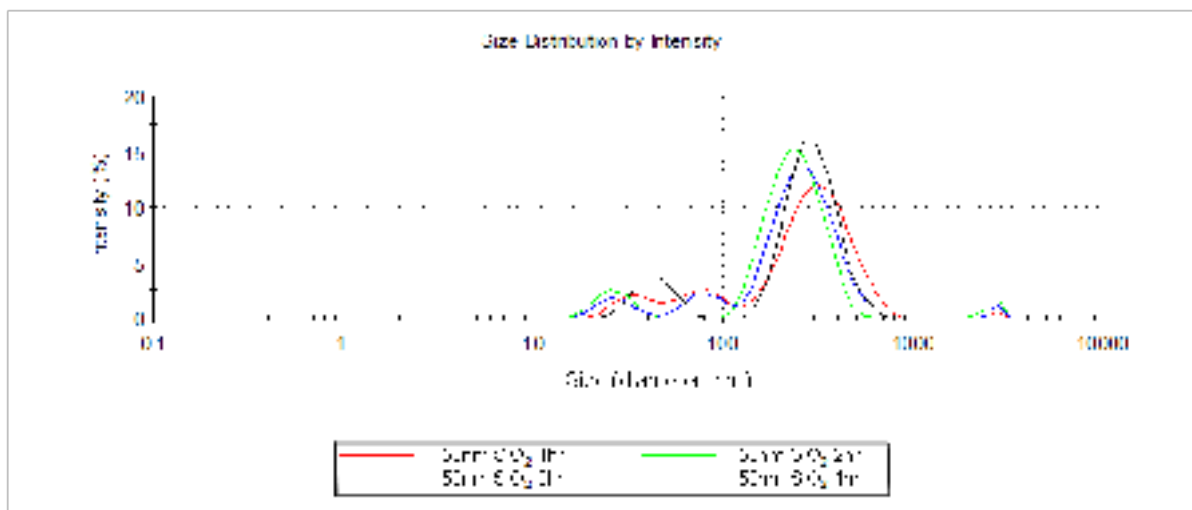


Figure 7.1. Dynamic light scattering plots of the size distribution of nominally 50 nm SiO₂ nanoparticles dispersed in the transport assay medium at 1-hour increments following the preparation of the initial dispersion.

Table 7.3. Detailed description of the average size (Z-ave) of the nominally 50 nm SiO₂ nanoparticles dispersed in the transport assay medium, at 1-hour increments following the preparation of the initial dispersion. Some agglomeration and polydispersity of the 50 nm SiO₂ nanoparticles was found on incubation in the assay medium at 37°C over 4 hours. This was attributed to the interaction of the 50 nm SiO₂ nanoparticles with proteins within the assay medium, which changes the surface charge and thus the electrostatic stabilisation of the nanoparticles.

Sample time (h)	Z-ave (nm)	Peak 1 (nm)	Peak intensity (%)	PDI	Peak width (nm)
1	175.	334.4	77.9	0.632	123.0
2	185.1	247.4	88.0	0.576	77.12
3	189.6	279.9	83.4	0.569	99.38
4	201.7	304.0	84.4	0.623	91.91

From the measurements in [Table 7.2](#), it is clear that all three sizes of SiO₂ nanoparticles were aggregated in the assay medium at both 37°C and 4°C, and their PDI values were above 0.3 in all cases, which was nearly three times higher than the PDI values in water ([Table 7.1](#)). However, although the 50 nm SiO₂ nanoparticles underwent agglomeration in the assay medium that far exceeded the hydrodynamic size in de-ionised water, the final size (~270 nm) of the 50 nm SiO₂ nanoparticles was still smaller than the pore size of the 0.4 µm PET transwell, and therefore the 50 nm SiO₂ nanoparticles were further investigated to determine the mechanism of transport through the BBB.

7.2 Pre-incubation of the Nanoparticles in the Assay Medium – Effect of the Protein Corona on Particle Stability

The stability of 50 nm and 200 nm SiO₂ nanoparticles as a function of time was assessed in an effort to improve the quality of the dispersions being presented to the BBB model. The aim of this experiment was to decrease the particle aggregation in the BBB assay medium (which contains 3% foetal calf serum). The 50 nm or 200 nm SiO₂ nanoparticles were pre-incubated in 55% foetal bovine serum (FBS) for 1 hour in order to form the nanoparticle protein corona, and were then either centrifuged once

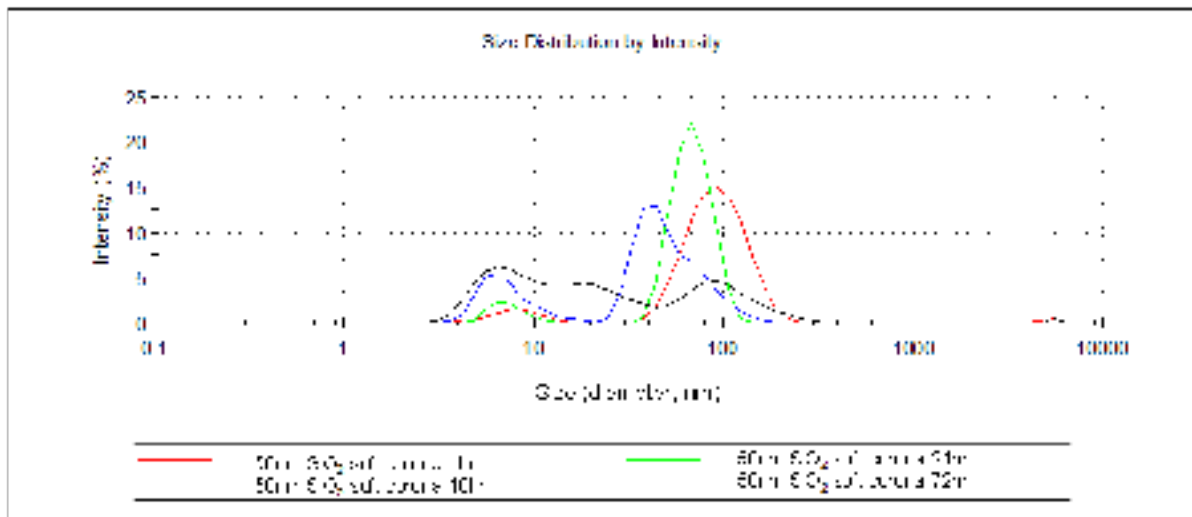


Figure 7.2. Dynamic light scattering data for 50 nm SiO₂ nanoparticles over 72 hours post formation of the nanoparticle soft corona (incubation of particles in 55% foetal bovine serum (FBS) for 1 hour followed by centrifugation and re-suspension in the blood–brain barrier transport assay medium to form the soft corona). Note that the peak at <10nm is due to the presence of protein clusters in the medium.

and re-suspended in the BBB transport assay medium (3% FBS) to form the soft corona (Figs 7.2 and 7.3 for the 50 nm and 200 nm SiO₂ nanoparticles, respectively), or centrifuged and washed three times to form the hard corona (Figs 7.3 and 7.4 for the 50 nm and 200 nm SiO₂ nanoparticles, respectively), before being re-suspended in the assay medium. Samples were then analysed with DLS from 1 to 72 hours to monitor the change in the dispersion quality over the time, both to determine the optimal preparation time for the particle dispersion prior to introduction to the apical chamber, and as preparation

for the longer-term exposure studies that are planned. Note that the 4-hour exposure experiments shown in this report were due to an experimental limitation in the set-up, whereby the exposure assay was performed without the cells being maintained under a 5% CO₂ atmosphere, which meant that the monolayer decayed beyond 4 hours. This limitation has recently been overcome by establishing the assays inside a cell culture incubator under a 5% CO₂ atmosphere, allowing us to study nanoparticle transport over longer times (e.g. up to 72 hours).

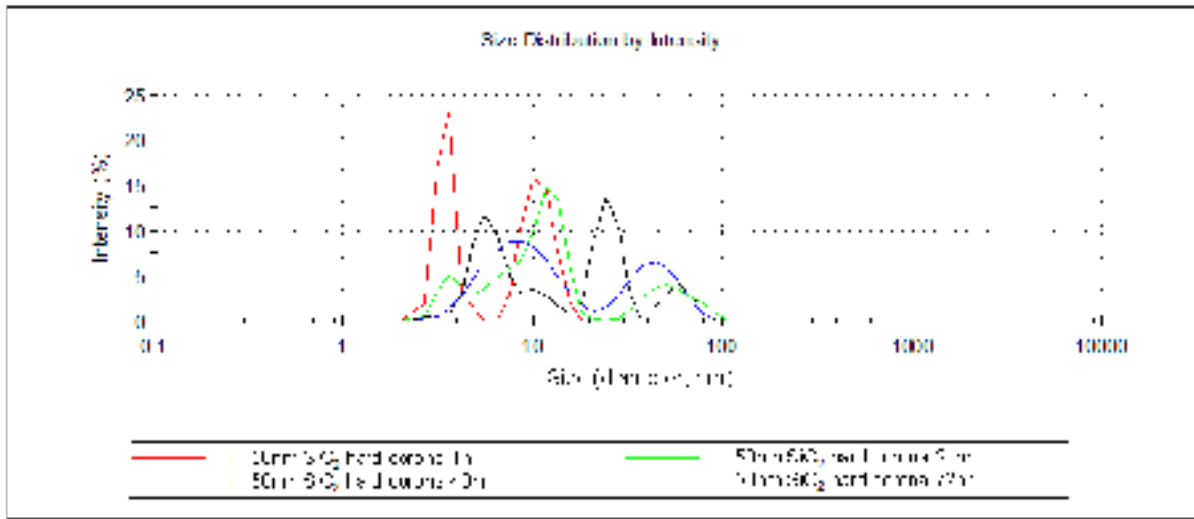


Figure 7.3. Dynamic light scattering data for 50 nm SiO₂ nanoparticles over 72 hours post formation of hard corona (incubation of particles in 55% foetal bovine serum [FBS] for 1 hour followed by centrifugation and three washes to form the hard corona before being re-suspended in the assay medium).

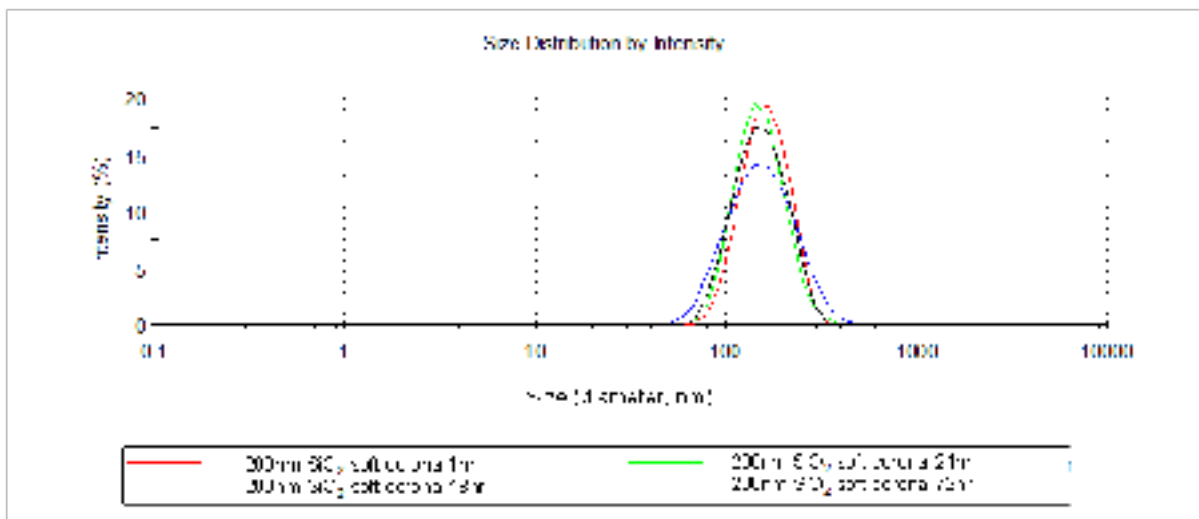


Figure 7.4. Dynamic light scattering data for 200 nm SiO₂ nanoparticles over 72 hours post formation of the nanoparticle soft corona (incubation of particles in 55% foetal bovine serum (FBS) for 1 hour followed by centrifugation and re-suspension in the blood–brain barrier transport assay medium to form the soft corona).

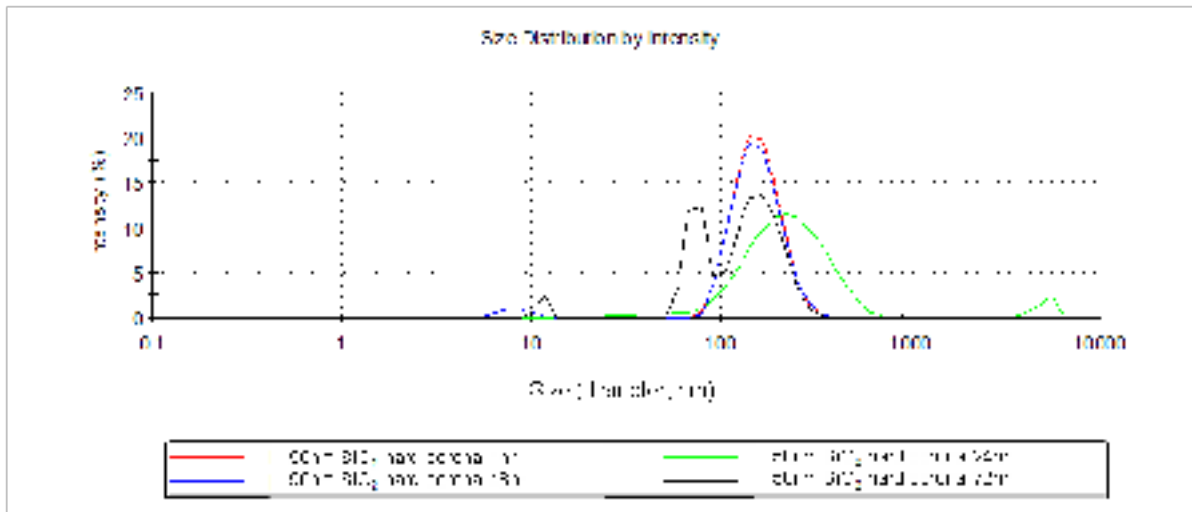


Figure 7.5. Dynamic light scattering data for 200 nm SiO₂ over 72 hours post formation of hard corona (incubation of particles in 55% foetal bovine serum (FBS) for 1 hour followed by centrifugation and three washes to form the hard corona before being re-suspended in the assay medium).

From these data it is clear that the formation of a soft corona on the 50 nm SiO₂ nanoparticles stabilises the particles somewhat. The 50 nm SiO₂ nanoparticle soft corona remains close to the nominal size of the particle over time but with a PDI of ~0.35, as shown in [Table 7.4](#).

The 50 nm SiO₂ nanoparticles have a dynamic change in hard corona over time. Removing the soft corona of 50 nm SiO₂ nanoparticles prior to re-dispersion in the assay medium causes particle aggregation initially (1 hour); however, the particles seem to stabilise somewhat by 48 hours (Z-ave diameter 117.62 nm, PDI 0.23), then aggregate once more by 72 hours (Z-ave diameter 459.7 nm, PDI 0.583), as shown in [Table 7.4](#)

and [Figure 7.5](#).

Table 7.4. Dynamic light scattering data for the The 200 nm SiO₂ nanoparticle stability does not improve through addition/removal of the soft corona until at least 72 hours post incubation in assay medium. The diameter of the 200 nm SiO₂ nanoparticles particles remains at ~130–140 nm nm, with PDI values that range from 0.164 to 0.459 until 48 hours post incubation in the assay medium, as shown in [Table 7.5](#). The 200 nm SiO₂ nanoparticle hard corona particles seem to stabilise somewhat in the assay medium post 72 hours incubation.

particle size (Z-ave) and size distribution of 50 nm SiO₂ nanoparticles in the presence of the soft and hard protein coronas.

Sample Name	T (°C)	Z-Ave (d.nm)	Peak 1	% Intensity	PdI	Width (d.nm)
50nm SiO ₂ Soft corona 1 hr	37	79.87	48.1	93	0.36	32.84
50nm SiO ₂ Soft corona 24hr	37	124.6	35.53	92	0.217	15.4
50nm SiO ₂ Soft Corona 48hr	37	98.76	27.21	74.6	0.35	23.08
50nm SiO ₂ Soft Corona 72hr	37	69.85	7.968	40.9	0.207	5.74
50nm SiO ₂ Hard corona 1 hr	37	9484	5.399	52.8	0.576	1.919
50nm SiO ₂ Hard corona 24hr	37	524.2	5.343	65.8	0.538	3.123
50nm SiO ₂ Hard Corona 48hr	37	117.62	4.485	65.1	0.23	3.681
50nm SiO ₂ Hard Corona 72hr	37	459.7	5.928	40.7	0.583	1.311

Table 7.5. Dynamic light scattering data for the particle size (Z-ave) and size distribution of 200 nm SiO₂ nanoparticles in the presence of the soft and hard protein coronas.

Sample Name	T (°C)	Z-Ave (d.nm)	Peak 1	% Intensity	Pdl	Width (d.nm)
200nm SiO ₂ Soft corona 1 hr	37	142.2	83.18	100	0.164	46.83
200nm SiO ₂ Soft corona 24hr	37	142.3	77.78	100	0.221	46.86
200nm Si Soft Corona 48hr	37	125.3	81.48	100	0.27	63.53
200nm Si Soft Corona 72hr	37	129.7	157.5	100	0.209	48.29
200nm SiO ₂ Hard corona 1 hr	37	153.7	83.18	100	0.322	45.3
200nm SiO ₂ Hard corona 24hr	37	142.3	77.78	100	0.285	44.2
200nm SiO ₂ Hard Corona 48hr	37	191.8	81.48	100	0.459	110.2
200nm SiO ₂ Hard Corona 72hr	37	198.2	161.2	66.4	0.289	45.47

The formation of a soft corona on 50 nm SiO₂ nanoparticles is most suitable for assessment of the mechanism of particle interaction with the BBB due to

its decreased aggregation. Additional studies could be carried out to identify the protein corona and how this affects nanoparticle transport through the monolayer.

8 Determination of Mechanisms for Nanoparticle Passage through the Blood–brain Barrier Model

8.1 Transport of 50 nm SiO₂ Nanoparticles Through the *In Vitro* Blood–brain Barrier Model

A key advantage of nanoparticles, which makes them very attractive as potential drug carriers for nanomedicine and nanotherapy, is that nanoparticles also access the endogenous active transport mechanisms of cells, likely as a result of attracting proteins and protein complexes to their surface (Hellstrand et al., 2009) and thereby presenting a biological identity to the cellular membranes (Walczyk et al., 2010). Thus, in analogy with the transport data for the positive control protein (ApoE), it is expected that the transport of the 50 nm SiO₂ nanoparticles should also be significantly different in the presence and absence of cellular energy.

Transport assays for green-fluorescent-labelled 50 nm SiO₂ nanoparticles, presented to the apical chamber at a concentration of 100 µg/ml, were performed by the two teams as the final step in the internal benchmarking process. One should be critical of several aspects of these conditions. First, dye leakage has been found to be a highly significant element in uptake studies within this laboratory, and given the small amounts of transport involved here, this is an even more serious issue. Indeed,

several explorations with a variety of commercially available labelled nanoparticles indicate that most of the apparent transport derives from leeching dye diffusing across the barrier. One should also note the rather high doses used in this study (to increase the signal to noise ratio), and this undesirable element of such studies should be addressed in future as such concentrations do not represent a realistic exposure dose.

SiO₂ nanoparticle transport across the BBB was tested using the hCMEC/D3 BBB model over 4 hours. The experimental procedure was performed as described in Appendix I. Based on the previous optimisation studies, the 0.4 µm PET transwell (Corning Costar 3460) was chosen as a permeable support for the transport study; the PET transwells were coated with rat tail collagen I and fibronectin before cell seeding. To evaluate SiO₂ transport efficiency in the BBB model, three parameters were measured: apparent permeability coefficient (P_{app}), transport mass and average transport percentage. The calculation methods for P_{app} and transport mass were described in Section 5. The average transport percentage was calculated by dividing the transported mass in the basolateral chamber after 4 hours with the initial compound mass at $T = 0$ in the apical chamber (the initial nanoparticle dose).

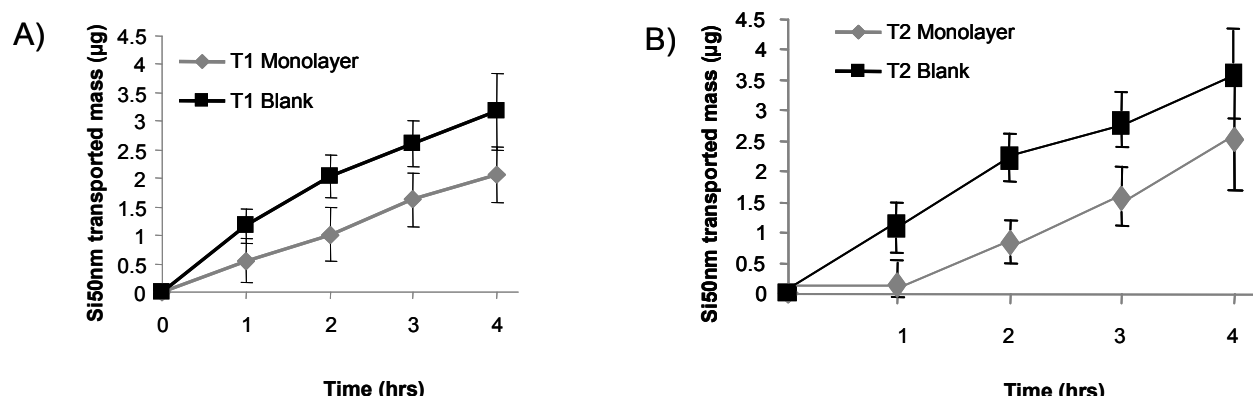


Figure 8.1. Comparison of 50 nm SiO₂ nanoparticle transport assays over 4 hours. Similar transported mass values through the *in vitro* blood–brain barrier (BBB) model were obtained for both teams within the internal benchmarking study, showing the reproducibility of the BBB monolayer in the study of nanoparticle uptake. (Data are mean \pm standard deviation, $3 \leq n \leq 6$. Two-way ANOVA showed no significant differences of 50 nm SiO₂ nanoparticle transport on comparison of the two teams' monolayer or blank values over time.)

The transport of the 50 nm SiO₂ nanoparticles across the BBB, under the normal tissue culture conditions, when the cellular process are occurring normally, is reduced to ~ (or approximately) 50% of the values in the absence of the cell layer (the blank filter alone), suggesting that the cellular monolayer is acting to prevent the nanoparticles from equilibrating across the BBB, and that some active transport of nanoparticles across the BBB is occurring, as shown in Fig. 8.1. In addition, the 50 nm SiO₂ nanoparticles did not reach equilibrium within the blank transwell, as 4 hours after exposure of 50 nm SiO₂ nanoparticles to the apical chamber, approximately 7% of the original dose had crossed the 0.4 µm filter, as read by the level of fluorescence in the basal chamber. This may be due to a combination of 50 nm SiO₂ nanoparticles agglomeration to ~200 nm in the assay medium and the non-linear shape of the 0.4 µm pores within the filter membrane. Ongoing optimisations of these models will be necessary to investigate the detailed mechanism of the passage of 50 nm SiO₂ nanoparticles through the model BBB, and in particular to reduce the influence of the filter membrane, while maintaining the cellular barrier reproducibility. These can be somewhat opposing needs in practice.

As FD4 was used previously as a marker of paracellular permeability, ApoE was used in as a marker for receptor-mediated transcytosis through the hCMEC/D3 cell monolayer. The percentage transported mass of ApoE after 4 hours was ~40% of the original exposure dose (Fig. 8.2). This is perhaps unsurprising as it has been reported that ApoE can enter the brain through the bloodstream. Approximately 7% of the 50 nm SiO₂ nanoparticle exposure dose crossed the monolayer, and the initial high exposure dose of 100 µg/ml highlights the robust properties of this cell line to impede the transport of foreign molecules. The exact mechanism of transport is as yet unknown; however, it has been shown that a protein corona surrounds nanoparticles in physiological medium, and these proteins guide the nanoparticle–cell interaction. Further investigation into the exact corona formed on 50 nm SiO₂ nanoparticles in assay media will be instructive on this matter.

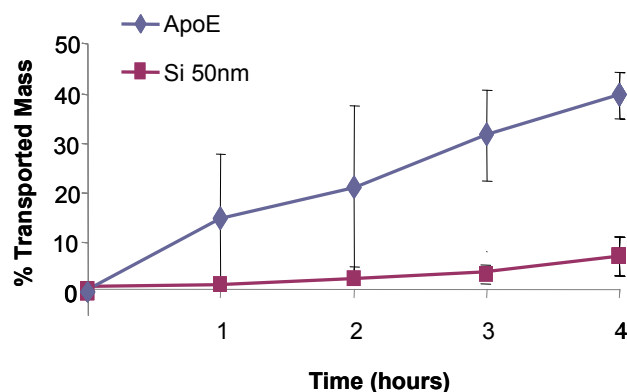


Figure 8.2. Percentage transported mass of 50 nm SiO₂ nanoparticles and apolipoprotein E (ApoE) transcytosis control. A higher percentage of ApoE was found to cross the blood–brain barrier monolayer compared to 50 nm SiO₂ nanoparticles (3 ≤ n ≤ 6) as expected.

8.2 Effect of SiO₂ Nanoparticles Size on Efficiency of Crossing the Blood–brain Barrier Model

As shown in Fig. 8.3 the flux curves of various SiO₂ nanoparticles through the hCMEC/D3 cell BBB model were plotted to investigate the effect of nanoparticle size on transport through the barrier at 37°C. After 4 hours, less than 2 µg of 50 nm SiO₂ crossed the BBB, which accounted for 4.3% of the initial mass applied to the apical chamber (50 µg). On the other hand, 2% of 100 nm SiO₂ and less than 0.9% of 200 nm SiO₂ penetrated the BBB monolayer. The transported amount of 50 nm SiO₂ nanoparticles was significantly higher than for 100 nm and 200 nm SiO₂ nanoparticles, indicating a size advantage of 50 nm SiO₂ nanoparticles for transport through the BBB model. The smaller nanoparticle is more efficient at crossing the monolayer, as expected. However, none of the three SiO₂ nanoparticles could penetrate the BBB monolayer in a large quantity based on their applied amounts. This phenomenon implies that the hCMEC/D3 cell model physically restricted exogenous compounds from crossing the BBB model.

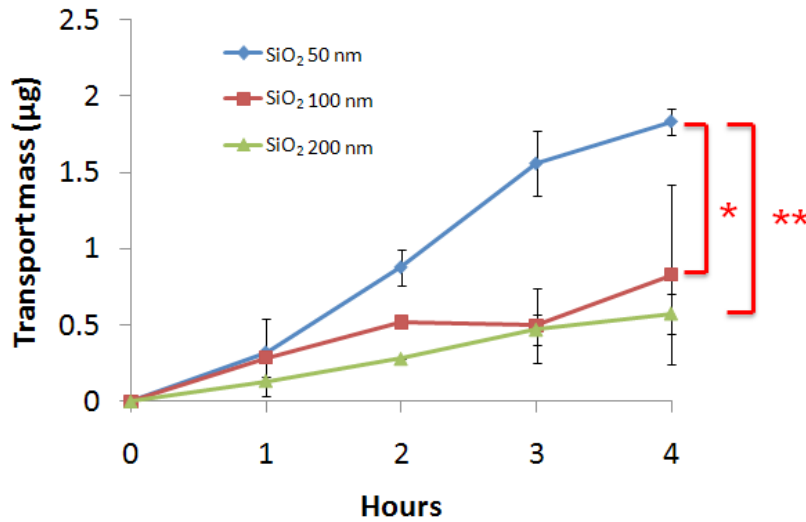


Figure 8.3. SiO₂ nanoparticle fluxes through the blood–brain barrier monolayer over 4 hours at 37°C, for 50, 100 and 200 nm SiO₂ particles. After 4 hours, the transport amount of 50 nm SiO₂ nanoparticles was significantly higher than that of 100 nm and 200 nm SiO₂ nanoparticles. (Student *t*-test was performed using two unequal variances. Data represent means of $n = 3 \pm$ standard deviation; * indicates $p < 0.05$, ** indicates $p < 0.001$.)

Moreover, when 50 nm SiO₂ nanoparticles were applied to blank transwells (Fig. 8.4), more than 6% was collected in the basolateral side after 4 hours, compared to only 4% transported through the BBB monolayers. This significant difference demonstrates

the permeable property of 0.4 µm PET membranes toward 50 nm SiO₂ nanoparticles. However, a further optimisation is still needed with blank transwells as the 6% transport rate (of the applied dose) is still very low.

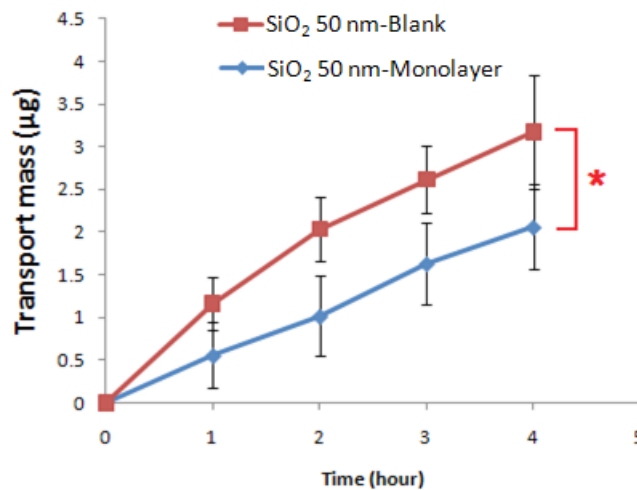


Figure 8.4. 50 nm SiO₂ nanoparticle fluxes across 0.4 µm blank polyester transwells and blood–brain barrier (BBB) monolayers over 4 hours. The transported mass of SiO₂ nanoparticles through blank transwells was significantly higher than the transwells with the BBB monolayer. (Data represent means of $n = 4 \pm$ standard deviation; significance assessed using the Student *t*-test; * indicates $p < 0.05$.)

8.3 Temperature-dependent Nanoparticle Transport Across the Blood–brain Barrier Model

A temperature-dependent transport study of ApoE, as the positive control for transcytosis, and SiO₂ nanoparticles through hCMEC/D3 monolayers was performed to study the cellular energy requirements in nanoparticles transcytosis. The ApoE was labelled with Alexa Fluor 647 fluorescent dye to allow its visualisation and to allow it to serve as a transcytotic marker. All the tests were performed at both 37°C and 4°C, as shown in [Fig. 8.5](#) for the 50 nm SiO₂ nanoparticles and ApoE.

Apolipoprotein E is a plasma protein that acts as a ligand for low-density lipoprotein receptors and, through its interaction with these receptors, participates in the

transport of cholesterol and other lipids among various cells of the body (Mahley, 1988). In endothelial cells, ApoE can be internalised and transcytosed together with its lipoprotein receptors LDL-R (Kreuter, 2004; Dergunov, 2004) and LRP (Knott et al., 1986; Croy et al., 2004), which are expressed on endothelial apical membranes. It was shown in the literature that the transport rate of apolipoprotein A-1 in human microvascular endothelial cells was reduced at 4°C compared to 37°C (Rohrer et al., 2006). In the present study, the transport patterns of ApoE at 37°C and 4°C (as shown in [Fig. 8.5B](#)) were consistent with the literature (Rohrer et al., 2006). ApoE was able to transcytose into the hCMEC/D3 BBB at 37°C, and its transport was dependent on the ATP supply from endothelial cells.

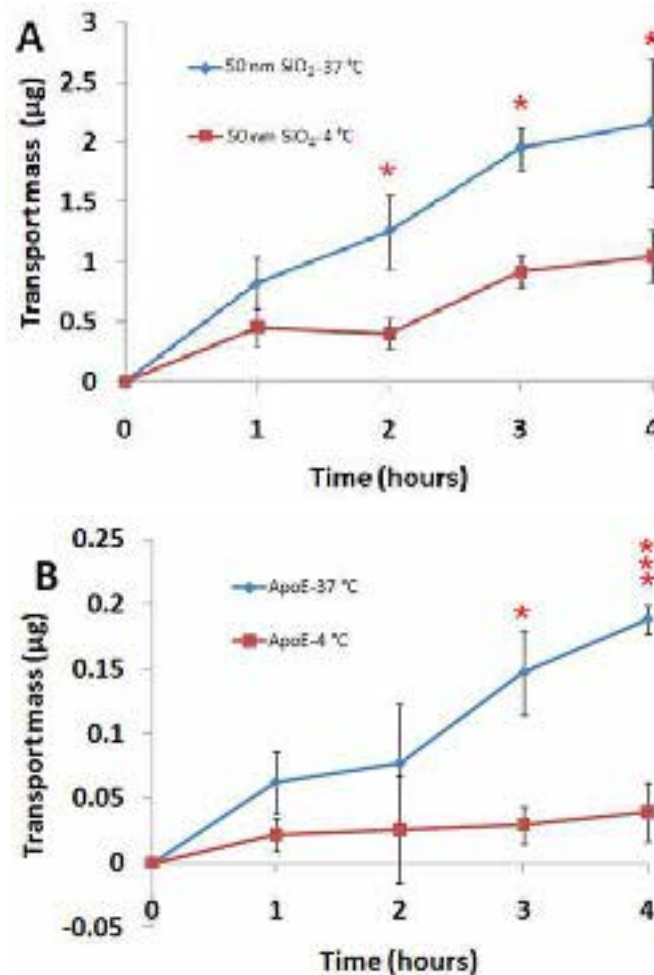


Figure 8.5. Transport of 50 nm SiO₂ nanoparticles and apolipoprotein E (ApoE) through the blood–brain barrier (BBB) model at 37°C and 4°C. (A) ‘50 nm SiO₂-37°C’ represents the flux curve of 50 nm SiO₂ through the BBB model at 37°C; ‘50 nm SiO₂-4°C’ represents 50 nm SiO₂ nanoparticles crossing the BBB model at 4°C. (B) ‘ApoE-37 °C’ represents the transport of ApoE crossing the BBB model at 37°C; ‘ApoE-4 °C’ represents ApoE crossing the BBB model at 4°C. (Student *t*-test was performed using two unequal variances. Data represent mean values ± standard deviation, *n* = 4; * indicates *p* < 0.05, *** indicates *p* < 0.0001.)

The permeability and transport percentage values of 50 nm SiO₂ nanoparticles and ApoE after 4 hours are given in Table 8.1, and shown in Figs 8.5 and 8.6. As shown in Fig. 8.5, 50 nm SiO₂ and ApoE were transported at 4°C to a significantly lower amount than at 37°C, after 4 hours. The permeability (Fig. 8.6A) and transport amount of 50 nm SiO₂ at 37°C (Table 8.1) were twice those found at 4°C. On the other hand, permeability of the positive control ApoE (Fig. 8.6B) at 37°C was almost four times higher than at 4°C,

and its transported mass after 4 hours at 37°C was five times higher than at 4°C. Similarly, a decrease in the permeability and transport percentage occurred in the 100 nm and 200 nm SiO₂ at 4°C (the flux and permeability figures are not shown), and the difference between 37°C and 4°C was nearly two-fold. In conclusion, the transport efficiencies of SiO₂ nanoparticles and ApoE at 37°C were significantly higher than at 4°C, indicating the temperature dependence of compound transport across the BBB.

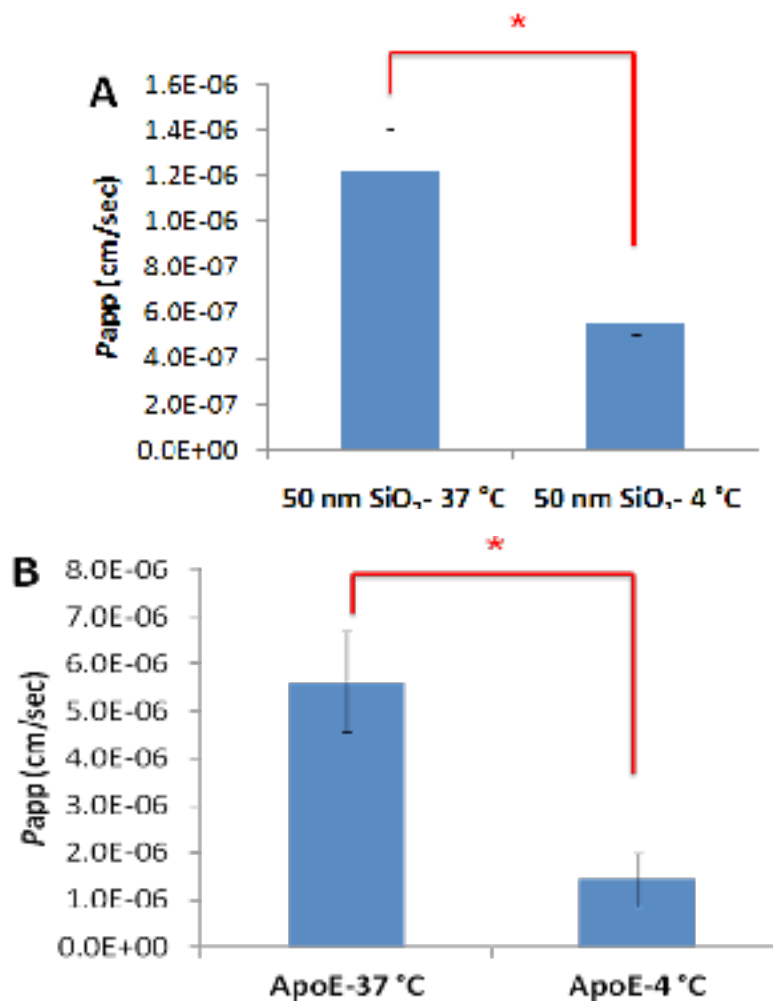


Figure 8.6. Apparent permeability (P_{app}) measurement of 50 nm SiO₂ nanoparticles and apolipoprotein E (ApoE) across the hCMEC/D3 blood–brain barrier (BBB) models at 37°C and 4°C. (A) ‘50 nm SiO₂-37°C’ and ‘50 nm SiO₂-4°C’ represent the apparent permeability of the BBB models to 50 nm SiO₂ nanoparticles at 37°C and 4°C, respectively. (B) ‘ApoE-37°C’ and ‘ApoE-4°C’ represent the apparent permeability of the BBB models to ApoE at 37°C and 4°C, respectively. (Student *t*-test was performed using two unequal variances. Data represent means of $n = 4 \pm$ standard deviation; * indicates $p < 0.05$.)

Table 8.1. Permeability and transport percentage comparison among SiO₂ nanoparticles and apolipoprotein E after 4 hour transport studies at 37°C and 4°C. (* indicates that flux curves and permeability figures were not shown in this section.)

Testing substance	Applied amount (µg/ml)	Temp. (°C)	Study duration (h)	Apparent permeability (×10 ⁻⁶ cm/s)	Average transport percentage (%)
50 nm SiO ₂	100	37	4	1.2 ± 0.2	4.3
50 nm SiO ₂	100	4	4	0.6 ± 0.05	2.1
* 100 nm SiO ₂	100	37	4	0.6 ± 0.1	2.0
* 100 nm SiO ₂	100	4	4	0.4 ± 0.3	0.9
* 200 nm SiO ₂	100	37	4	0.4 ± 0.08	0.9
* 200 nm SiO ₂	100	4	4	0.2 ± 0.05	0.4
ApoE	1.98	37	4	5.6 ± 1.1	19
ApoE	1.98	4	4	1.4 ± 0.6	3.94

A temperature reduction from 37°C to 4°C potentially decreases the ATP supply to support endocytic vesicle movement in the cytomembrane, and further leads to slowing of substance transport via the clathrin- and caveolae-dependent endocytosis pathways. The temperature dependence of cellular protein transport was previously investigated with an *in vitro* lymphatic endothelial cell model (O'Morchoe et al., 1984), which showed that if vesicular transport is required for the intercellular uptake process, the rate of protein movement is temperature-dependent due to cellular ATP participation in endocytic vesicle transport (Anderson, 1981). Conversely, if the protein moves by a non-cytoplasmic process (or non-transendothelial transport), such as diffusion among adjacent cells (tight junction), then temperature should have comparatively little influence on the rate of protein paracellular transport (O'Morchoe et al., 1984).

Based on the results shown here, ApoE and SiO₂ nanoparticles presented the same temperature-

dependent transport pattern in this BBB model, suggesting that the nanoparticles are also taken up by the hCMEC/D3 BBB using an active, receptor-mediated pathway. Also, due to the consistent profile of the ApoE and 50 nm SiO₂ nanoparticle fluxes in the BBB model, it is assumed that 50 nm SiO₂ nanoparticles potentially crossed the BBB monolayer by transcytosis; further imaging evidence, e.g. light microscopy or electron microscopy, would be required to prove this.

8.4 Bi-directional Transport Assays through the hCMEC/D3 Blood–brain Barrier Monolayers

With ApoE as the transcytosis positive control, a bi-directional transport study of 50 nm SiO₂ nanoparticles through the hCMEC/D3 monolayers was performed. The permeability values of 50 nm SiO₂ nanoparticles and ApoE through the BBB model are given in [Table 8.2](#).

Table 8.2. Bi-directional transport of 50 nm SiO₂ nanoparticles and apolipoprotein E through the hCMEC/D3 BBB monolayers.

	50 nm SiO ₂	50 nm SiO ₂	ApoE	ApoE
Transport direction	Apical to basolateral	Basolateral to apical	Apical to basolateral	Basolateral to apical
Apparent permeability (×10 ⁻⁶ cm/s)	1.29 ± 0.04	0.92 ± 0.12	7.65 ± 1.74	3.82 ± 1.0
Uptake ratio ($P_{app,ab}/P_{app,ba}$)	1.4		2.0	
Applied dose (µg/ml)	100	100	100	100
Temperature (°C)	37	37	37	37
Duration (h)	4	4	4	4

As shown in Fig. 8.7, a significantly larger amount of 50 nm SiO₂ nanoparticles was transported from the apical (A) to basolateral (B) chamber than from the basolateral to the apical chamber. The permeability value of A to B was significantly higher than B to A in the 50 nm SiO₂ nanoparticle transport study. In this study, ApoE was also used as the transcytotic control. As discussed above, ApoE shows predominantly transport from the apical to the basolateral side of the BBB, because receptors expressed on the apical membrane of the endothelium, such as LDL-R (Kreuter, 2004; Dergunov, 2004) promote ApoE transcytosis in the BBB (Rohrer et al., 2006). Consistently, the uptake ratio of A to B divided by B to A was 2.0, indicating increased ApoE transport from A to B. In a similar manner, the uptake ratio of 50 nm SiO₂ nanoparticles was calculated as 1.4 after 4 hours. Additionally, ApoE transport from A to B was significantly higher than 50 nm SiO₂ transport from A to B, as shown in Fig. 8.7, as expected.

These findings demonstrate the likelihood of active transport of 50 nm SiO₂ nanoparticles from the apical side to the basolateral side of the hCMEC/D3 monolayers, with a similar pattern as for the ApoE positive control. However, at this point it still cannot be concluded that SiO₂ nanoparticle transport is conducted in an ApoE-like receptor-mediated pathway. SiO₂ nanoparticle transcytosis may involve some specific mediators on the apical membrane of the BBB, or may be caused by a paracellular diffusion effect.

Thus to fully understand and confirm nanoparticle transport mechanisms, it is essential to perform imaging of SiO₂ nanoparticle transport in this BBB model. Another important aspect is to examine the roles of clathrin or other endocytosis-related proteins in SiO₂ nanoparticle vesicle transport. An ApoE receptor antibody can also be used to inhibit the ApoE uptake pathway and try to find if there is a connection between ApoE receptors and SiO₂ nanoparticle transport in the BBB.

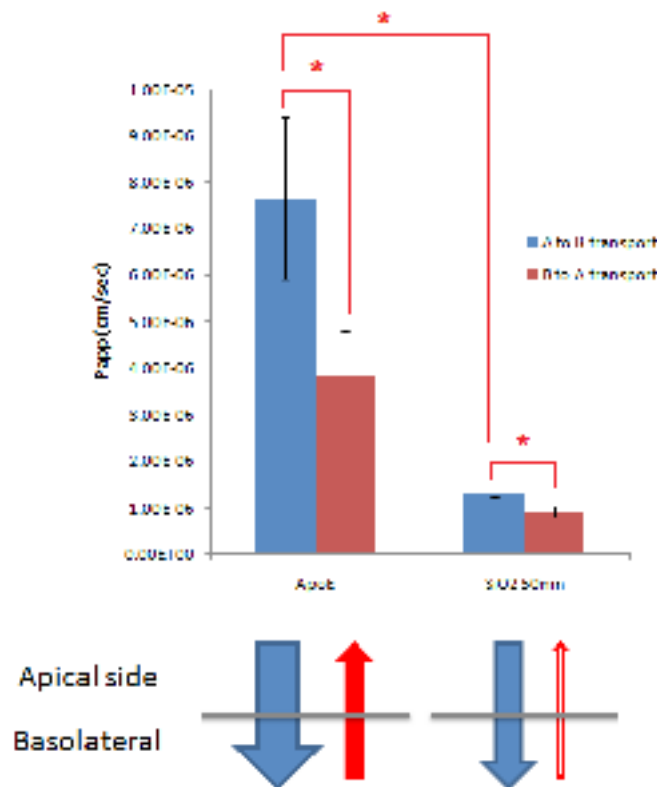


Figure 8.7. Bi-directional transport study of apolipoprotein E (ApoE) and 50 nm SiO₂ nanoparticles' apparent permeability through the blood–brain barrier (BBB). 'A to B transport' indicates transport from the apical side to the basolateral side of the BBB monolayer; 'B to A transport' represents transport from the basolateral side to the apical side of the BBB monolayer. Apparent permeability (*P*_{app}) values were calculated for the transport experiments in directions A to B and B to A. (Data represent means of *n* = 4 ± standard deviation; * indicates *p* < 0.05.)

8.5 Endocytosis and Internalisation of SiO₂ Nanoparticles by hCMEC/D3 Cells

A unique aspect of biological barriers is that the cells are polarised, whereas the same cells grown on a glass slide to less than confluency are not, so in the latter case particles will not exit from the basolateral side (transcytose), but the mechanisms of uptake and early transport are the same, making this approach suitable to study early stages of nano-particle barrier interaction.

To study nanoparticle uptake by hCMEC/D3 cells, flow cytometry analysis was performed. hCMEC/D3 cells were incubated with 25 µg/ml 50 nm SiO₂ nanoparticles for 1, 2, 3, 4, 6, 8 and 24 hours. Exposed cells were analysed by flow cytometry using a 20 mW 488 nm argon laser for excitation; fluorescence emission was collected through a 520 nm band pass filter. Unexposed cells were also measured as negative controls. The exposed cells' fluorescence intensity was divided by the untreated cells', and the ratios were plotted as fold increase (y-axis) in Fig. 8.8. From this experiment it can

be seen that 50 nm SiO₂ nanoparticles accumulated in cells in a time-dependent manner. By the end of 4 hours, fluorescence intensity of exposed cells increased more than 10-fold compared to that of unexposed cells. After 24 hours, the fluorescence intensity of nanoparticle-exposed cells was more than 40-fold higher than that of unexposed cells, as shown in Fig. 8.8.

Subsequently, nanoparticle accumulation in hCMEC/D3 cells was visualised using confocal microscopy. As shown in Fig. 8.9B, a considerable amount of 50 nm SiO₂ nanoparticles were observed in the hCMEC/D3 cells after 2 hours of exposure. After 24 hours of exposure (Fig. 8.9C), 50 nm SiO₂ nanoparticles remained in hCMEC/D3 cells in high quantity. These findings demonstrate that 50 nm SiO₂ nanoparticles were taken up by hCMEC/D3 endothelial cells in a time-dependent manner. Note that for these studies, the hCMEC/D3 cells were grown on collagen-coated glass coverslips and not in the transwells, so the cells were at 70% confluency and were not polarised, thus the tight junctions between cells were not in place.

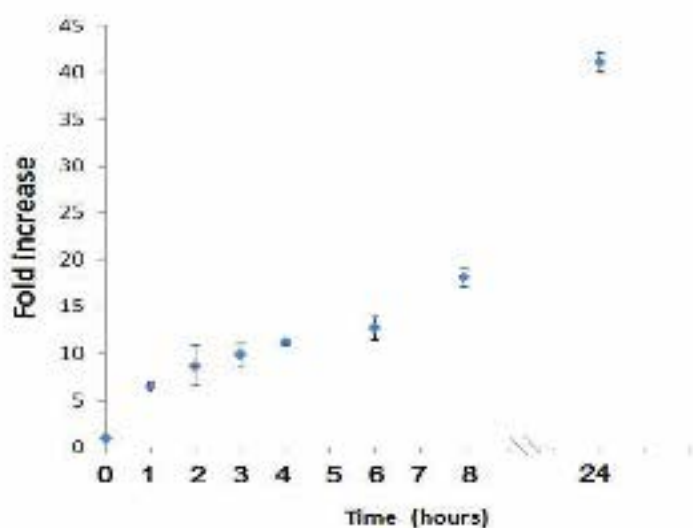


Figure 8.8. 50 nm SiO₂ nanoparticle uptake in hCMEC/D3 cells over 24 hours. Cells were exposed to 25 µg/ml 50 nm SiO₂ nanoparticles over different periods of time. Nanoparticle intensity was measured with flow cytometry. Nanoparticle fluorescence intensity in exposed cells for the indicated times was divided by the unexposed control cell fluorescence in order to obtain the uptake ratio ('Fold increase'). (Data represent mean values of $n = 3 \pm$ standard deviation.)

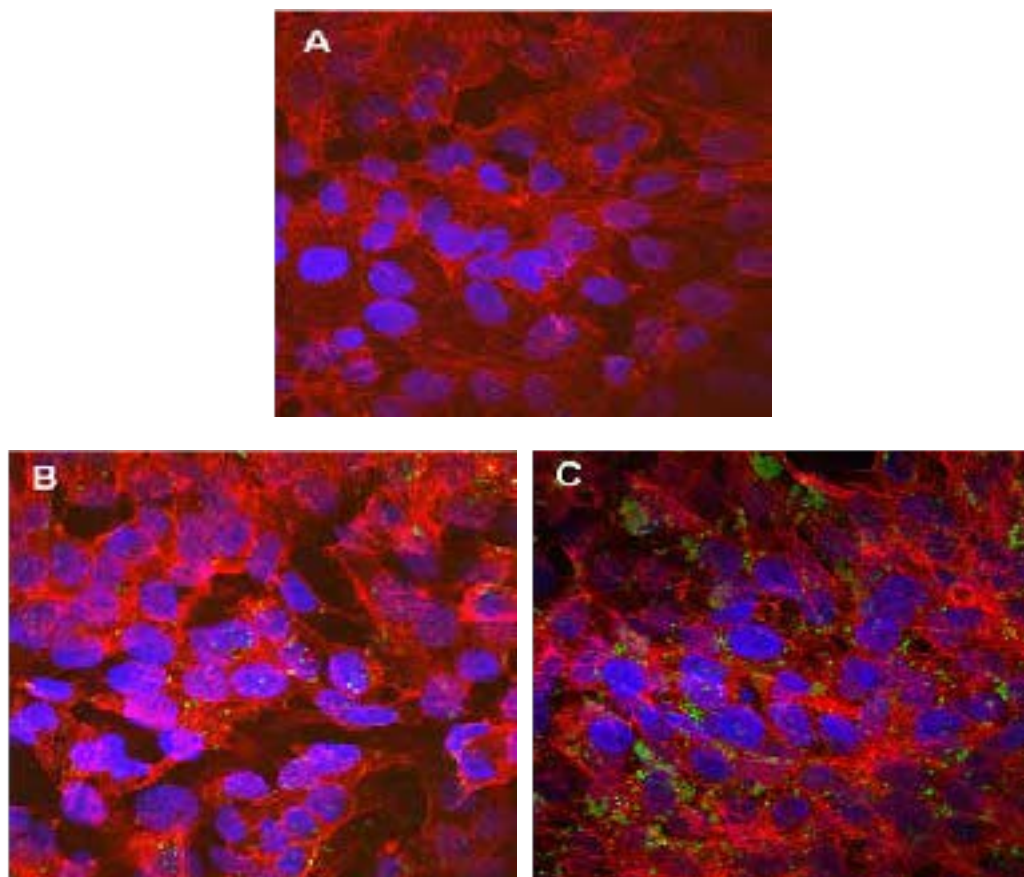


Figure 8.9. Visualisation of SiO₂ nanoparticles in hCMEC/D3 cells using confocal microscopy. (A) Unexposed hCMEC/D3 cells were grown on collagen-coated cover slips. (B) hCMEC/D3 cells were exposed to 25 µg/ml 50 nm SiO₂ nanoparticles for 2 hours. (C) hCMEC/D3 cells were exposed to 25 µg/ml 50 nm SiO₂ nanoparticles for 24 hours. Blue represents 4',6-diamidino-2-phenylindole counterstaining for nuclei, red represents phalloidin Texas-red staining for F-actin, and green represents 50 nm SiO₂ nanoparticles.

8.6 Co-localisation of SiO₂ Nanoparticles in Lysosomes of hCMEC/D3 Cells

Previous studies of the interactions of Kisker silica nanoparticles of sizes 50–200 nm have shown that several different cell types take up these particles very effectively, and that the nanoparticles localise almost exclusively to the lysosomes (Shapero et al., 2011). Thus, a key question to understand was whether the uptake and localisation of the 50 nm SiO₂ nanoparticles follows a similar trajectory and kinetics in the hCMEC/D3 cells.

In fluorescence microscopy, co-localisation refers to the observation of a spatial overlap between two (or more) different fluorescent labels and is used to

see if the different 'targets' are located in the same area of the cell. To confirm nanoparticle localisation in the lysosomes, an immunostaining assay was performed, followed by confocal microscopy analysis. After exposure of the hCMEC/D3 cells to 50 nm SiO₂ nanoparticles over 2, 4, 12 and 24 hours, cells were stained with 4',6-diamidino-2-phenylindole (DAPI) (blue, which stains the nucleus) and LAMP1 antibody (red, binds to lysosomes) as described in Appendix I. The results of this assay showed that after 4 hours, SiO₂ nanoparticles co-localised with cell lysosomes (the white dots in [Fig. 8.10D](#)). At 12 hours and 24 hours, more co-localisation was observed as shown in [Figs 8.10F](#) and [8.10H](#), suggesting time-dependent nanoparticle internalisation within cellular lysosomes.

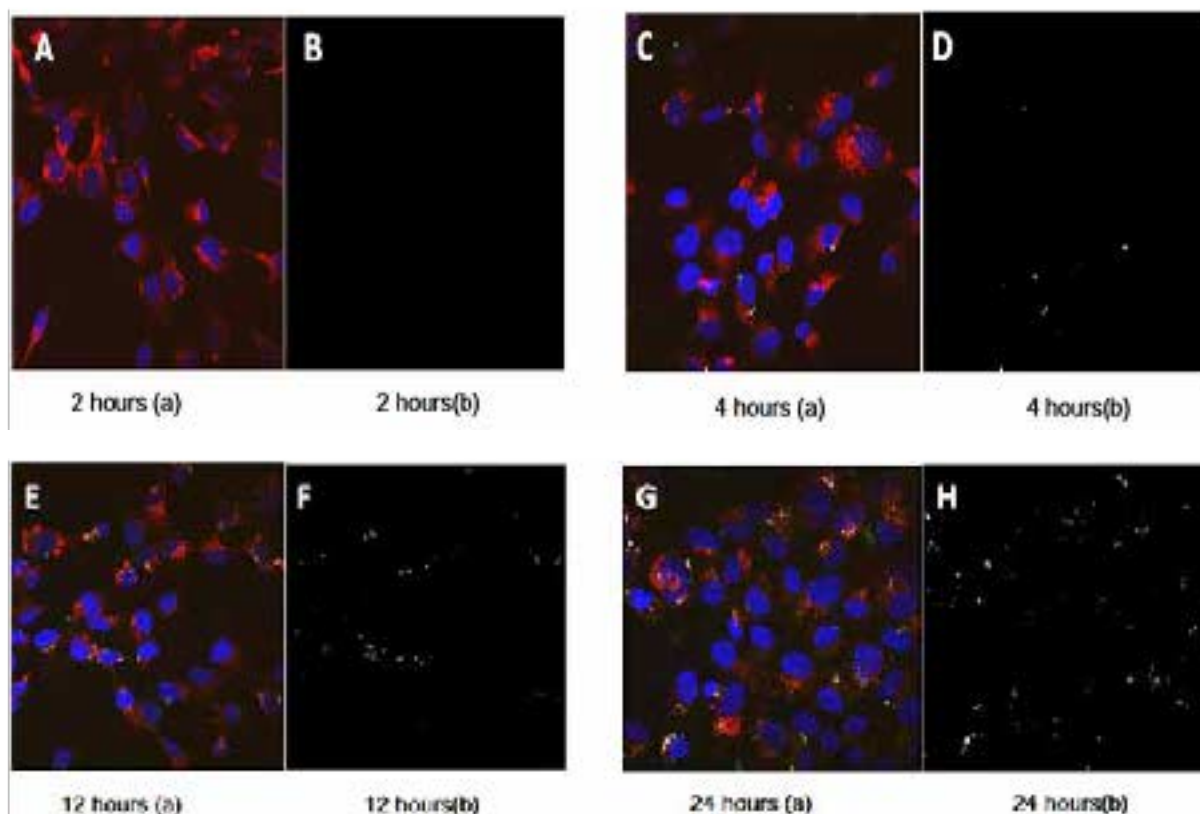


Figure 8.10. Confocal microscopy analysis of 50 nm SiO₂ nanoparticle co-localisation with lysosomes over 24 hours. hCMEC/D3 cells were exposed to 25 µg/ml 50 nm SiO₂ nanoparticles for 2, 4, 12 and 24 hours. Cells were stained as described in Appendix I. Blue represents nuclei, red lysosomes, green SiO₂ nanoparticles, and white is co-localisation of nanoparticles and lysosomes. In images A, C, E and G, colours were merged, and in images B, D, F and H, only white was shown.

8.7 Visualisation of Cellular Endocytosis of 50 nm SiO₂ Nanoparticles by hCMEC/D3 Cells using Electron Microscopy

The hCMEC/D3 cells were cultivated on collagen-coated dishes, and then exposed to 50 nm SiO₂ nanoparticles for 5 minutes, 1 hour, 4 hours and 24 hours. At each time point, ultra-thin sections were obtained for electron microscopy analysis, and images from different time points were captured. Results showed that nanoparticles were initially associated with

the apical membrane of endothelial cells ([Figs 8.11A](#) and [8.11B](#)) and were engulfed by the membrane and internalised into the cytosol inside vesicular bodies ([Fig. 8.11C](#)). In addition, the internalised SiO₂ nanoparticles were observed to be contained within membrane-bound vesicles, mostly localised at the perinuclear region. Free nanoparticles in the cytosol were not observed. Some SiO₂ nanoparticles were transported through early endosomes to lysosomes after 4 hours, and by 24 hours, all uptaken nanoparticles were found in lysosomes ([Fig. 8.11D](#)).

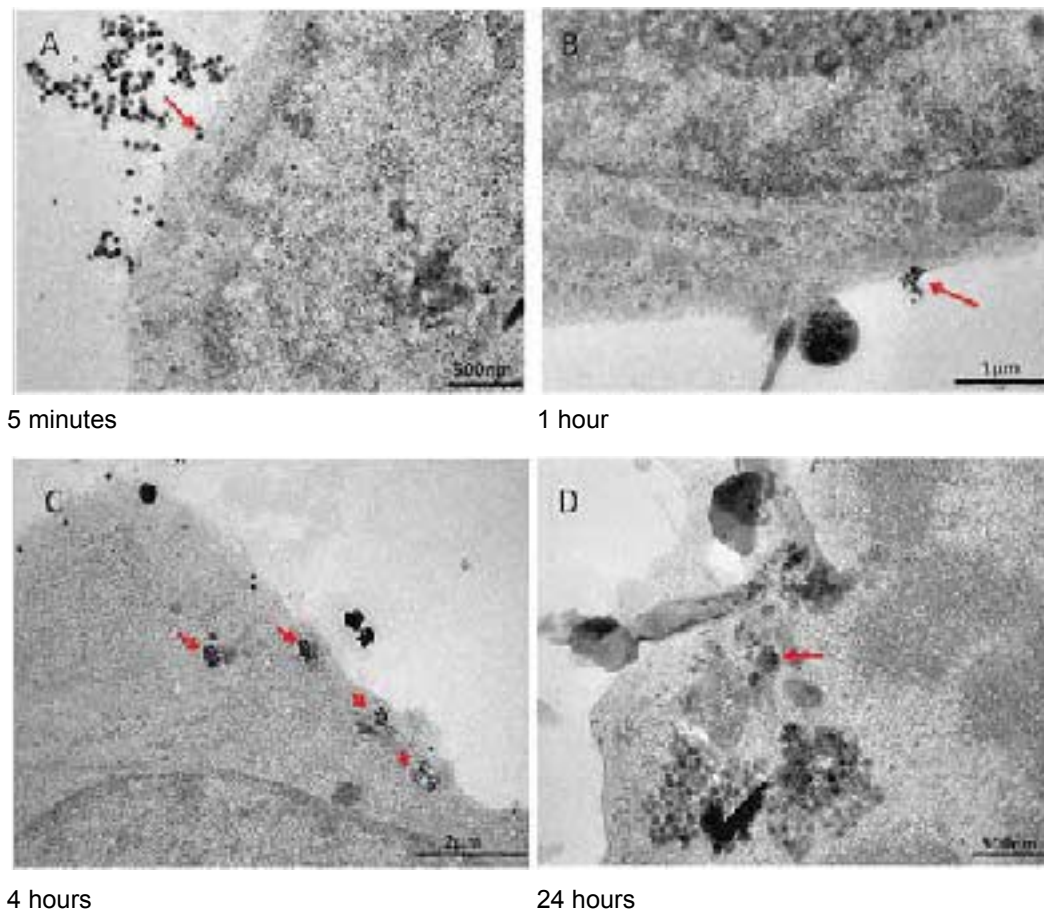


Figure 8.11. Internalisation of 50 nm SiO₂ nanoparticles by hCMEC/D3 cells. Cells were grown on collagen-coated glass dishes before being exposed to 25 µg/ml 50 nm SiO₂ nanoparticles for 5 minutes, 1 hour, 4 hours and 24 hours. Ultra-thin sections were cut and then analysed by electron microscopy. Nanoparticles initially associated with cellular membranes (A, B) later transferred or absorbed onto cell membranes (B), endocytic vesicle transfer (C), and lysosomal accumulation (C, D).

8.8 Transcytosis of 50 nm SiO₂ Nanoparticles across the hCMEC/D3 Blood–brain Barrier Model

Electron microscopy analysis was used to demonstrate and confirm the SiO₂ nanoparticle transport mechanism in the hCMEC/D3 BBB model. As shown in [Fig. 8.12](#), a cell monolayer (grown on the PET transwell) treated with 100 µg/ml 50 nm SiO₂ nanoparticles for 4 hours retained barrier integrity over the 4-hour exposure period. The mechanism of nanoparticle transport was analysed in this monolayer.

As shown in [Fig. 8.13A](#), SiO₂ nanoparticles were initially associated with the BBB endothelial apical membrane. Endocytic vesicles were observed accumulated underneath the plasma membrane. Particles further adhered to the membrane and were engulfed into vesicles. Furthermore, some particles were transferred to early endosomes and were later directed to multi-vesicular bodies. Finally, particles reached the lysosomes for cellular degradation. In Section 8.7 it was shown that SiO₂ nanoparticles were not degraded in lysosomes and were able to remain there over 24 hours. However, lysosomes were not the only destination

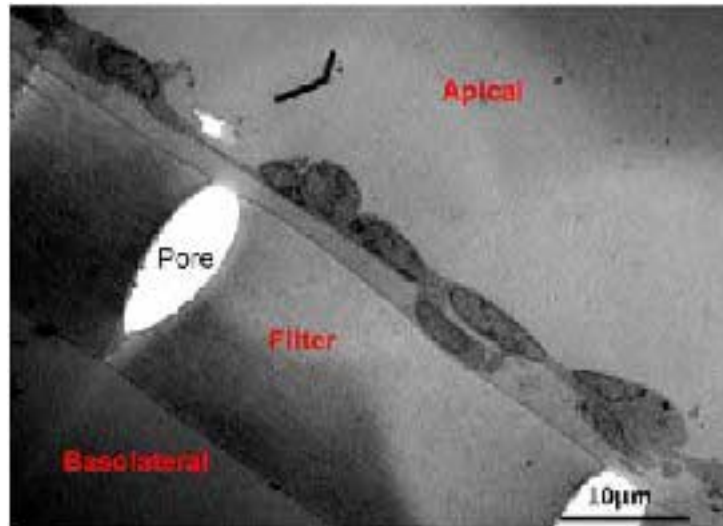


Figure 8.12. The hCMEC/D3 blood–brain barrier monolayer on the 0.4 μm porous polyester transwell after 4 hours exposure to 100 μg/ml 50 nm SiO₂ nanoparticles. The transwell was coated with rat tail type I collagen and fibronectin before cell seeding. Scale bar is 10 μm.

for nanoparticle transport in the BBB case, i.e. when the cell monolayer was grown on the transwell filters and the cells were polarised. In this case, some SiO₂ nanoparticles were observed to bypass the lysosomal degradation pathway (the red arrow '5' in [Fig. 8.13A](#)), and reached the basolateral membrane (still inside a vesicular body, likely a basosome).

Furthermore, in [Fig. 8.13B](#), cell membranes were lifting up and actively engulfing SiO₂ nanoparticles

by phagocytosis. Finally, direct transendothelial vesicle transfer of SiO₂ nanoparticles is shown in [Fig. 8.13C](#). Endocytic vesicles accumulated inside the cytoplasm (the red arrow in [Fig. 8.13C](#)), and clear vesicular-bound transfer of nanoparticles was observed. All these findings visually prove that SiO₂ nanoparticles were transferred across the *in vitro* BBB model, most likely via a transcytosis pathway.

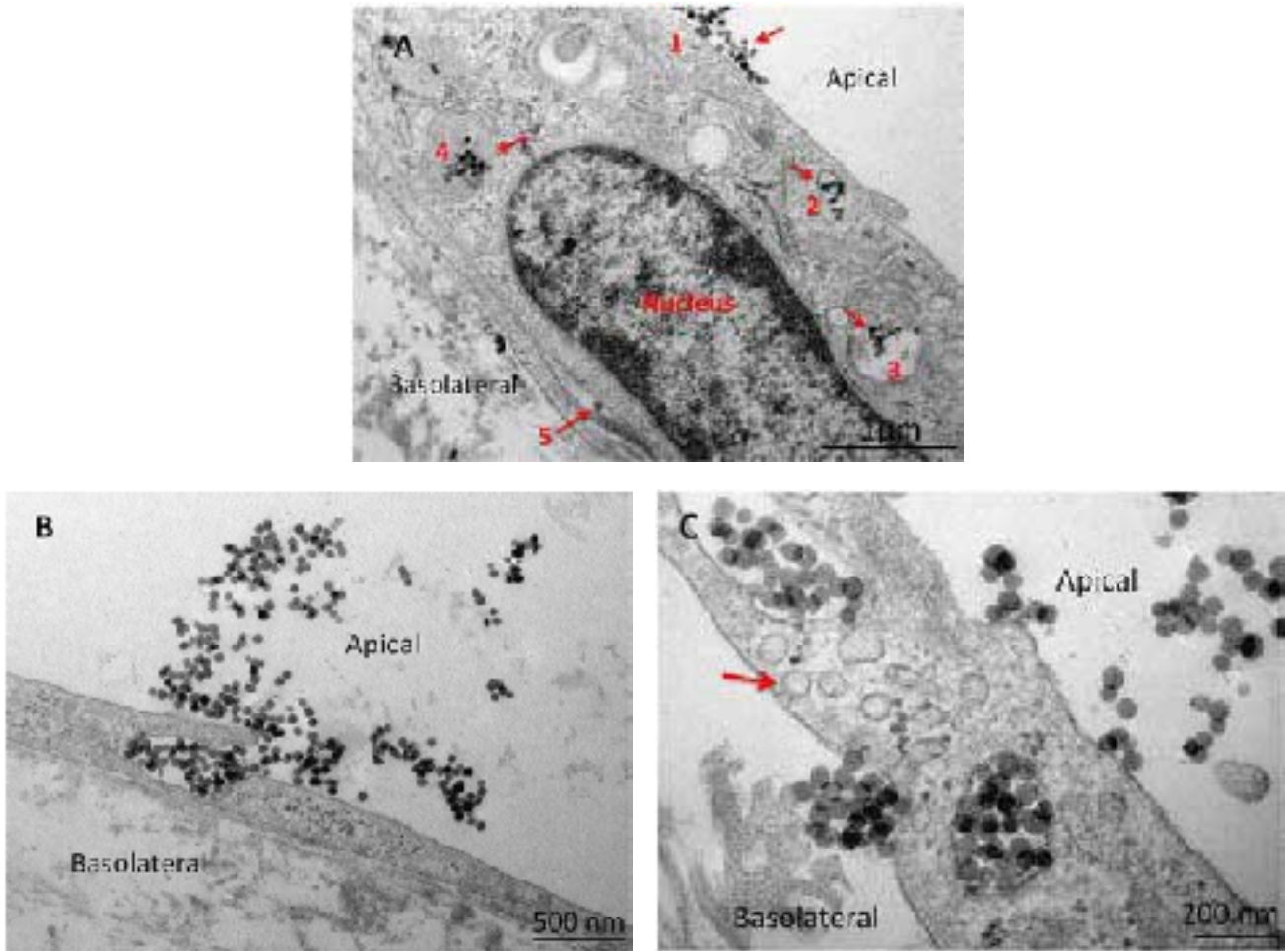


Figure 8.13. Transmission electron microscopy analysis of transport of 50 nm SiO₂ nanoparticles across the *in vitro* BBB model. (A) Transendothelial transport of 50 nm SiO₂ nanoparticles through the hCMEC/D3 blood-brain barrier (BBB) monolayer. Nanoparticles initially associated with the apical plasma membrane, where many endocytic vesicles were accumulated underneath the membrane (1). Some particles then translocated into early endosomal compartments (2), and some were found in the late endosomes (3) and the lysosomes (4). Relatively fewer particles bypassed the lysosomal degradation pathway and were found at the basolateral membrane (5). Scale bar represents 1 μm. (B) Phagocytosis-like engulfment of 50 nm SiO₂ nanoparticles in the hCMEC/D3 BBB monolayer. Scale bar represents 500 nm. (C) Vesicle-mediated transcytosis of 50 nm SiO₂ nanoparticles through the BBB monolayer. Scale bar represents 200 nm.

9 Correlation of Protein Coronas on Particles with Passage through the Blood–brain Barrier

There was an earlier allusion to the issue of protein binding to nanoparticles and the formation of the nanoparticle protein corona in biological fluids, including cellular assay media containing even small amounts of serum proteins. Several nanoparticles have been shown to preferentially bind ApoE, which (as discussed several times in this report) is a known brain-transporter protein. In fact, this turns out to be quite general for different nanoparticles, many adsorbing specific proteins, but often with some component of the apolipoprotein complexes (e.g. one or more of the many apolipoproteins) (Lundqvist et al., 2008). Now, although the mechanism is not yet understood, apolipoprotein E (ApoE) is associated with an elevated risk of Alzheimer's disease (and possibly other neurodegenerative diseases) via multiple routes. It has been suggested that its role as a cholesterol transporter in the brain is combined with complicating effects on aggregation of amyloid, development of neuritic plaques, phosphorylation of tau protein and mitochondrial neurotoxicity (Reiman, 2007). It is clear that selective association of ApoE to nanoparticles (Cedervall et al., 2007a, 2007b) could provide a transport mechanism for small nanoparticles to reach the brain, which may then lead to highly undesirable effects on arrival, especially for nanoparticles that were never intended to reach the brain. Note carefully that *this is not a proof of any form of connection to human disease*. It is merely a caution that the question should be considered.

Within the general point there is the possibility to develop a unique understanding of how, and why, specific nanoparticles arrive at the brain. As shown in Section 8, it is possible to follow the trajectory of the nanoparticles as they are transported into and across the cells of the BBB in a time-resolved manner if they are labelled suitably and/or are sufficiently electron-dense to allow for TEM imaging. For those nanoparticles that can be identified in the basolateral chambers of the transwells, which have been actively transported across the BBB, it is possible to recover the nanoparticles and begin to study their protein coronas before and after transport through the BBB. This would

then allow determination of the nature of the corona and its evolution as it passes through different organs, and help to rationalise why some particles (even though sufficiently small access the brain, and others do not. It is strongly suspected that the difference lies in the protein corona picked up on entry, and the material-dependent manner in which proteins can unbind and exchange, as the nanoparticle identity evolves while passing into different organs.

While a full evaluation of the nanoparticle protein corona before and after transcytosis was beyond the scope of this 2-year project, some preliminary efforts in this direction have been made, with very promising results. Thus, hCMEC/D3 cells were cultivated on PET transwells with a pore size of 0.4 μm , and then exposed to 50 nm SiO_2 nanoparticles for 4 hours. The solutions in the basolateral chambers of several samples were pooled in order to ensure that sufficient particles were recovered following transcytosis through the BBB, to allow determination of their protein coronas. At each time point, ultra-thin sections were obtained for TEM analysis, and images from different time points were captured. After 4 hours, the remaining particles in the apical chamber were also recovered, and their coronas were also determined. The process for recovery of the particles and their hard protein coronas was the same for both apical and basolateral chamber particles: the samples were centrifuged to form a particle pellet, and the supernatant containing the unbound proteins was removed. Particles were washed three times in physiological buffer saline (PBS) with centrifugation and removal of the supernatant each time. The final particle pellet was re-suspended in PBS and bound proteins – the hard corona – were removed from the particles then separated by one-dimensional polyacrylamide gel electrophoresis (1D-PAGE), as described in Appendix I. Results showed some significant differences in the protein coronas before (apical chamber) and after (basolateral chamber) transcytosis through the BBB, as shown in [Fig. 9.1](#). Further work is ongoing to correlate the proteins in the corona with transcytosis efficiency.

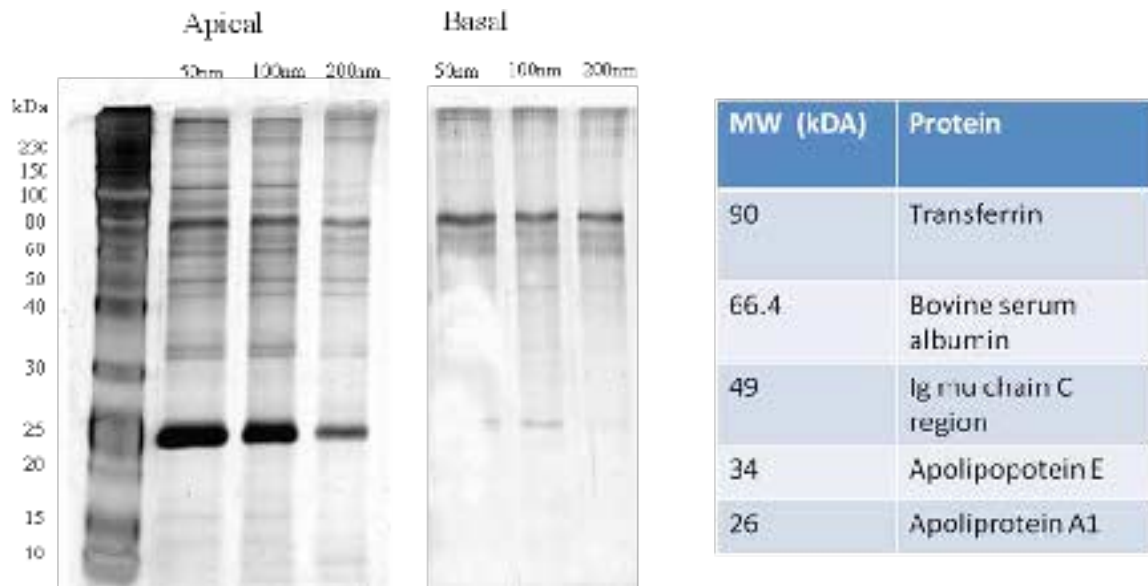


Figure 9.1. SDS-PAGE gel of serum proteins obtained from 50 nm SiO₂ nanoparticles after 4 hours in the apical chamber in assay media containing 3% foetal calf serum, or following transcytosis through the hCMEC/D3 blood–brain barrier (BBB) monolayer into the basolateral chamber. Experiments were performed in collaboration with Dr Marco Monopoli. The protein table on the right-hand side lists possible proteins contained in the nanoparticle protein coronas, but further mass spectrometry analysis has yet to be completed to verify these. Apolipoprotein A-1 could aid in nanoparticle transcytosis across the BBB. The decrease in intensity of the protein bands from the 50 nm SiO₂ nanoparticles compared to the 200 nm SiO₂ nanoparticles from the basolateral chamber is consistent with the decrease in the amount of transported mass of 200 nm SiO₂ nanoparticles compared to the 50 nm SiO₂ nanoparticles, as also shown in [Fig. 8.3](#).

10 Development of a Risk-assessment Protocol for Nanoparticle Uptake into the Brain

The overall objective of this project was to determine if engineered nanoparticles could constitute a significant neurotoxicological risk to humans as a consequence of their small size enabling them to reach the brain.

In the context of public health, risk assessment is the process of quantifying the probability of a harmful effect to individuals or populations from certain human activities. In most countries, the use of specific chemicals is not allowed unless it can be shown that they do not increase the risk of death or illness above a specific threshold. Within Europe, and applicable to Ireland also, the current regulation for chemicals is REACH (EC) No. 1907/2006 (EC, 2006) and the associated guidance documents from the European Chemicals Agency (ECHA, 2007, 2008).

In the estimation of the potential risks, three or more steps are involved, requiring the inputs of different disciplines:

- 1 *Hazard identification* aims to determine the qualitative nature of the potential adverse consequences of the contaminant (e.g. chemical, radiation, noise, etc.) and the strength of the evidence showing that it can have that effect. For chemical hazards, this is done by drawing from the results of the sciences of toxicology and epidemiology.
- 2 *Dose–response analysis* aims to determine the relationship between dose and the probability or the incidence of effect (dose–response assessment). In many contexts, the complexity of this step derives mainly from the need to extrapolate results from experimental animals (e.g. mouse, rat) to humans, and/or from high to lower doses. In addition, the differences between individuals due to genetics or other factors mean that the hazard may be higher for particular groups, called susceptible populations.

An alternative to dose–response estimation is to determine the concentration unlikely to yield observable effects, that is, a no-effect concentration. In developing such a dose, to account for the largely unknown effects of animal to human extrapolations,

increased variability in humans or missing data, a prudent approach is often adopted by including safety factors in the estimate of the ‘safe’ dose, typically a factor of 10 for each unknown step.

- 3 *Exposure quantification* aims to determine the amount of a contaminant (dose) that individuals and populations will receive. This is done by examining the results of the discipline of exposure assessment. Particular care is taken to determine the exposure of the susceptible population(s).

Finally, the results of the three steps above are combined to produce an estimate of risk. Because of the different susceptibilities and exposures, this risk will vary within a population.

Thus, it is clear that for a significant risk to be present, there needs to be both exposure and hazard. In the case of neurotoxicity, the target organ is the brain, thus a key element of this project was to assess the capacity of nanoparticles to access the brain via the BBB.

10.1 Exposure Assessment

The primary routes of occupational and/or consumer exposure to nanoparticles include inhalation, transdermal absorption and ingestion (Borm et al., 2006; Maynard and Kuempel, 2005). From each of these routes, nanoparticles enter the systemic circulatory system, and from there are distributed through the body. There is evidence (Semmler et al., 2004; Kreyling et al., 2002), now incontrovertible (Kreyling et al., 2007), that some engineered nanoparticles (e.g. 6 nm and 18 nm gold nanoparticles), entering intravenously or via the lungs, can reach the brains of small animals. Indeed, they lodge in almost all parts of the brain, and there are no efficient clearance mechanisms to remove them once there. Furthermore, there are suggestions that nanoscale particles arising from urban pollution reach the brains of animals (Calderón-Garcidueñas et al., 2002, 2003; Elder et al., 2007), and nanoscale particles have been found in target brain areas (olfactory bulb, frontal cortex) in children resident in Mexico City (Calderón-Garcidueñas et al., 2004). However, whether such nanoparticles are

reaching the brain via the BBB or via the olfactory bulb is not yet fully clear, although recent results from within the EU FP7 NeuroNano project shed some light on this question (see Section 11 of this report for further details).

Thus, the key question that the present project aimed to address was if nanoparticles can reach the brain. To achieve this, the overall objective was further divided into a series of sub-objectives (see also Section 2) aimed at understanding and quantifying the potential for nanoparticles to reach the brain, as follows:

- Understand what constitutes a lead nanoparticle candidate for passing the BBB;
- Quantify transport efficiency to the brain;
- Understand the detailed pathways that nanoparticles take to reach the brain.

Each of these sub-objectives addresses the issue of exposure – i.e. whether (and how) nanoparticles reach the brain by crossing the BBB. From Sections 6–9 of this report, it is clear that nanoparticles, even up to 200 nm in size, can and do transcytose across the *in vitro* model BBB. Much of the work reported here has been on the particles that showed the highest rate of transcytosis through the *in vitro* BBB model, in order to allow validation of the model, and to have sufficient particles crossing the barrier to allow study of the process. Thus, 50 nm SiO₂ nanoparticles were shown to be transported effectively across the model BBB, with mechanistic studies (Section 8) confirming the transport mechanism as transcytosis. Approximately 5% of the 50 nm SiO₂ nanoparticles exposure dose of 100 µg/ml crossed the monolayer within 4 hours. The low transport relative to this initial high exposure dose highlights the robustness of the BBB formed by this cell line, and its ability to impede the transport of foreign molecules to the brain. Even with the 200 nm SiO₂ nanoparticles, approximately 1% of the applied dose (100 µg/ml) crossed the monolayer within 4 hours.

Thus, the model BBB can effectively discriminate between particles of different sizes, and clearly demonstrates that nanoparticles can potentially reach the brain. However, it is important to note that an exposure concentration of 100 µg/ml is extremely high from a physiological viewpoint, and humans are extremely unlikely to ever be exposed to nanoparticle concentrations this high, even in the case of particles injected directly into the bloodstream for nanodiagnostic

or nanotherapeutic purposes. For this reason, ongoing work will use a much lower exposure dose, and focus on longer, more sustained exposure times (up to 72 hours), with the possible development of a model to look at amounts of nanoparticles reaching the brain via the BBB following long-term or chronic exposure.

However, as these and other nanoparticles were effectively able to transport across the BBB, it is clear that nanoparticles certainly pose a risk from the exposure viewpoint, and where those particles are also shown to present a hazard, there is significant concern about how to develop processes to ensure that nanoparticles (other than those designed to delivery specific therapies) do not reach the brain – so-called safety by design.

10.2 Hazard Assessment

Assessment of the hazard of nanoparticles towards the brain was beyond the scope of the present project, although as detailed below, some assessment of cytotoxicity was carried out, primarily to confirm that the observed nanoparticle access to the brain was not a result of the nanoparticles killing the cells, thereby damaging the cell–cell tight junctions that provide the barrier function.

Within the EU FP7 NeuroNano project, which was secured on the basis of preliminary results that emerged from this EPA STRIVE Fellowship, the cytotoxicity of the Kisker SiO₂ nanoparticles (yellow-green labelled, 50 nm, 100 nm and 200 nm) and the PS-COOH nanoparticles utilised in Section 5 (Invitrogen, yellow-green labelled, 50 nm, 100 nm and 200 nm) to the hCMEC/D3 cells has been assessed using the MTT (3-(4,5-dimethylthiazol-2-yl)-2,5-diphenyltetrazolium bromide) assay. The MTT assay is a colourmetric assay that measures the reduction of MTT, a yellow tetrazole, to purple formazan in living cells (Mosmann, 1983). The absorbance of this coloured solution can be quantified by measuring at a certain wavelength (usually ~500 nm), and a change in the efficiency of the cellular reduction is associated with cell death. Two particle concentrations were assessed (25 µg/ml and 100 µg/ml), and the cytotoxicity of the particles was assessed for up to 72 hours of exposure of the hCMEC/D3 cells to the nanoparticles, with time points at 4, 24, 48 and 72 hours. To mimic both the cells in culture on glass slides and the cells grown on the BBB transwell, two different conditions were studied: non-confluent cells (70% confluence) and a

cell monolayer (100% confluence). To account for the potential interference in the fluorescence assay from the presence of the nanoparticles (which are themselves fluorescent, and could potentially adsorb either reactant or product dyes, thereby reducing their concentration in solution without being indicative of cytotoxicity), the values were normalised according to the interference of the nanoparticles' fluorescence with the MTT reagent.

Data for the six nanoparticles studied are shown in [Fig. 10.1](#) for the 48-hour time point, and as can be clearly seen, none of the tested nanoparticles displayed any significant amount of cytotoxicity to the hCMEC/D3 cells

or to the hCMEC/D3 monolayer, indicating a low hazard for these particles. This is not unexpected, as it was necessary to choose a nanoparticle that did not severely damage or disrupt the integrity of the BBB in order to validate the model for assessment of nanoparticle transport and to confirm nanoparticle transport through the BBB. Thus, if the chosen nanoparticles were highly toxic to the BBB cells, barrier functionality could not be maintained, and a very significant portion of the nanoparticles crossing into the basolateral chamber would likely have crossed as a result of breakages in the barrier integrity resulting from cell death. This would

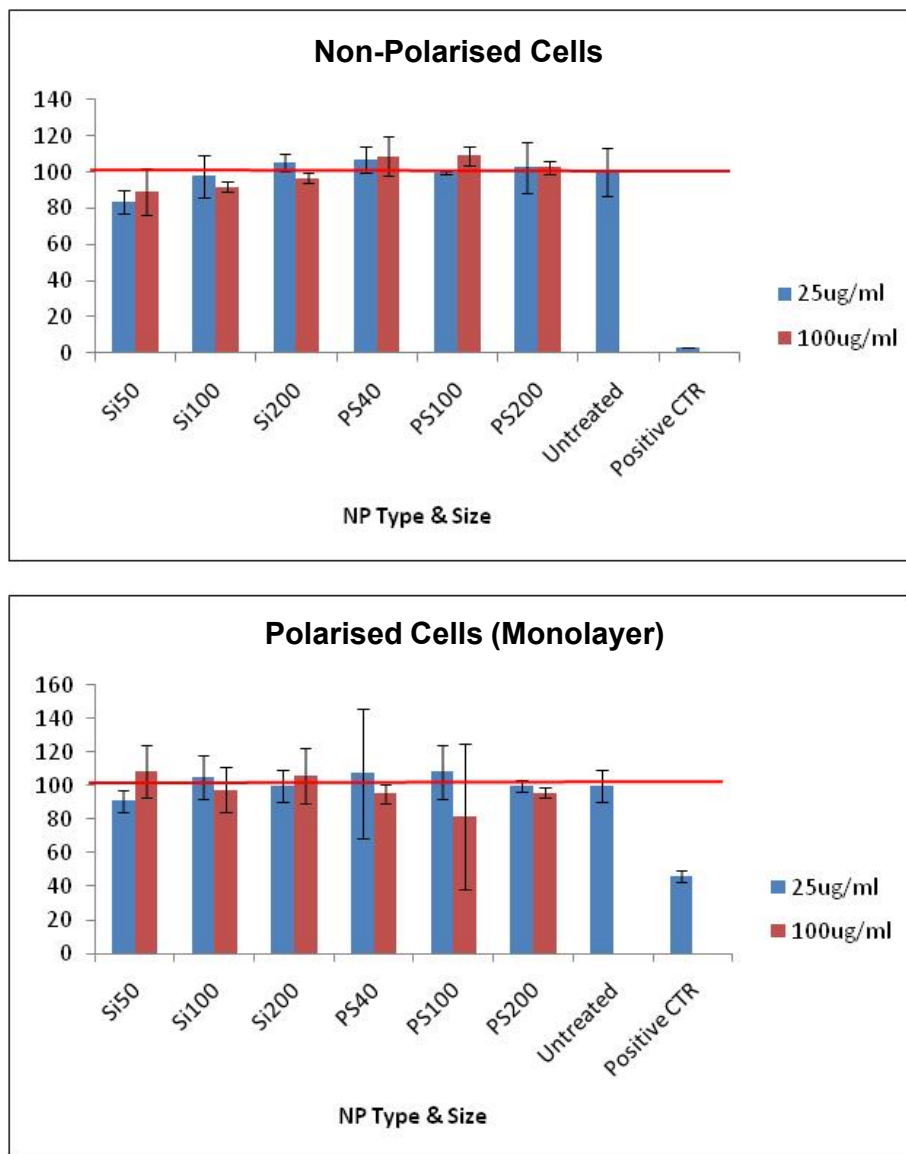


Figure 10.1. MTT assay of cytotoxicity of SiO₂ nanoparticles (NPs) (50 nm, 100 nm and 200 nm) and carboxylate modified polystyrene (PS-COOH) nanoparticles (50 nm, 100 nm and 200 nm) to hCMEC/D3 cells after 48 hours of exposure to cells at 70% confluency and 100% confluency (cell monolayer). A positive control (positive CTR) was added to ensure that the assay was functioning correctly.

be notable from a sudden increase in particles reaching the basolateral chamber on a similar timescale to the cell death, which was not observed in the examples reported here.

10.3 Risk Assessment

Based on the data presented in Sections 6–9 on the low potential of the SiO₂ nanoparticles to reach the brain via the BBB, where transcytosis occurred for less than 5% of the applied dose of 50 nm SiO₂ nanoparticles over 4 hours, even with an extremely large initial particle dose, coupled with the data in Section 10.2 on the low hazard of these nanoparticles, an initial risk assessment would be that there is a very small risk posed by the Kisker SiO₂ nanoparticles for neurotoxicity. This is in good agreement with other work by this group that has assessed the uptake of these same Kisker SiO₂ nanoparticles in lung epithelial cells, and also found that the cells were able to take up the particles effectively and contain them in the lysosomes with no apparent impact on the cell viability or cell division (Shapero et al., 2011).

However, as mentioned in Section 10.1, these are very short-term acute exposure tests only, and additional experimental modifications are required in order to enable the system to be utilised for longer-term, chronic and repeat dose experiments. The work described in this report is being continued within the EU FP7 NeuroNano project, which was secured subsequently to the EPA STRIVE Fellowship, on the basis of preliminary data generated within the EPA STRIVE Fellowship. Thus, with the longer-term exposure studies, and an extension to additional nanoparticles, such as doped ceria and/or radiolabelled TiO₂ nanoparticles being prepared within the NeuroNano project, a wider panel of particles is available with a mode for detection of the particles in the basolateral chamber, and these are currently being assessed.

The NeuroNano project (2009–2012) involves multiple European and international partners, and was developed to build on the EPA STRIVE Fellowship but to include a much broader experimental scope, including *in vivo* experiments for nanoparticle biodistribution and behavioural effects induced by exposure to nanoparticles in an Alzheimer's mouse knockout model. Within NeuroNano, a more detailed risk assessment model is being developed for neurotoxicity. This model

will also consider additional hazard aspects, beyond the simple cytotoxicity described here, such as the potential for nanoparticles to induce reactive oxygen species (ROS) and thereby induce DNA damage and/or inflammation in accordance with the ROS paradigm (Xia et al., 2006), and whether the nanoparticles can also induce protein fibrillation (Linse et al., 2007), which is a key symptom in neurodegenerative diseases such as Alzheimer's and Parkinson's.

From the NeuroNano project, a quite significant body of quantitative *in vivo* evidence is beginning to emerge indicating that nanoparticles reach the brain following exposure by a range of different routes, although the amount of nanoparticles that reach the brain is size, composition and exposure route dependent (see Section 11 for further details). Additionally, data are emerging that suggest that all nanoparticles can modulate the rate of protein fibrillation, suggesting that it is a surface phenomenon, although whether the rate of fibrillation is accelerated or decelerated seems to be a function of the available nanoparticle surface area relative to the protein concentration, and may also be related to the flexibility of the proteins. Finally, oxidative stress data suggest that even within a single particle type (e.g. TiO₂), factors such as the crystal phase and the capping agents used to help disperse the nanoparticles may contribute to the reactive oxygen generation potential of nanoparticles.

Thus, work is being done to build these elements into the risk assessment aspect of the project, and to further develop the preliminary risk assessment that has been performed within the more limited scope of this project.

During the 2.25 years of the project, significant experimental difficulties were encountered, and are now resolved, meaning that a much wider panel of particles can now be assessed using the *in vitro* BBB model. Additionally, following the publication of the first paper from the EPA STRIVE BBB Fellowship project on the establishment and internal validation of the model BBB (Nic Ragnail et al., 2011), requests have come in from other groups that would like to establish a similar *in vitro* BBB model in their labs, which also suggests that additional data will be generated externally to build up knowledge in this emerging field, thereby enabling more robust risk assessments to be performed in the medium term.

11 Validation of the Human Blood–brain Barrier Model Against *In Vivo* Biodistribution Data

A key element of ensuring that the data generated *in vitro* are meaningful, and to help to build the case for the *in vitro* BBB as a screening tool for risk assessment, is to compare the *in vitro* results with data from *in vivo* studies in animals exposed to the same nanoparticles. Initially, the intention was for this comparison to be with data from the literature, but fortuitously, during the lifetime of the EPA STRIVE BBB Fellowship, the Dawson group was awarded the EU FP7 NeuroNano project, to investigate the potential role of nanoparticles in neurodegenerative diseases, with specific emphasis on Alzheimer's and Parkinson's diseases. Thus, preliminary data are emerging from the NeuroNano project on the same sets of particles as have been used in the *in vitro* studies, in particular the 50 nm PS-COOH particles.

11.1 Intra-cerebro-ventricular Injection of Animals with Nanoparticles

In an attempt to determine the infiltration potential of nanoparticles into brain tissue directly, Sprague Dawley rats were anaesthetised using isoflurane, shaved around the cranial region and prepared in a stereotaxis for injection. Two control animals were used. Engineered nanoparticles (10 μ l of each) in the form of ceria (64 nm) $n = 3$, gold (50 nm) $n = 2$, carboxyl-modified polystyrene (20 nm) $n = 2$ and titania (3–9 nm) $n = 4$ were introduced by intra-cerebro-ventricular (ICV) injection using a 20 μ l Hamilton gas-tight syringe. Animals were stitched and allowed to recover for 24 hours, after which they were culled and perfused through the heart using a 4% Perfluoroalkoxy solution. Brains were harvested from each animal and stored in combination fixative before dissection.

The fate of fluorescent carboxylate-modified polystyrene particles (20 nm) after ICV injection was investigated using fluorescent microscopy. Striking fluorescence was found along the injection path and in the ventricle lining in cryotome sections, as shown in [Fig. 11.1](#). The surrounding tissue also seemed to show some fluorescence, potentially indicating some limited transport of particles out of the bloodstream, although the background fluorescence of formaldehyde fixed tissue makes it difficult to detect nanoparticles in the tissue. Fluorescent polystyrene nanoparticles were not found in either the resin or the paraffin sections. Further adaptations of the processing are being made to improve the detection of particles in the brain tissue.

However, as very limited amounts of particles leave the bloodstream, and since routes of administration other than ICV are extremely unlikely to result in concentrations of particles sufficiently high for detection, some improvement of the methodology is required. The team at the University of Ulster at Coleraine who performed the *in vivo* exposure has recently acquired a stimulated emission depletion (STED) microscope, which has much improved resolution, so this work is now being continued. STED is a fluorescence microscopy technique that uses the non-linear de-excitation of fluorescent dyes to overcome the resolution limit imposed by diffraction with standard confocal laser scanning microscopes and conventional far-field optical microscopes. The results found with fluorescent PS-COOH nanoparticles were also confirmed by TEM with ceria particles, as shown in [Fig. 11.2](#).

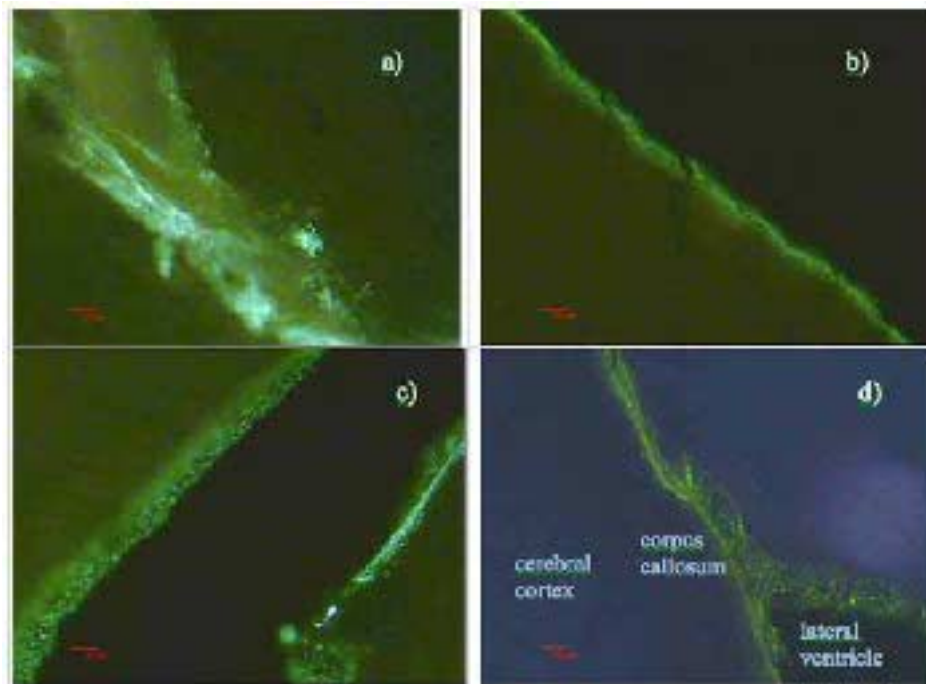


Figure 11.1. Fluorescence light microscopy images of the distribution of fluorescently-labelled 20 nm carboxylate modified polystyrene (PS-COOH) nanoparticles in a mouse brain. Nanoparticles were found along the injection track through the cerebral cortex (a) and in the lining of the ventricular system (third ventricle (b) and lateral ventricle with a fluorescein isothiocyanate filter (c) and with a DAPI filter, probably showing some agglomerated nanoparticles in the tissue (d)). Scale bars are 50 µm.

Ceria nanoparticles were found mainly along the ICV injection path and along the walls of the ventricle. The ventricle was free of nanoparticles, probably due to the perfusion process with combination fixative. However, huge clusters of particles could be found in

compartments adjacent to the ventricle and even in the tissue. Scattered single clusters of about 3–20 particles were found in the brain tissue in the vicinity of the ventricle and injection path.

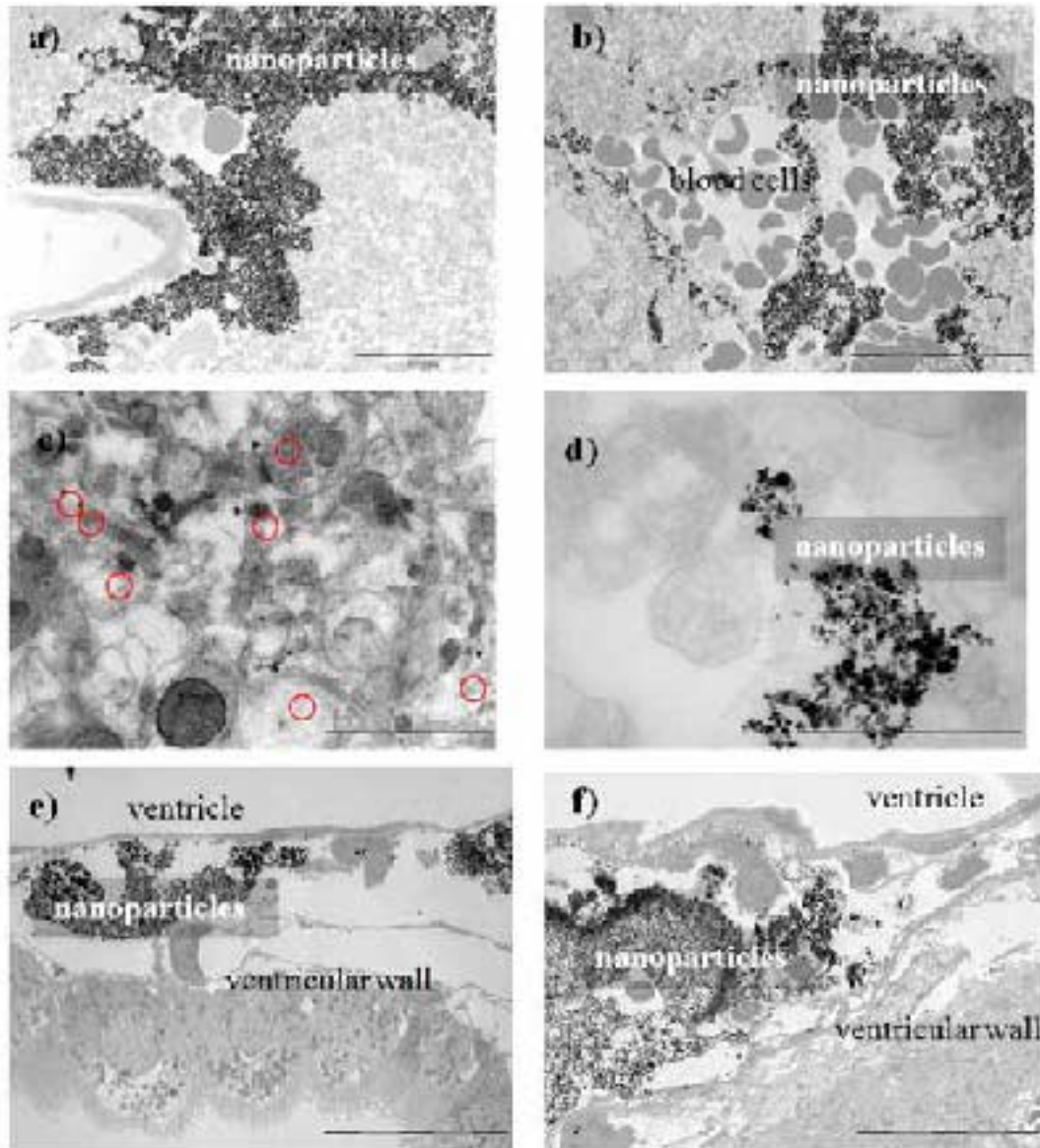


Figure 11.2. Transmission electron microscopy images of ceria nanoparticles in a mouse brain. In comparison with the carboxylate modified polystyrene (PS-COOH) nanoparticle data above, ceria nanoparticles were found along the injection site, in the ventricle but also in the brain tissue. (a, b) show ceria nanoparticles around the lesion (see blood cells present). (c, d) show particles in the brain tissue (red circles in c). (e, f) show particles along the ventricle.

12 Conclusions and Recommendations

By careful application of a robust protocol, it has been possible to obtain quantitatively reproducible results across two teams regarding the transport of a simple macromolecule (FD4), and a known brain transporter protein (ApoE) through an *in vitro* BBB model based on hCMEC/D3 cells that form a monolayer and tight junctions when grown on transwell filters coated with collagen-fibronectin. By comparison with the results in the literature for paracellular transport of FD4, the apparent permeability P_{app} of 3.45×10^{-6} cm/s was relatively lower than published values, indicating that this model maintained a good-quality monolayer with functioning tight-junctions. The appropriate functioning of a receptor-mediated transport mechanism was also confirmed, based on the reproducible, and temperature-dependent, transport of the positive control ApoE shown by each team. This internal benchmarking validation of the *in vitro* BBB model confirmed the formation and barrier functionality of the *in vitro* model human BBB.

Having validated the hCMEC/D3 BBB model, preliminary studies using fluorescently labelled SiO₂ and PS-COOH nanoparticles were performed using a range of transwell membrane compositions and pore sizes in order to optimise the system design, and to identify appropriate nanoparticles for in-detail mechanistic studies to probe how, and why, some nanoparticles can be actively transported across the BBB. Serial equilibration experiments on various 0.4 µm or 3.0 µm porous membranes made of different materials were tested with the PS-COOH and SiO₂ nanoparticles in order to find a permeable transwell compatible with the purpose of nanoparticle application and barrier growth. Results showed that various sizes of PS-COOH particles were not able to equilibrate over 24 hours in all available transwells, but SiO₂ nanoparticles did. DLS characterisation of the different nanoparticles in the transport assay media showed that the PS-COOH nanoparticles were somewhat aggregated under the exposure conditions, although the hydrodynamic sizes in the assay medium were still smaller than the 0.4 µm pores in the PET membrane. TEM imaging was unable to confirm the presence of PS-COOH nanoparticles in either the 0.4 µm or 3.0 µm transwell

filters, as a consequence of the similar electron density properties of the nanoparticles and the PET and PTFE membranes that made visualisation of the polystyrene nanoparticles difficult. Based on these experiments, the SiO₂ nanoparticles (50 nm, 100 nm and 200 nm) were selected for detailed mechanistic studies.

The transport of 50 nm, 100 nm and 200 nm SiO₂ nanoparticles across the BBB was assessed in detail. As expected, a size exclusion effect was observed in the fluxes of the differently sized nanoparticles across the BBB over 4 hours. 50 nm SiO₂ dominated the other two sizes and showed the highest transported amount after 4 hours. Temperature-dependence studies revealed that the SiO₂ nanoparticle transport mechanism is energy-dependent, and is thus an active process involving cellular energy and engagement of cellular machinery and cellular receptors. A transcytotic protein, ApoE, was applied as a positive control. In endothelial cells, ApoE acts as a ligand for low-density lipoprotein receptors and assists transport of cholesterol and other lipids into the brain. In this study, similar patterns of fluxes and permeability at 4°C and 37°C were observed for both ApoE and SiO₂ nanoparticles, and temperature-dependence was observed in both ApoE and SiO₂ nanoparticle transport processes. Furthermore, a bi-directional transport, where the transport from apical to basolateral chambers and from basolateral to apical chambers was assessed, also pointed to an active uptake of both ApoE and SiO₂ nanoparticles, as the permeability of the barrier towards particles was much higher going from apical to basolateral compared to transport from the basolateral to apical chamber due to the presence of specific receptors for uptake localised on the apical side of the cell.

To evaluate the possible pathways of nanoparticle endocytosis and transcytosis, flow cytometry, confocal microscopy and electron microscopy were together employed to study cellular uptake. It was shown that SiO₂ nanoparticles accumulated in hCMEC/D3 cells and were internalised in cellular lysosomes after 4 hours. In the barrier model, ultra-thin sections were obtained to analyse the transport pathway of nanoparticles within

barrier cells. Using electron microscopy, 50 nm SiO₂ nanoparticles were found in endocytic vesicles, early endosomes, multi-vesicular bodies and lysosomes of the hCMEC/D3 cell monolayer. Some particles successfully escaped lysosomal degradation and were transcytosed into the basolateral membrane of the barrier. Additional images showed that after phagocytosis, some SiO₂ nanoparticles were able to cross the barrier by direct transendothelial vesicular transfer through the endothelial cells. These findings demonstrate that SiO₂ nanoparticles can be transcytosed in the hCMEC/D3 BBB model and are able to cross the *in vitro* BBB model.

The preliminary risk assessment of the potential for SiO₂ nanoparticles to induce neurotoxicity suggests that the low potential of the SiO₂ nanoparticles to reach the brain via the BBB (less than 5% of the applied dose of 50 nm SiO₂ nanoparticles was transcytosed in 4 hours), coupled with the low hazard of these nanoparticles, indicate that there is very little risk posed by the Kisker SiO₂ nanoparticles for neurotoxicity. However, these are very short-term acute exposure tests only, and additional experimental modifications are required in order to enable the system to be utilised for longer-term, chronic and repeat dose experiments. Additionally, the simple cytotoxicity assay reported here does not account for more subtle impacts from nanoparticles, such as DNA damage or inflammation, or signalling impacts resulting from conformational changes of proteins adsorbed to the nanoparticles.

Based on the work presented here, the recommendation is that having established and validated the human *in vitro* BBB model for short-term acute studies as intended, there should now be a follow-on study whereby some of the key issues for risk assessment would be further developed, such as using the model for longer-term (e.g. 72-hour) exposure studies, and for repeat dose and chronic exposure studies, and that these be coupled with a fuller hazard assessment. Additionally, a much wider panel of nanoparticles needs to be assessed, including particles such as ceria, titania, gold and carbon nanotubes. Within the NeuroNano project, approaches to label these particles with radioisotopes to allow for their detection in the basolateral chamber are being developed, thereby expanding the range of accessible nanoparticles. This has been somewhat of

a limitation to date, as a result of the limits of detection of ultraviolet and fluorescence measurements, which makes detection of very low nanoparticle concentrations difficult, and of unlabelled nanoparticles extremely challenging.

Additionally, it has recently emerged that direct contact with nanoparticles is not required in order for toxicity effects to be observed. A recent paper in *Nature Nanotechnology* has shown a new type of toxicity, whereby metal nanoparticles (potentially releasing metal ions) or metal ions can cause DNA damage and chromosome aberrations in human cells from the other side of a cellular barrier, i.e. without passing through the barrier and without direct contact between the nanoparticle and the DNA (Bhabra et al., 2009). This novel indirect toxicity is mediated by intercellular signalling within the barrier through connexin and pannexin channels, and involves transmission of purine nucleotides including ATP and Ca wave propagation within the cellular barrier. This new mechanism shares some features of other secondary cellular responses to cell injury, and has some features in common with the radiation- or chemical-induced bystander effect. Until now, genotoxic responses mediated across cellular barriers have not been described, although a recent paper from work within the EU FP6 NanoInteract consortium has also suggested that indirect DNA damage resulted from SiO₂ nanoparticles that appeared to be mediated from the lysosomes, as extensive electron microscopy studies on the localisation of the SiO₂ nanoparticles failed to find any evidence of the nanoparticles anywhere except in the lysosomes (Park et al., 2010). Note, however, that the Kisker SiO₂ nanoparticles used in the EPA STRIVE Fellowship were not included in the panel of SiO₂ nanoparticles used in the genotoxicity study, so whether these particular fluorescently-labelled SiO₂ nanoparticles also induce DNA damage is not yet known. However, having established the conditions under which nanoparticles do not pass through the transwell filters, the BBB model could also be used to assess indirect impacts from nanoparticles that do not get through the membrane. Thus, the system could be set up such that the particles are confined in the apical chamber, and the effects of the nanoparticles on signalling to cells grown in the basolateral chamber could be assessed.

13 Key Messages for Policy Makers

Based on the information presented above, whereby nanoparticles of common materials such as silica and polystyrene appear to be able to utilise active transport mechanisms across the human BBB model, even at sizes up to 200 nm, it is clear that nanoparticles cannot be considered as chemicals for risk assessment purposes. Thus, it is recommended that the EPA consider nanomaterials as biological entities in terms of the assessment of their environmental safety and exposure and promote the development of new assays for assessment of the potential hazards posed by nanomaterials for human health and the environment.

It is further recommended that significant additional research be performed as to the mechanism and kinetics of uptake using a wider panel of appropriately labelled nanoparticles, as well as longer exposure times, repeat dose exposure studies, and so on. This should also be coupled with appropriate assessment of the functional impacts (toxicity) of the nanoparticles towards a range of brain cell types in order to allow a more complete risk assessment of different types of nanomaterials to be carried out.

Given the limited amount of data at present regarding the environmental exposure to nanoparticles in Ireland, it is recommended that the EPA develop a strategy to begin to monitor potential emissions of nanoparticles into water, soil and air from industry.

In the immediate term, this could be implemented via a mandatory reporting system whereby companies utilising nanomaterials in processes or products must report on this use and the type and quantities of nanomaterials being utilised, as well as the potential sources of emission of nanomaterials. This could be followed by appropriate monitoring/measurement strategies as required.

Finally, it is recommended that further high-quality research be conducted to characterise the hazard posed by the emission of those nanomaterials identified in the mandatory reporting process described above, specifically to at-risk consortia (filter-feeding marine bivalves and estuarine benthic communities), and also to assess models for vulnerable human populations, such as injured gut and lung models, etc., as well as in terms of the fate in the environment (dissolution, sedimentation, etc.).

Given Ireland's heavy investment in nanoscience and nanotechnologies, and our desire to be a knowledge economy, leadership in terms of nanosafety assessment would ensure that Ireland contributes to the development of appropriate regulation. Being a regulatory-leader (rather than follower) would give Ireland's enterprise a first-mover advantage in the nano-revolution and in the commercialisation of nano-enabled products.

References

- ABBOTT, N.J., RONNBACK, L. and HANSSON, E. (2006) Astrocyte-endothelial interactions at the blood–brain barrier. *Nat. Rev. Neurosci.*, **7**, 41–53.
- ALZHEIMER EUROPE (2006) *Dementia in Europe – Yearbook 2006*.
- AMBRUOSI, A., KHALANSKY, A.S., YAMAMOTO, H., GELPERINA, S.E., BEGLEY, D.J. and KREUTER, J. (2006) Biodistribution of polysorbate 80-coated doxorubicin-loaded [14C]-poly(butyl cyanoacrylate) nanoparticles after intravenous administration to glioblastoma-bearing rats. *J. Drug Target.*, **14**, 97–105.
- ANDERSON, G.W. (1981) *Cell surface membrane structure and the function of endothelial cells*. New York, Plenum Press.
- ARTURSSON, P. (1990) Epithelial transport of drugs in cell culture. I: a model for studying the passive diffusion of drugs over intestinal absorptive (Caco-2) cells. *J. Pharm. Sci.*, **79**, 476–82.
- BALL, P. (2006) Nanoparticles in sun creams can stress brain cells. *BioEd Online*. <http://www.bioedonline.org/news/news.cfm?art=2592>
- BHABRA, G., SOOD, A., FISHER, B., CARTWRIGHT, L., SAUNDERS, M., EVANS, W.H., SURPRENANT, A., LOPEZ-CASTEJON, G., MANN, S., DAVIS, S.A., HAILS, L.A., INGHAM, E., VERKADE, P., LANE, J., HEESOM, K., NEWSON, R. and CASE, C.P. (2009) Nanoparticles can cause DNA damage across a cellular barrier. *Nat. Nanotechnol.*, **4**, 876–83.
- BLASI, P., GIOVAGNOLI, S., SCHOUBBEN, A., RICCI, M. and ROSSI, C. (2007) Solid lipid nanoparticles for targeted brain drug delivery. *Adv. Drug Deliv. Rev.*, **59**, 454–77.
- BORM, P.J.A., ROBBINS, D., HAUBOLD, S., KUHLBUSCH, T., FISSAN, H., DONALDSON, K., SCHINS, R.P.F., STONE, V., KREYLING, W., LADEMANN, J., KRUTMANN, J., WARHEIT, D. and OBERDORSTER, E. (2006) The potential risks of nanomaterials: a review carried out for ECETOC. *Particle Fibre Toxicology*, **3**, 11.
- BRIGGER, I., MORIZET, J., AUBERT, G., CHACUN, H., TERRIER-LACOMBE, M.J., COUVREUR, P., VASSAL, G. (2002) Poly(ethylene glycol)-coated hexadecylcyanoacrylate nanospheres display a combined effect for brain tumor targeting. *J. Pharmacol. Exp. Ther.*, **303**, 928–36.
- CALDERÓN-GARCIDUEÑAS, L., AZZARELLI, B., ACUNA, H., GARCIA, R., GAMBLING, T.M., OSNAYA, N., MONROY, S., DEL ROSARIO TIZAPANTZI, M., CARSON, J.L., VILLARREAL-CALDERON, A. and REWCASTLE, B. (2002) Air pollution and brain damage. *Toxicol. Pathol.*, **30**, 373–89.
- CALDERÓN-GARCIDUEÑAS, L., MARONPOT, R.R., TORRES-JARDON, R., HENRÍQUEZ-ROLDÁN, C., SCHOONHOVEN, R., ACUÑA-AYALA, H., VILLARREAL-CALDERÓN, A., NAKAMURA, J., FERNANDO, R., REED, W., AZZARELLI, B. and SWENBERG, J.A. (2003) DNA damage in nasal and brain tissues of canines exposed to air pollutants is associated with evidence of chronic brain inflammation and neurodegeneration. *Toxicol. Pathol.*, **31**, 524–38.
- CALDERÓN-GARCIDUEÑAS, L., REED, W., MARONPOT, R.R., HENRIQUEZ-ROLDAN, C., DELGADO-CHAVEZ, R., CALDERÓN-GARCIDUEÑAS, A., DRAGUSTINOVIS, I., FRANCO-LIRA, M., ARAGON-FLORES, M., SOLT, A.C., ALTENBURG, M., TORRES-JARDON, R. and SWENBERG, J.A. (2004) Brain inflammation and Alzheimer's-like pathology in individuals exposed to severe air pollution. *Toxicol. Pathol.*, **32**, 650–8.
- CALVO, J.P., GOURITIN, B., CHACUN, H., DESMAELE, D., D'ANGELO, J., NOEL, J.P., GEORGIN, D., FATTAL, E., ANDREUX, J.P. and COUVREUR, P. (2001) Long-circulating PEGylated polycyanoacrylate nanoparticles as new drug carrier for brain delivery. *Pharm. Res.*, **18**, 1157–66.
- CEDERVALL, T., LYNCH, I., FOY, M., BERGGÅRD, T., DONNELLY, S.C., CAGNEY, G., LINSE, S. and DAWSON, K.A. (2007a) Detailed identification of plasma proteins adsorbed on copolymer nanoparticles. *Angew. Chem. Int. Ed.*, **46**, 5754–6.
- CEDERVALL, T., LYNCH, I., LINDMAN, S., NILSSON, H., THULIN, E., LINSE, S. and DAWSON, K.A. (2007b) Novel methods to quantify binding rates and affinities of proteins to nanoparticles. Effects of nanoparticle composition and size. *PNAS*, **104**, 2050–5.
- CHANG, J., JALLOULI, Y., KROUBIA, M., YUAN, X.-B., FENG, W., KANG, C.-S., PU, P.-Y. and BETBEDER, D. (2009) Characterization of endocytosis of transferrin-coated PLGA nanoparticles by the blood–brain barrier. *Internat. J. Pharma.*, **379**, 285–92.

- CHATTOPADHYAY, N., ZASTRE, J., WONG, H.L., WU, X.Y. and BENDAYAN, R. (2008) Solid lipid nanoparticles enhance the delivery of the HIV protease inhibitor, atazanavir, by a human brain endothelial cell line. *Pharm. Res.*, **25**, 2262–71.
- CROY, J.E., BRANDON, T. and KOMIVES, E.A. (2004) Two apolipoprotein E mimetic peptides, ApoE(130-149) and ApoE(141-155)₂, bind to LRP1. *Biochemistry*, **43**, 7328–35.
- CUCULLO, L., COURAUD, P.O., WEKSLER, B., ROMERO, I.A., HOSSAIN, M., RAPP, E. and JANIGRO, D. (2007) Immortalized human brain endothelial cells and flow-based vascular modeling: a marriage of convenience for rational neurovascular studies. *J. Cereb. Blood Flow Metab.*, **28**, 312–28.
- DEHOUCQ, B., FENART, L., DEHOUCQ, M.P., PIERCE, A., TORPIER, G. and CECCHELLI, R. (1997) A new function for the LDL receptor: transcytosis of LDL across the blood–brain barrier. *J. Cell Biol.*, **138**, 877–89.
- DERGUNOV, A.D. (2004) Apolipoprotein E structure and substrate and receptor-binding activities of triglyceride-rich human plasma lipoproteins in normo- and hypertriglyceridemia. *Biochemistry*, **69**, 720–37.
- DESCAMPS, L., DEHOUCQ, M.P., TORPIER, G. and CECCHELLI, R. (1996) Receptor-mediated transcytosis of transferrin through blood–brain barrier endothelial cells. *Am. J. Physiol.*, **270**, 1149–58.
- DIAMOND, J.M. and WRIGHT, E.M. (1969) Molecular forces governing non-electrolyte permeation through cell membranes. *Proc. R. Soc. Lond. B. Biol. Sci.*, **171**, 273–316.
- DOBROVOLSKAIA, M.A., MCNEIL, S.E. (2007) Immunological properties of engineered nanomaterials. *Nat. Nanotechnol.*, **2**, 469–78.
- DUFFY, K.R. and PARDRIDGE, W.M. (1987) Blood–brain barrier transcytosis of insulin in developing rabbits. *Brain Res.*, **420**, 32–8.
- EC, Registration, Evaluation, Authorization and Restriction of Chemicals (REACH). Regulation (EC) No. 1907/2006 of the European Parliament and of the Council. *Off. J. Eur. Commun.* **2006**, L396/17, 1-849.
- European Chemicals Agency (ECHA) *Guidance for identification and naming of substances under REACH*. http://guidance.echa.europa.eu/guidance_en.htm; 2007.
- ECHA *Guidance on information requirements and chemical safety assessment. Chapter R.7a: Endpoint specific guidance*; European Chemicals Agency. Available at http://guidance.echa.europa.eu/docs/guidance_document/information_requirements_en.htm; 2008.
- ELDER, A., COUDERC, J.P., GELEIN, R., EBERLY, S., COX, C., XIA, X., ZAREBA, W., HOPKE, P., WATTS, W., KITTELSON, D., FRAMPTON, M., UTELL, M. and OBERDORSTER, G. (2007) Effects of on-road highway aerosol exposures on autonomic responses in aged, spontaneously hypertensive rats. *Inhal. Toxicol.*, **19**, 1–12.
- FISCHER, H., GOTTSCHLICH, R., SEELIG, A. (1998) Blood–brain barrier permeation: molecular parameters governing passive diffusion. *J. Membr. Biol.*, **165**, 201–11.
- FORSTER, C., BUREK, M., ROMERO, I.A., WEKSLER, B., COURAUD, P.O. and DRENCKHAHN, D. (2008) Differential effects of hydrocortisone and TNF α on tight junction proteins in an *in vitro* model of the human blood–brain barrier. *J. Physiol.*, **586**, 1937–49.
- FRANK, H.J., PARDRIDGE, W.M., JANKOVIC-VOKES, T., VINTERS, H.V. and MORRIS, W.L. (1986) Insulin binding to the blood–brain barrier in the streptozotocin diabetic rat. *J. Neurochem.*, **47**, 405–11.
- GHOSE, A.K., VISWANADHAN, V.N. and WENDOLOSKI, J.J. (1999) A knowledge-based approach in designing combinatorial or medicinal chemistry libraries for drug discovery. 1. A qualitative and quantitative characterization of known drug databases. *J. Comb. Chem.*, **1**, 55–68.
- HELLSTRAND, E., LYNCH, I., ANDERSSON, A., DRAKENBERG, T., DAHLBÄCK, B., DAWSON, K.A., LINSE, S. and CEDERVALL, T. (2009) Complete high-density lipoproteins in nanoparticle corona. *FEBS J.*, **276**, 3372–81.
- HUBATSCH, I., RAGNARSSON, E.G.E. and ARTURSSON, P. (2007) Determination of drug permeability and prediction of drug absorption in Caco-2 monolayers. *Nature Protocol*, **2**, 2111–19.
- HUWYLER, J., WU, D. and PARDRIDGE, W.M. (1996) Brain drug delivery of small molecules using immunoliposomes. *Proc. Natl. Acad. Sci. U.S.A.*, **93**, 14164–9.
- KETABI-KIYANVASH, N., HEROLD-MENDE, C., KASHFI, F., CALDEIRA, S., TOMMASINO, M., HAEFELI, W.E. and WEISS J. (2007) NKIM-6. A new immortalized human brain capillary endothelial cell line with conserved endothelial characteristics. *Cell Tissue Res.*, **328**, 19–29.
- KIM, H.R., ANDRIEUX, K., GIL, S., TAVERNA, M., CHACUN, H., DESMAËLE, D., TARAN, F., GEORGIN, D. and COUVREUR, P. (2007) Translocation of poly(ethylene glycol-cohexadecyl) cyanoacrylate nanoparticles into rat brain endothelial cells: role of apolipoproteins in receptor-mediated endocytosis. *Biomacromolecules*, **8**, 793–9.

- KNOTT, T.J., PEASE, P.J., POWELL, L.M., WALLIS, S.C., RALL JR, S.C., INNERARITY, T.L., BLACKHART, B., TAYLOR, W.H., MARCEL, Y., MILNES, R., JOHNSON, D., FULLER, M., LUSIS, A.J., MCCARTY, B.J., MAHLEY, R.W., LEVY-WILSON, B. and SCOTT, J. (1986) Complete protein sequence and identification of structural domains of human apolipoprotein B. *Nature*, **323**, 734–8.
- KREUTER, J. (2004) Influence of the surface properties on nanoparticle-mediated transport of drugs to the brain. *J. Nanosci. Nanotechnol.*, **4**, 484–8.
- KREUTER, J., HEKMATARA, T., DREIS, S., VOGEL, T., GELPERINA, S. and LANGER, K. (2007) Covalent attachment of apolipoprotein A-1 and apolipoprotein B-100 to albumin nanoparticles enables drug transport into the brain. *J. Control. Release*, **118**, 54–8.
- KREUTER, J., SHAMENKOV, D., PETROV, V., RAMGE, P., CYCHUTEK, K., KOCH-BRANDT, C. and ALYAUTDIN, R. (2002) Apolipoprotein-mediated transport of nanoparticle-bound drugs across the blood–brain barrier. *J. Drug Target.*, **10**, 317–25.
- KREYLING, W., MÖLLER, W., SEMMLER-BEHNKE, M. and OBERDÖRSTER, G. (2007) *Particle dosimetry: deposition and clearance from the respiratory tract and translocation towards extra-pulmonary sites*. Boca Raton, Francis & Taylor.
- KREYLING, W.G., SEMMLER, M., ERBE, F., MAYER, S., TAKENAKA, S. and SCHULTZ, J. (2002) Translocation of ultrafine insoluble iridium particles from lung epithelium to extrapulmonary organs is size dependent but very low. *Toxicol. Env. Health. Part A*, **65**, 1513–30.
- KUSCH-PODDAR, M., DREWE, J., ISABELLE FUX, I. and GUTMANN, H. (2005) Evaluation of the immortalized human brain capillary endothelial cell line BB19 as a human cell culture model for the blood–brain barrier. *Brain Research.*, **1064**, 21–31.
- LINSE, S., CABALEIRO-LAGO, C., XUE, W.-F., LYNCH, I., LINDMAN, S., THULIN, E., RADFORD, S.E. and DAWSON, K.A. (2007) Nucleation of protein fibrillation by nanoparticles. *PNAS*, **104**, 8691–6.
- LUNDQVIST, M., STIGLER, J., CEDERVALL, T., ELIA, G., LYNCH, I. and DAWSON, K. (2008) Nanoparticle size and surface properties determine the protein corona with possible implications for biological impacts. *PNAS*, **105**, 14265–70.
- LYNCH, I., ANNA SALVATI, A. and DAWSON, K.A. (2009) What does the cell see? *Nature Nanotechnology*, **4**, 2.
- MAHLEY, R.W. (1988) Apolipoprotein E: cholesterol transport protein with expanding role in cell biology. *Science*, **240**, 622–30.
- MARRINK, S.J., JÄHNIG, F., BERENDSEN, H.J. (1996) Proton transport across transient single-file water pores in a lipid membrane studied by molecular dynamics simulations. *Biophys. J.*, **71**, 632–47.
- MAYNARD, A.D. and KUEMPEL, E.D. (2005) Airborne nanostructured particles and occupational health. *J Nanoparticle Research*, **7**, 587–614.
- MICHAELIS, K., HOFFMANN, M.M., DREIS, S., HERBERT, E., ALYAUTDIN, R.N., MICHAELIS, M., KREUTER, J. and LANGER, K. (2006) Covalent linkage of apolipoprotein E to albumin nanoparticles strongly enhances drug transport into the brain. *J. Pharm.*, **317**, 1246–53.
- MOSMANN, T. (1983) Rapid colorimetric assay for cellular growth and survival: application to proliferation and cytotoxicity assays. *J. Immunological Methods*, **65**, 55–63.
- NIC RAGNAILL, M., BROWN, M., YE, D., BRAMINI, M., CALLANAN, S., LYNCH, I. and DAWSON, K.A. (2011) Internal benchmarking of a human blood–brain barrier cell model for screening of nanoparticle uptake and transcytosis. *Eur. J. Pharma. & Biopharma.*, article in press, doi:10.1016/j.ejpb.2010.12.
- OECD WORKING PARTY ON MANUFACTURED NANOMATERIALS: LIST OF MANUFACTURED NANOMATERIALS AND LIST OF ENDPOINTS FOR PHASE ONE OF OECD TESTING PROGRAMME. *ENV/JM/MONO(2008)13/REV*; Organisation for Economic Cooperation and Development: 2008.
- OLIVIER, J.C., FENART, L., CHAUVET, R., PARIAT, C., CECHELLI, R. and COUET, W. (1999) Indirect evidence that drug brain targeting using polysorbate 80-coated polybutylcyanoacrylate nanoparticles is related to toxicity. *Pharm. Res.*, **16**, 1836–42.
- OMIDI, Y., CAMPBELL, L., BARAR, J., CONNELL, D., AKHTAR S. and GUMBLETON, M. (2003) Evaluation of the immortalised mouse brain capillary endothelial cell line, b.End3, as an *in vitro* blood–brain barrier model for drug uptake and transport studies. *Brain Res.*, **990**, 95–112.
- O’MORCHOE, C.C.C., JONES, W.R., JAROSZ, H.M., O’MORCHOE, P.J. and FOX, L.M. (1984) Temperature dependence of protein transport across lymphatic endothelium *in vitro*. *J. Cell Biology*, **98**, 629–40.
- PALUMBO, P., PICCHINI, U., BECK, B., VAN GELDER, J., DELBAR, N. and ANDREA DEGAETANO, A. (2008) A general approach to the apparent permeability index. *J. Pharmacokinetics and Pharmacodynamics*, **35**, 235–48.
- PARDRIDGE, W.M. (2001) *Brain drug targeting: the future of brain drug development*. Cambridge University Press.

- PARDRIDGE, W.M. (2007) Blood brain barrier delivery. *Drug Discovery Today*, **12**, 54–61.
- PARDRIDGE, W.M. and MIETUS, L.J. (1979) Transport of steroid hormones through the rat blood–brain barrier. Primary role of albumin-bound hormone. *J. Clin. Invest.*, **64**, 145–54.
- PARK, M.V., VERHAREN, H.W., ZWART, E., HERNANDEZ, L.G., VAN BENTHEM, J., ELSAESSER, A., BARNES, C., MCKERR, G., HOWARD, C.V., SALVATI, A., LYNCH, I., DAWSON, K.A. and DE JONG, W.H. (2010) Genotoxicity evaluation of amorphous silica nanoparticles of different sizes using the micronucleus and the plasmid lacZ gene mutation assay. *Nanotoxicology*, 24 August (epublication ahead of print).
- PETRI, B., BOOTZ, A., KHALANSKY, A., HEKMATARA, T., MÜLLER, R., UHL, R., KREUTER, J. and GELPERINA, S. (2007) Chemotherapy of brain tumour using doxorubicin bound to surfactant-coated poly(butyl cyanoacrylate) nanoparticles: revisiting the role of surfactants. *J. Control. Release*, **117**, 51–8.
- PHIBBS-RIZZUTO, P. (2007) Study of nanoparticles' effect on protein important, but more research needed. *Daily Environment Report*, **107**, A-4.
- POLLER, B., GUTMANN, H., KRÄHENBÜHL, S., WEKSLER, B., ROMERO, I., COURAUD, P.O., TUFFIN, G., DREWE, J. and HUWYLER, J. (2008) The human brain endothelial cell line hCMEC/D3 as a human blood–brain barrier model for drug transport studies. *J. Neurochem.*, **107**, 1358–68.
- PRUDHOMME, J.G., SHERMAN, I.W., LAND, K.M., MOSES, A.V., STENGLEIN, S. and NELSON, J.A. (1996) Studies of Plasmodium falciparum cytoadherence using immortalized human brain capillary endothelial cells. *Int. J. Parasitol.*, **26**, 647–55.
- REGINA, A., ROMERO, I.A., GREENWOOD, J., ADAMSON, P., BOURRE, J.M., COURAUD, P.O. and ROUX, F. (1999) Dexamethasone regulation of P-glycoprotein activity in an immortalized rat brain endothelial cell line, GPNT. *J. Neurochem.*, **73**, 1954–63.
- REIMAN, E.M. (2007) Linking brain imaging and genomics in the study of Alzheimer's disease and aging. *Ann. N.Y. Acad. Sci.*, **1097**, 94–113.
- ROHRER, L., CAVELIER, C., FUCHS, S., SCHLÜTER, M.A., VÖLKER, W., VON ECKARDSTEIN, A. (2006) Binding, internalization and transport of apolipoprotein A-1 by vascular endothelial cells. *Biochimica et Biophysica Acta*, **176**, 186–94.
- ROUX, F., DURIEU-TRAUTMANN, O., CHAVEROT, N., CLAIRE, M., MAILLY, P., BOURRE, J.M., STROSBERG, A.D. and COURAUD, P.O. (1994) Regulation of gamma-glutamyl transpeptidase and alkaline phosphatase activities in immortalized rat brain microvessel endothelial cells. *J. Cell. Physiol.*, **159**, 101–13.
- SARIN, H., KANEVSKY, A.S., WU, H., BRIMACOMBE, K.R., FUNG, S.H., SOUSA, A.A., AUH, S., WILSON, C.M., SHARMA, K., ARONOVA, M.A., LEAPMAN, R.D., GRIFFITHS, G.L., HALL, M.D. (2008) Effective transvascular delivery of nanoparticles across the blood–brain tumor barrier into malignant glioma cells. *J. Transl. Med.*, **6**, 80.
- SCHINKEL, A.H. (1999) P-glycoprotein, a gatekeeper in the blood–brain barrier. *Adv. Drug Deliv. Rev.*, **36**, 179–94.
- SEMMLER, M., SEITZ, J., ERBE, F., MAYER, P., HEYDER, J., OBERDORSTER, G. and KREYLING, W.G. (2004) Long-term clearance kinetics of inhaled ultrafine insoluble iridium particles from the rat lung, including transient translocation into secondary organs. *Inhal. Toxicol.*, **16**, 453–9.
- SHAPER, K., FENAROLI, F., LYNCH, I., COTTELL, D.C., SALVATI, A. and DAWSON, K.A. (2011) Time and space resolved uptake study of silica nanoparticles by human cells. *Mol. Biosyst.*, **7**, 371–8.
- SILVA, G.A. (2008) Nanotechnology approaches to crossing the bloodbrain barrier and drug delivery to the CNS. *BMC Neuroscience*, **9** (Suppl. 3), S4.
- STEIN, W.D. (1967) *The movement of molecules across cell membranes*. Academic Press.
- TOSI, G., COSTANTINO, L., RIVASI, F., RUOZI, B., LEO, E., VERGONI, A.V., TACCHI, R., BERTOLINI, A., VANDELLI, M.A. and FORNI, F. (2007) Targeting the central nervous system: *in vivo* experiments with peptide-derivatized nanoparticles loaded with loperamide and rhodamine-123. *J. Control. Release*, **122**, 1–9.
- TRAUBLE, H. (1971) The movement of molecules across lipid membranes: a molecular theory. *J. Membr. Biol.*, **4**, 193–208.
- WALCZYK, D., BALDELLI-BOMBELLI, F., CAMPBELL, A., LYNCH, I. and DAWSON, K.A. (2010) What the cell “sees” in bionanoscience. *JACS*, **132**, 5761–8.
- WEKSLER, B.B., SUBILEAU, E.A., PERRIÈRE, N., CHARNEAU, P., HOLLOWAY, K., LEVEQUE, M., TRICOIRE-LEIGNEL, H., NICOTRA, A., BOURDOULOUS, S., TUROWSKI, P., MALE, D.K., ROUX, F., GREENWOOD, J., ROMERO, I.A., COURAUD, P.O. (2005) Blood–brain barrier-specific properties of a human adult brain endothelial cell line. *FASEB J.*, **19**, 1872–4.

WU, D. and PARDRIDGE, W.M. (1999) Blood–brain barrier transport of reduced folic acid. *Pharm. Res.*, **16**, 415–19.

XIA, T., KOVOCHICH, M., BRANT, J., HOTZE, M., SEMPFF, J., OBERLEY, T., SIOUTAS, C., YEH, J.I., WIESNER, M.R. and NEL, A.E. (2006) Comparison of the abilities of ambient and manufactured nanoparticles to induce cellular toxicity according to an oxidative stress paradigm. *Nano Lett.*, **6**, 1794–807.

Acronyms and Annotations

AET	Active efflux transport
ApoE	Apolipoprotein E
ATP	Adenosine-5'-triphosphate
BBB	Blood–brain barrier
BCEC	Brain capillary endothelial cells
bFGF	Basic fibroblast growth factor
CMT	Carrier-mediated transport
CNS	Central nervous system
CO ₂	Carbon dioxide (gas)
DAPI	4',6-diamidino-2-phenylindole
DLS	Dynamic light scattering
EBM-2	Endothelial basal medium
EGF	Epidermal growth factor
EU FP7	European Commission Seventh Framework Programme
FBS	Foetal bovine serum FCS Foetal calf serum
FD4	Fluorescein isothiocyanate labelled dextran, molecular weight 4 kDa
H-bond	Hydrogen bond
hCMEC/D3	Immortalised human capillary microvascular endothelial cell
ICV	Intra-cerebro-ventricular
IGF-1	Insulin-like growth factor 1
LDL	Low-density lipoprotein
mM	Millimolar
MTT	3-(4,5-dimethylthiazol-2-yl)-2,5-diphenyltetrazolium bromide
MW	Molecular weight
OECD	Organisation for Economic Co-operation and Development
P_{app}	Apparent permeability
PBS	Phosphate buffered saline
PDI	Polydispersity index
PET	Polyester
PS-COOH	Carboxylate modified polystyrene
PTFE	Polytetrafluoroethylene
RMT	Receptor-mediated transport

ROS	Reactive oxygen species
rpm	Revolutions per minute
SiO ₂	Silicon dioxide (silica)
STED	Stimulated emission depletion
TEER	Transendothelial electrical resistance
TEM	Transmission electron microscopy
TiO ₂	Titanium dioxide
VEGF	Vascular endothelial growth factor
Z-ave	Average size

Appendix I: Experimental Details

Cell Culture

Immortalised human brain capillary microvascular endothelial cells (hCMEC/D3) were obtained from Florence Miller, B.B. Weksler (Inserm, France). The original brain endothelial cells were isolated from human brain tissue following surgical excision of an area of the temporal lobe of an adult female with epilepsy. The hCMEC/D3 cell line was formed by immortalisation of the aforementioned endothelial cells by lentiviral transduction of the catalytic subunit of human telomerase and SV40-T antigen (8). The hCMEC/D3 cells were used between passage 7–10. For culturing, 50,000 cells were seeded in a collagen-coated flask (25 cm³, Becton Dickinson) and supplemented with endothelial basal medium (EBM-2) containing vascular endothelial growth factor (VEGF), insulin-like growth factor-1 (IGF-1), epidermal growth factor (EGF), basic fibroblast growth factor (bFGF), foetal calf serum (FCS, 2%), gentamicin sulphate/amphotericin B and hydrocortisone (Lonza Biosciences). For migration assays, cells were supplemented with growth factor depleted EBM-2 assay medium containing bFGF, 2% FCS, hydrocortisone and 10 mM 4-(2-hydroxyethyl)-1-piperazineethanesulfonic acid during monolayer formation. Cells were cultured in an incubator at 37°C with 5% CO₂/95% air and saturated humidity. The cell culture medium was changed every two days, and the monolayer medium twice weekly.

Transport Assays and P_{app} Determination

The *in vitro* BBB system was prepared on a 12-well format on a PET membrane transwell (1.12 cm², 0.4 µm pore size, Corning). Membrane inserts were coated with 200 µl collagen-fibronectin (15% rat tail collagen and 15% bovine fibronectin, Invitrogen) 1 day prior to use, and stored at 37°C in a dry incubator. For transport experiments, hCMEC/D3 cells were seeded in 500 µl assay media at a density of 5×10^5 cells per 1.2 cm² filter in the apical compartment and 1500 µl assay media in the basolateral compartment. The assay medium was changed twice weekly. Transport assays

were conducted 7–10 days after seeding. Both the apical and basolateral chambers were washed twice with assay medium directly before experiments began. The transport study set-up involved application of 500 µl assay medium containing FD4 (200 µg/ml), SiO₂ nanoparticles (50 nm, 100 µg/ml) or ApoE (1.98 µg/ml) to the transwell apical compartment. The basolateral compartment contained 1500 µl assay medium and transwells were placed in an orbital shaker at 37°C. Samples of 100 µl assay medium were removed from the basolateral compartment every 15 minutes in the case of FD4, and every hour for ApoE and 50 nm SiO₂ nanoparticles, and aliquoted into black flat-bottomed 96-well plates. The 100 µl sample was replaced with assay medium after each sampling. The fluorescence of FD4, ApoE and 50 nm SiO₂ nanoparticles was determined using a fluorimeter with an excitation/emission wavelength of 490 nm/515 nm for FD4, 485 nm/514 nm for 50 nm SiO₂ nanoparticles and 650 nm/668 nm for ApoE. A standard curve of fluorescence was calculated for each molecule in order to determine sample concentration. The apparent permeability (P_{app}) was calculated according to the method of Artursson (1990) using the equation

$$P_{app} = \frac{dQ}{dt} \times \frac{1}{A \times C_0 \times 60},$$

where dQ/dt is the amount of FD4, 50 nm SiO₂ nanoparticles or ApoE transported per minute (ng/min), A is the surface area of the filter (cm²), C_0 is the initial concentration of FD4, 50 nm SiO₂ nanoparticles or ApoE, and 60 is the conversion from minutes to seconds.

Confocal Microscopy

Cells were plated on 35mm plates with 15mm diameter glass coverslips at densities ranging from 1.25×10^5 to 1.8×10^5 cells and treated as described above for the transport assay sample preparation. For actin visualization, cells were washed with 3 x 1ml PBS, permeabilized for 5 minutes with 0.1% saponin from Quillaja bark (Sigma, St. Louis, MO), washed again

with 3 x 1ml PBS then incubated at room temperature for 20 minutes with 2% Texas Red-X Phalloidin (Invitrogen) and 0.5% Bovine Serum Albumin (BSA) in PBS. Slides were then washed with 3 x 1ml PBS, treated for 3 minutes with DAPI to stain the nuclei, washed with 1ml PBS, and then mounted onto slides for imaging. For lysosome staining, samples were washed with 3 x 1ml PBS, fixed for 20 minutes with 1ml 4% Formaline, permeabilized for 5 mins of 1ml 1% saponin from Quillaja bark (Sigma), and incubated for 30 minutes at room temperature with a blocking solution of 1% Albumin Bovine Serum Fraction V (Sigma) in PBS-T to prevent non specific binding. Samples were incubated for 1 hour at room temperature with a primary antibody of 1:200 mouse mAb to LAMP [H4A3] (Abcam, Cambridge, UK), washed with 3 x 1ml PBS, and then incubated at room temperature for 1hr with 1:400 dilution of AlexaFluor 647 Goat Anti-mouse IgG (H+L) as a secondary antibody. Samples were washed 3 x 1ml PBS and incubated for 3 minutes with DAPI before mounting with MOWIOL on slides for imaging. The cells were observed using a Carl Zeiss LSM 510 Meta laser scanning confocal microscope (Zeiss, Munchen, Germany) with lasers at 364nm (DAPI), 488nm (FD4 labelled SiO₂ nanoparticles), 543nm (Phalloidin), and 633nm (LAMP antibody).

Transmission Electron Microscopy

Seven-day-old hCMEC/D3 monolayers were exposed to 100 µg/ml 50 nm SiO₂ nanoparticles in an orbital shaker (100 rpm) for 1 hour at 37°C. Permeable filters containing a confluent monolayer of endothelial cells were fixed with glutaraldehyde (2.5% volume by volume) in Sorensen phosphate buffer for 1 hour at room temperature, and post-fixed with osmium tetroxide (1% weight by volume) in de-ionised water for 1 hour. After dehydration in a graded series of 70%, 90% and 100% ethanol and embedding in epoxy resin, sections were cut perpendicular to the monolayer with a Leica Microtome, contrasted with 2% uranyl acetate and lead citrate, and examined with an electron microscope (TECNAI).

Nanoparticle Dispersion and Characterisation

SiO₂ Nanoparticles

Yellow-green fluorescently-labelled 50 nm SiO₂ nanoparticles were purchased from Kisker-Biotech. The size of these nanoparticles dispersed in assay media was determined with a Malvern Zetasizer 3000HSa. The particles were diluted in 1.5 ml assay medium to reach a 100 µg/ml concentration. The solution of particles was incubated at 37°C in an orbital shaker over 4 hours, and sampled each hour. The measurements were conducted at 37°C by transferring 500 µl of the stock solution to a square cuvette for DLS analysis. DLS analyses the velocity distribution of particle movement by measuring dynamic fluctuations of light scattering intensity caused by the Brownian motion of the particle. This technique yields a hydrodynamic radius, or diameter, which is calculated via the Stokes–Einstein equation from the aforementioned measurements.

Polystyrene Nanoparticles

Polystyrene nanoparticles (Yellow-green fluorescently labelled, 40 nm from Invitrogen) were used without further modification or purification. All stock solutions were stored at 4 °C.

Nanoparticle dispersions were prepared by diluting the concentrated nanoparticle stock solutions into the assay medium used for cell culture at room temperature, immediately prior to the experiments on cells, with an identical time delay between diluting and introducing to the cells for all experiments. The medium was kept at room temperature and not pre-warmed to 37 °C to ensure better nanoparticle dispersions. Particles were diluted and measured as above for SiO₂ nanoparticles.

Protein Corona Determination

Particle suspensions were incubated with assay medium and introduced to the apical chamber of the transwells. Following 4 hours of exposure, the particles from the apical and basolateral chambers were assessed for their protein coronas as follows.

The samples were centrifuged to pellet the particle–protein complexes. The pellet was re-suspended in PBS (10 mM phosphate, 0.15 M NaCl, 1 mM EDTA, pH 7.5), transferred to a new vial and centrifuged again to pellet the particle–protein complexes. This procedure was repeated three times. After the third washing step, the supernatant did not contain any detectable amount of proteins. The proteins were eluted from the particles by adding SDS-sample buffer to the pellet and boiling the solution. The proteins

were separated by 12% SDS-PAGE, and stained using Coomassie blue.

Statistical Analysis

Statistical analysis was carried out by two-way ANOVA and Bonferroni post-test on transport studies of both 50 nm SiO₂ nanoparticles and ApoE, as well as on the TEER measurements (GraphPad Prism 4.0). A *p*-value of less than 0.05 was deemed significant.

An Ghníomhaireacht um Chaomhnú Comhshaoil

Is í an Ghníomhaireacht um Chaomhnú Comhshaoil (EPA) comhlachta reachtúil a chosnaíonn an comhshaoil do mhuintir na tíre go léir. Rialaímid agus déanaimid maoirsiú ar ghníomhaíochtaí a d'fhéadfadh truailliú a chruthú murach sin. Cinntímid go bhfuil eolas cruinn ann ar threochtaí comhshaoil ionas go nglactar aon chéim is gá. Is iad na príomhnithe a bhfuilimid gníomhach leo ná comhshaoil na hÉireann a chosaint agus cinntiú go bhfuil forbairt inbhuanaithe.

Is comhlacht poiblí neamhspleách í an Ghníomhaireacht um Chaomhnú Comhshaoil (EPA) a bunaíodh i mí Iúil 1993 faoin Acht fán nGníomhaireacht um Chaomhnú Comhshaoil 1992. Ó thaobh an Rialtais, is í an Roinn Comhshaoil, Pobal agus Rialtais Áitiúil.

ÁR bhFREAGRACHTAÍ

CEADÚNÚ

Bíonn ceadúnais á n-eisiúint againn i gcomhair na nithe seo a leanas chun a chinntiú nach mbíonn astuithe uathu ag cur sláinte an phobail ná an comhshaoil i mbaol:

- áiseanna dramhaíola (m.sh., líonadh talún, loisceoirí, stáisiúin aistriúcháin dramhaíola);
- gníomhaíochtaí tionsclaíocha ar scála mór (m.sh., déantúsaíocht cógaisíochta, déantúsaíocht stroighne, stáisiúin chumhachta);
- diantalmhaíocht;
- úsáid faoi shrian agus scaoileadh smachtaithe Orgánach Géinathraithe (GMO);
- mór-áiseanna stórais peitreal; agus
- scardadh dramhuisce.

FEIDHMIÚ COMHSHAOIL NÁISIÚNTA

- Stiúradh os cionn 2,000 iniúchadh agus cigireacht de áiseanna a fuair ceadúnas ón nGníomhaireacht gach bliain.
- Maoirsiú freagrachtaí cosanta comhshaoil údarás áitiúla thar sé earnáil - aer, fuaim, dramhaíl, dramhuisce agus caighdeán uisce.
- Obair le húdaráis áitiúla agus leis na Gardaí chun stop a chur le gníomhaíocht mhídhleathach dramhaíola trí chomhordú a dhéanamh ar líonra forfheidhmithe náisiúnta, díriú isteach ar chiontóirí, stiúradh fiosrúcháin agus maoirsiú leigheas na bhfadhbanna.
- An dlí a chur orthu siúd a bhriseann dlí comhshaoil agus a dhéanann dochar don chomhshaoil mar thoradh ar a ngníomhaíochtaí.

MONATÓIREACHT, ANAILÍS AGUS TUAIRISCIÚ AR AN GCOMHSHAOIL

- Monatóireacht ar chaighdeán aer agus caighdeán aibhneacha, locha, uisce taoide agus uisce talaimh; leibhéil agus sruth aibhneacha a thomhas.
- Tuairisciú neamhspleách chun cabhrú le rialtais náisiúnta agus áitiúla cinntiú a dhéanamh.

RIALÚ ASTUITHE GÁIS CEAPTHA TEASA NA HÉIREANN

- Caimníochtú astuithe gáis ceaptha teasa na hÉireann i gcomhthéacs ár dtiomantas Kyoto.
- Cur i bhfeidhm na Treorach um Thrádáil Astuithe, a bhfuil baint aige le hos cionn 100 cuideachta atá ina mór-ghineadóirí dé-ocsaíd charbóin in Éirinn.

TAIGHDE AGUS FORBAIRT COMHSHAOIL

- Taighde ar shaincheisteanna comhshaoil a chomhordú (cosúil le caighdeán aer agus uisce, athrú aeráide, bithéagsúlacht, teicneolaíochtaí comhshaoil).

MEASÚNÚ STRAITÉISEACH COMHSHAOIL

- Ag déanamh measúnú ar thionchar phleananna agus chláracha ar chomhshaoil na hÉireann (cosúil le pleananna bainistíochta dramhaíola agus forbartha).

PLEANÁIL, OIDEACHAS AGUS TREOIR CHOMHSHAOIL

- Treoir a thabhairt don phobal agus do thionscal ar cheisteanna comhshaoil éagsúla (m.sh., iarratais ar cheadúnais, seachaint dramhaíola agus rialacháin chomhshaoil).
- Eolas níos fearr ar an gcomhshaoil a scaipeadh (trí cláracha teilifíse comhshaoil agus pacáistí acmhainne do bhunscoileanna agus do mheánscoileanna).

BAINISTÍOCHT DRAMHAÍOLA FHORGHNÍOMHACH

- Cur chun cinn seachaint agus laghdú dramhaíola trí chomhordú An Chláir Náisiúnta um Chosc Dramhaíola, lena n-áirítear cur i bhfeidhm na dTionscnamh Freagrachta Táirgeoirí.
- Cur i bhfeidhm Rialachán ar nós na treoracha maidir le Trealamh Leictreach agus Leictreonach Caite agus le Srianadh Substaintí Guaiseacha agus substaintí a dhéanann ídiú ar an gcrios ózón.
- Plean Náisiúnta Bainistíochta um Dramhaíl Ghuaiseach a fhorbairt chun dramhaíl ghuaiseach a sheachaint agus a bhainistiú.

STRUCHTÚR NA GNÍOMHAIREACHTA

Bunaíodh an Ghníomhaireacht i 1993 chun comhshaoil na hÉireann a chosaint. Tá an eagraíocht á bhainistiú ag Bord lánaimseartha, ar a bhfuil Príomhstíúrthóir agus ceithre Stíúrthóir.

Tá obair na Ghníomhaireachta ar siúl trí ceithre Oifig:

- An Oifig Aeráide, Ceadúnaithe agus Úsáide Acmhainní
- An Oifig um Fhorfheidhmiúchán Comhshaoil
- An Oifig um Measúnacht Comhshaoil
- An Oifig Cumarsáide agus Seirbhísí Corparáide

Tá Coiste Chomhairleach ag an nGníomhaireacht le cabhrú léi. Tá dáréag ball air agus tagann siad le chéile cúpla uair in aghaidh na bliana le plé a dhéanamh ar cheisteanna ar ábhar imní iad agus le comhairle a thabhairt don Bhord.

Science, Technology, Research and Innovation for the Environment (STRIVE) 2007-2013

The Science, Technology, Research and Innovation for the Environment (STRIVE) programme covers the period 2007 to 2013.

The programme comprises three key measures: Sustainable Development, Cleaner Production and Environmental Technologies, and A Healthy Environment; together with two supporting measures: EPA Environmental Research Centre (ERC) and Capacity & Capability Building. The seven principal thematic areas for the programme are Climate Change; Waste, Resource Management and Chemicals; Water Quality and the Aquatic Environment; Air Quality, Atmospheric Deposition and Noise; Impacts on Biodiversity; Soils and Land-use; and Socio-economic Considerations. In addition, other emerging issues will be addressed as the need arises.

The funding for the programme (approximately €100 million) comes from the Environmental Research Sub-Programme of the National Development Plan (NDP), the Inter-Departmental Committee for the Strategy for Science, Technology and Innovation (IDC-SSTI); and EPA core funding and co-funding by economic sectors.

The EPA has a statutory role to co-ordinate environmental research in Ireland and is organising and administering the STRIVE programme on behalf of the Department of the Environment, Heritage and Local Government.